**Title**
Chemistry and biochemistry of 13 C hyperpolarized magnetic resonance using dynamic nuclear polarization

**Permalink**
https://escholarship.org/uc/item/78032550

**Journal**
Chemical Society Reviews, 43(5)

**ISSN**
0306-0012

**Authors**
Keshari, Kayvan R
Wilson, David M

**Publication Date**
2014-03-07

**DOI**
10.1039/c3cs60124b

Peer reviewed

# Chemistry and biochemistry of 13C hyperpolarized magnetic resonance using dynamic nuclear polarization

**Kayvan R. Keshari**[a,b] and **David M. Wilson**[c,†]

[a]Department of Radiology, Memorial Sloan-Kettering Cancer Center (MSKCC), New York, NY 10065, USA

[b]Molecular Pharmacology and Chemistry Program, Memorial Sloan-Kettering Cancer Center (MSKCC), New York, NY 10065, USA

[c]Department of Radiology and Biomedical Imaging, University of California San Francisco (UCSF), 1700 4th St., Byers Hall 203, San Francisco, California, USA 94158

## Abstract

The study of transient chemical phenomena by conventional NMR has proved elusive, particularly for non-$^1$H nuclei. For $^{13}$C, hyperpolarization using the dynamic nuclear polarization (DNP) technique has emerged as a powerful means to improve SNR. The recent development of rapid dissolution DNP methods has facilitated previously impossible *in vitro* and *in vivo* study of small molecules. This review presents the basics of the DNP technique, identification of appropriate DNP substrates, and approaches to increase hyperpolarized signal lifetimes. Also addressed are the biochemical events to which DNP-NMR has been applied, with descriptions of several probes that have met with *in vivo* success.

## 1. Introduction

The term "molecular imaging" has been used to describe techniques that directly or indirectly monitor and record the spatiotemporal distribution of molecular or cellular processes for biochemical, biologic, diagnostic, or therapeutic applications.[1] A variety of imaging methods fit this description, including positron emission tomography (PET), single photon emission computed tomography (SPECT), optical imaging, and Raman spectroscopy. The relevant chemistries are highly evolved for some of these fields, with the earliest SPECT camera developed in the 1960's and hundreds of PET tracers now described in the literature. Magnetic resonance imaging (MRI), whose origin is in nuclear magnetic resonance (NMR), was developed for clinical use as of the 1980's, and began with a structural emphasis. More recently, functional insights have been provided by several MRI innovations. *In vivo* magnetic resonance spectroscopy (MRS), use of gadolinium (Gd) chelates, and imaging of magnetic nanoparticles (MNP), to name a few, have permitted interrogation of basic cellular mechanisms on the molecular level.

[†]Department of Radiology and Biomedical Imaging, 505 Parnassus Ave, Room L-358, San Francisco, CA 94143. David.M.Wilson@ucsf.edu; Fax: +1-415-514-4714; Tel: +1-415-353-1668.

One limitation of MRS in particular is low sensitivity, a problem that has been addressed by hyperpolarization, where the spin polarization of a nucleus is enhanced beyond that seen at thermodynamic equilibrium. Hyperpolarized (HP) $^{129}$Xe and $^{3}$He have been achieved by optical pumping, with potential for low-radiation imaging of the lungs. For nuclei found in endogenous molecules (in particular carbon and nitrogen), the dynamic nuclear polarization (DNP) technique has emerged as a way to polarize small-molecule metabolites not readily observable by traditional MR. The dramatic signal enhancements obtained (up to $10^5$) allow not only the detection of the introduced metabolic agent, but also its metabolic products in real-time. Progress has been catalyzed by a remarkable technical achievement, namely, the retention of spin polarization in solution following low-temperature DNP in the solid state.[2] This process has been termed dissolution-DNP and is the focus of this review. New $^{13}$C probes, MRI methods, disease models, and biochemical insights have advanced the field significantly over the last decade, culminating in the first human trial using HP [1-$^{13}$C] pyruvate in prostate cancer patients.[3]

*In vivo* studies are only one application of DNP, which has also probed a variety of chemistries *in vitro*. DNP-NMR is particularly suited to processes that are rapid, transient, and dynamic since their study is difficult at thermodynamic equilibrium. The focus of this review is $^{13}$C, but several other spin 1/2 nuclei are amenable to DNP, including $^{15}$N, $^{29}$Si, and $^{89}$Y. This review presents the basics of the DNP technique, identification of appropriate DNP substrates, and approaches to increase HP signal lifetimes. Also addressed are the biochemical events to which DNP-NMR has been applied, with descriptions of several probes that have met with *in vivo* success.

## 2. WHY DNP?

### 2.1. Clinical development of $^1$H MRI/MRS

One of the major advances in biomedical imaging of the last century has been the development of MRI, which evolved from NMR. Since the pioneering work of Lauterbur and Mansfield, advances in MR imaging have progressed rapidly, with MRI now considered critical in the workup of patients suffering from a wide array of disorders. Nuanced discussion of the development of MRI is beyond the scope of this review.[4] Briefly, the vast majority of clinical MRI scans observe protons ($^1$H nuclei, spin 1/2), which are highly abundant in the body in the form of $H_2O$. In a typical NMR experiment, at thermal equilibrium these $^1$H spins precess about an applied magnetic field with a net magnetization, which may be perturbed and detected by appropriate radiofrequency radiation and detection. In MRI, the location of the detected signal in 3D-space is obtained by applying additional magnetic field gradients during detection. In conventional pulsed NMR, the return to thermal equilibrium is characterized by a relaxation time $T_1$.

While MRI provides morphometric information about the organs and/or disease studied, MRS is used to study metabolites in tissue, providing functional and biochemical insights. MRS is commonly performed during clinical scans of the brain and prostate gland.[5,6] The brain is ideal for MRS due to its relative lack of motion, and its comparatively high concentrations of metabolites that become altered in cancer, ischemia, and neurodegenerative disease. MRS is based on chemical shift, whereby the microenvironment

of $^1$H spins causes a small change in their spin frequency, expressed in parts-per-million (ppm). This frequency information is used to generate metabolite maps with spectra corresponding to various volume elements, or voxels.

## 2.2. Study of non-$^1$H nuclei at thermodynamic equilibrium

Of potential MR-observable nuclei, only $^1$H is currently used in clinical practice. Several features of $^1$H make it the ideal nucleus for MRI/MRS at thermodynamic equilibrium. These include (1) high natural abundance, (2) high concentration in the body, (3) large gyromagnetic ratio ($\gamma$), (4) short $T_1$ relaxation, and (5) presence in several metabolites that are relevant to human disease.

In contrast, other nuclei found in biomolecules, *e.g.*, the MR-active isotopes of carbon, oxygen, and nitrogen, are difficult to observe at thermodynamic equilibrium. Despite various shortcomings, several non-$^1$H nuclei have been used for MRS in man. $^{31}$P has been studied *in vivo*, with an emphasis on high-energy metabolites and lipid metabolism.[7–9] $^{23}$Na has been used to image sodium throughout the body, mostly focusing on the brain to assess changes with stroke and neurodegenerative disease.[10,11] While $^1$H, $^{23}$Na and $^{31}$P MRS studies have focused on endogenous nuclei, several other nuclei have been investigated following long infusions of small molecules containing MR-active nuclei. These include $^2$H, $^{19}$F and $^{13}$C. For example, following administration of [2-$^{13}$C] glucose and using low-power stochastic decoupling on a modified clinical 3 T scanner, incorporation of the label into glutamine, glutamate, aspartate, gamma-aminobutyric acid, and *N*-acetylaspartate was observed in the human brain.[12] In a separate study, [1-$^{13}$C] glucose and [6,6-$^2$H$_2$] were used to measure glucose metabolism in humans by assaying biofluids.[13] $^{19}$F studies have focused on the metabolism of fluorinated drugs.[14] The basic properties of nuclei studied at thermal equilibrium are presented in Table 1.

Clinical translation of non-$^1$H nuclear imaging has proved difficult. For these nuclei, a lower gyromagnetic ratio ($\gamma$) results in the need for extensive signal averaging; hence the necessity of utilizing species with short $T_1$ relaxation times. In nuclei that exhibit long $T_1$ relaxation times, signals are not fully relaxed upon acquisition and must be corrected, further impacting sensitivity. Typically, methyl carbons (*i.e.*, the methyl moiety of $^{13}$C lactate) are used for *in vivo* $^{13}$C spectroscopy, as they have shorter $T_1$'s.[15] Unfortunately, $^{13}$C nuclei typically have directly attached protons, leading to *J*-coupling and resonance splitting. When used in *ex vivo* MRS, $^1$H decoupling may be implemented, but this can be problematic for *in vivo* use. $T_2$ relaxation times can also negatively affect the ability to image certain nuclei, with acquisition times heavily dependent on transverse magnetization decay. For example, in the case of $^{31}$P, short $T_2$ relaxation times lead to broad spectroscopic lines and make it difficult to implement spectroscopic imaging sequences.[16] As will be subsequently discussed, the dissolution-DNP technique has emerged as a way to increase the MR signal for $^{13}$C and $^{15}$N, affording the needed signal enhancement for *in vivo* studies.

## 2.3. Enhancing the MR signal using DNP

The use of non-$^1$H nuclei in MRS, in particular $^{13}$C, has been partially motivated by the limited chemical shift range ($\delta \approx 10$ ppm) of metabolites of interest in the $^1$H spectrum.[17]

Deconvolution of the many metabolite resonances in the $^1$H spectrum is difficult. Additionally, strong signals from $^1$H's of water and lipids, relative to those of relevant metabolites, overwhelm the spectrum and are difficult to suppress.[18–20] Several strategies have been employed to overcome these limitations, including outer-voxel suppression, spectral editing techniques, and 2D-MRS. In the latter experiments, coherence transfer between *J*-coupled spins or *J*-coupling induced phase differences can be used to "uncover" nuclei of interest in a second frequency dimension.[21–23] These methods are commonly applied to *in vitro* NMR, but are relatively new to *in vivo* imaging and have been facilitated by the proliferation of high field-strength magnets (3 T and 7 T).

In contrast to the crowded $^1$H spectrum, peaks corresponding to $^{13}$C metabolites of interest occur over a much larger range, approximately 200 ppm. However, as previously mentioned, $^{13}$C applications *in vivo* have been limited by both nuclear features and the low concentrations of interrogated metabolites. The natural abundance of $^{13}$C, the NMR-active isotope, is only 1.1%. In addition, the gyromagnetic ratio ($\gamma$) of $^{13}$C is only 1/4 that of $^1$H, which further limits sensitivity. Finally, in contrast to water (60–70% of the human body), in which the concentration of $^1$H is approximately 110 M, the most concentrated metabolites (for example, ascorbate and lactate) are present in the mM range *in vivo*. Accordingly, MRI/MRS of endogenous $^{13}$C is not possible at reasonable imaging times.

Fortunately, HP MR has recently emerged as a way to dramatically improve sensitivity, with signal enhancements in solution routinely observed on the order of $10^4$ for a variety of small molecules. Both percent polarizations and signal enhancements are reported in the literature, with the latter term depending on field strength. For example, a $^{13}$C nucleus HP to 30% and studied at 3 T may be compared with its thermodynamic polarization at this field strength, namely 2.47 ppm. The corresponding enhancement factor would be $0.3/2.47 \times 10^{-6}$ or roughly $10^5$. In addition to $^{13}$C (the focus of this review), several other long $T_1$ nuclei have been polarized using the DNP technique, including $^{15}$N, $^{29}$Si, $^{89}$Y, and $^{129}$Xe, with potential applications in biomedical imaging (Table 2).[24–31] The PASADENA technique has also been used to polarize $^{13}$C metabolites of interest.[32–34] While the PASADENA method has the benefit of rapid polarization times, the DNP technique has the advantage of being applicable to a broad range of chemistries and metabolites, as will be discussed shortly.

## 2.4. Categories of $^{13}$C DNP probes

HP $^{13}$C agents can be divided into three categories according their discrete utilities: (1) endogenous molecules, modified only by $^{13}$C or $^2$H enrichment, (2) environmental sensors, and (3) molecules that interrogate and expand the reach of DNP-NMR as an imaging technique.

HP [1-$^{13}$C] pyruvate and [1,4-$^{13}$C$_2$] fumarate are examples of probes in the first category, used to follow basic biochemistry with many potential applications in oncologic imaging (REF). For this set of agents, the principal question is what the HP data reveals about flux through metabolic pathways, and how this information might help us better understand and treat disease. The second category of DNP agents may be non-endogenous and include [2-$^{13}$C] benzoylformic acid and [$^{13}$C,D$_3$]-*p*-anisidine (used to detect reactive oxygen species), $^{13}$C HCO$_3^-$ (used to interrogate pH) and salicylic acid (used to detect hydrophobic

binding *in vitro*).[35–38] These may also be applied to biologic problems, but the emphasis here is detecting chemical environment, usually by a reaction-based mechanism. The final category of $^{13}C$ probes includes many that are critical in advancing and understanding DNP-NMR technology. For example, $[2,3-^{13}C_2]$ diacetyl has been used to study spin polarization in the singlet state, allowing retention of HP signal beyond that dictated by $T_1$.[39] Modification of substrates by HP $[1,1'-^{13}C_2]$ acetic anhydride has demonstrated the transfer of hyperpolarization by chemical means,[40] while HP styrene has allowed direct visualization of living anionic intermediates during polarization.[41] For this last set of probes, the main emphasis is identifying special properties of DNP-NMR, and ways the technology itself can expand.

## 2.5. Mechanics of the dissolution-DNP experiment

The physics of DNP are beyond the scope of this review and are discussed elsewhere.[42] The DNP phenomenon, namely that the heating of one spin system could lead to cooling of another, was described as early as 1953 by Overhauser.[43] Solid-state experiments at low temperatures showed that high electron polarizations could be transferred, in part, to nuclear spins by microwave irradiation, at frequencies close to the resonance frequency of the electron spin. As early as the 1974, de Boer demonstrated that through thermal contact between nuclear and electronic spins, dynamic nuclear polarization is produced.[44] Hyperpolarization can occur by three main mechanisms: the solid effect, Overhauser enhancement, and thermal mixing. The mechanism requires the presence of unpaired electrons, which can be accomplished *via* addition of an electron paramagnetic agent (EPA), often an organic free radical. The choice of this radical and in turn its electron spin resonance (ESR) linewidth is indicative of the major mechanism used to achieve hyperpolarization. Very high polarizations (up to 50%) have been reported for $^{13}C$ in the solid state.[45] For applications in solution, fast heating/melting of the frozen sample (dissolution), with retention of spin polarization, was accomplished only recently by Ardenkjaer-Larsen *et al.*[2] Since this development, the field of DNP-NMR has progressed rapidly, with reports of several new MRI/MRS methods, DNP agents, and biochemical applications.

The components of a DNP sample include the MR-active nucleus of interest, an organic free radical, and a solvent that ensures homogeneous distribution of the radical, forming an amorphous solid or "glass" when frozen. In the DNP polarizer, at moderate magnetic field strength (up to 5 T) and liquid helium temperatures (1 K), electron spin polarization is at unity. Partial transfer of spin polarization is accomplished by microwave irradiation, with the solid-state polarization reaching a plateau at 1–2 hours for a typical sample. Several media have been employed for dissolution, but for biological applications an aqueous buffer is used. A chelating agent (typically ethylenedinitrotetraacetic acid, or EDTA) is often used to bind paramagnetic ions that might increase the relaxation rate. The solution is then ready for *in vitro* and *in vivo* applications, which are usually performed within 1–2 minutes following dissolution to minimize $T_1$-dependent loss of signal. For *in vivo* MR studies, special hardware is required to transmit and receive radiofrequency signals at the $^{13}C$ frequency. A dual-tuned coil is used to acquire $^1H$ anatomical imaging, for correlation

of $^{13}$C magnetic resonance spectroscopic imaging (MRSI) data with organs/tissues of interest. These components together facilitate the HP MR experiment.

Both dynamic and single time-point studies may be performed, as shown in Fig. 1. In this example, [1-$^{13}$C] pyruvate was HP and injected into a pig, with spectral data acquired from the porcine myocardium.[46] First, a dynamic experiment was conducted where a 10 cm axial slab was excited with a low flip angle (10°) pulse and a 2 s repetition time. The injection duration was approximately 15 s and the maximum HP pyruvate was also observed at this time point. HP pyruvate then underwent enzymatic conversion and its metabolic products (lactate 183 ppm, alanine 176.5 ppm and bicarbonate 161 ppm) observed as they formed in real time. This type of experiment is used to determine the timing of single time-point studies. Here the researchers chose to initiate the 3D MRSI sequence at 18 s after the start of the pyruvate injection. In this range they found relatively constant lactate and bicarbonate signals for 10–20 s. It is important to note that since this data is dynamic, the window chosen for imaging weights the ratios observed. Analysis of the 3D data shows differential metabolism to HP bicarbonate across the porcine heart, including localized bicarbonate in the myocardium as compared to the predominant pyruvate signal in the heart chamber.

*In vivo* metabolism of several HP $^{13}$C probes has been observed, as will be discussed in Section 11. In addition, many exciting *in vitro* experiments have shown the value of DNP for observing fast chemical reactions, characterizing binding in solution, and monitoring metabolism in engineered cellular systems or "bioreactors".

## 3. Considerations for DNP probe development

The prototype agent for dynamic nuclear polarization is [1-$^{13}$C] pyruvic acid, which has been used for the majority of *in vivo* studies, including a recent clinical trial in prostate cancer patients. The chemical structure of [1-$^{13}$C] pyruvic acid is shown in Fig. 2A. Pyruvic acid forms a glass as a neat liquid upon freezing, has a high concentration (14.2 M), readily dissolves several organic free radicals, and has a long spin–lattice relaxation constant ($T_1$), especially at clinically relevant magnetic field strengths (*i.e.*, 1.5 and 3 T). As discussed later, the biochemical features of this probe are also desirable, including low toxicity, rapid uptake, and fast conversion to metabolites that are readily observable by chemical shift. When designing new probes and predicting their chemical and biochemical behavior, the success of [1-$^{13}$C] pyruvic acid provides an important exemplar.

### 3.1. Identification of DNP candidates

In recent years, the pool of $^{13}$C agents for DNP has rapidly expanded, incorporating a large number of functional groups, and focusing on a broad range of physiologic processes. Although several features are considered essential for the viability of $^{13}$C DNP substrates as *in vitro* and *in vivo* agents, this review presents the versatility of DNP with respect to chemical structure. This section will also describe the basic preparation of a DNP sample, which includes an organic free radical and glass-forming solution of the $^{13}$C agent being studied. Generally, the DNP technique has been applied to small molecules (<200 Da) that contain a long $T_1$ nucleus. A large number of endogenous metabolites meet these criteria.

**3.1.1. Hyperpolarized lifetime and spin–lattice relaxation ($T_1$)**—In DNP, the critical property of a nucleus is its $T_1$, which determines its useful HP lifetime in solution. Following dissolution, 37% of the HP MR signal remains at $1T_1$, and only 5% at $3T_1$'s. For this reason, even MR studies with long $T_1$ probes are initiated within 1–2 minutes following dissolution. Dipolar coupling is the most important consideration, although the strong magnetic field dependence observed for some biomolecules indicates a significant contribution from chemical shift anisotropy (CSA), which scales with the square of the field $(B_0^2)$.[47] For $^{13}C$ nuclei in biomolecules of interest, dipolar coupling is usually with $^1H$, and depends on the number of intervening bonds.

Generally, nuclei with directly attached protons are not feasible candidates for DNP. For example, glucose is of broad interest in metabolic studies, but the $T_1$'s of the carbons are all <2 seconds.[48,49] To observe upstream glycolysis, two approaches have been used to overcome this limitation. The first is substitution of $^1H$ with $^2H$, a quadrupole nucleus (this will be discussed in detail in Section 5). The second is use of glucose surrogates, for example [2-$^{13}C$] fructose and [1-$^{13}C$] dehydroascorbate, which share several biochemical features with glucose. In both cases, both the probe and metabolite are of sufficiently long $T_1$ to observe in living systems. The structures of glucose (an aldo-sugar) and fructose (a keto-sugar) are shown in Fig. 2A. For a comprehensive discussion of magnetic dipole–dipole interactions, Levitt's text is suggested.[50]

If relaxation by dipolar coupling were the only mechanism observed, a modest increase in $T_1$ would be anticipated with increasing field strength. In fact, this is observed for [2-$^{13}C$] fructose, which exists predominantly as a hemi-ketal in aqueous solution. Also, the average $T_1$'s calculated for [U-$^{13}C_6$, $^2H_7$] glucose carbons are similar over a large magnetic field range (3–11.8 T).[49] However, for the majority of DNP substrates, a longer $T_1$ is observed at lower field strength. This is the result of chemical shift anisotropy, where circulating π-electrons cause local induced magnetic fields depending on their orientation with respect to the external field. This effect is expected in alkenes, carbonyls, and aromatic species. Since the majority of compounds polarized by DNP are carbonyls, higher field strength generally results in a lower $T_1$, sometimes significantly.[51,52] Therefore, the benefits of conducting DNP-NMR studies at higher field strength (increased spectral dispersion and improved SNR for $^1H$ correlative studies at thermal equilibrium) are partially offset by a reduced HP lifetime. Several $^{13}C$ probes have been HP and studied at varying field strengths (Table 3).

Dedicated studies have been performed to investigate the dependence of $T_1$ on magnetic-field strength for $^{13}C$ compounds. The $T_1$ dispersion of [1-$^{13}C$] acetate was measured by shuttling the sample in and out of an NMR spectrometer, with the local field determined by the fringe field of the magnet.[53] For this study, the spin–lattice relaxation rates ($1/T_1$) of [1-$^{13}C$] acetate in $D_2O$ were measured from 2 mT to 18.8 T (most state-of-the-art clinical MR scanners are 1.5–3.0 T), with and without the presence of TEMPO radical. The results demonstrate relaxation due to intra-molecular dipolar effects, chemical shift anisotropy, and presence of the paramagnetic species. Significantly, long $T_1$'s are identified in the clinically-relevant range, with higher relaxation rates observed at both very low and high fields. High fields (up to 14 T) are often employed for *in vitro* and preclinical (animal) studies,[54] while

low fields are experienced by HP samples during transfer from the DNP apparatus to the magnet.

These results confirming the dependent relationship of $T_1$ on magnetic-field strength were tested using an alternate method, employing HP [1-$^{13}$C] pyruvate with a fast field-cycling relaxometer, at relaxation fields varying between 0.237 mT and 0.705 T.[55] The authors investigated these low-field $T_1$'s since the magnetic field surrounding the DNP apparatus is normally near or at the earth's field. [1-$^{13}$C] pyruvate was polarized by DNP, and dissolved in aqueous pH 7.8 buffer at a concentration of 80 mM, which is similar to the concentration employed in preclinical *in vivo* studies. The authors found that the relaxation time for the C1 nucleus was approximately 46.9 s at the earth's magnetic field (0.05 mT) compared to 65 s at 3 T, suggesting the utility of a "holding field" through which the HP solution could be transferred following dissolution to avoid loss of sample magnetization.

**3.1.2. Molecular size**—Small molecules are usually employed in DNP given (1) ease of synthesis (2) high aqueous solubility and (3) relevance in fast metabolism. In addition, for small molecules $T_1$ decreases as a function of the increasing correlation time ($\tau_c$) seen with increasing molecular size. This relationship is described in Fig. 3, and was investigated using HP $^{13}$C MR spectroscopy in a series of *N*-acetylated glycine peptides (glycine, diglycine and triglycine).[40] This study showed a significant reduction in $T_1$ with increasing molecular weight, for similar chemical structures. Therefore, it is not surprising that the highest reported DNP enhancements are for small molecules (the molecular weight of pyruvic acid is 88 Da).

At high molecular weights, as seen in polymers and larger proteins, the opposite trend in $T_1$ is expected. Recently, solution NMR of HP polypeptides was described, for both a short peptide (bacitracin A) and full-length protein (L23).[56] This technique required both $^{13}$C enrichment and partial deuterium substitution, to minimize loss of $T_1$ due to dipolar coupling. Bacterial cultures were grown in media containing $^{13}$C$_6$-glucose and 80% D$_2$O, leading to approximately 50% total fractional enrichment. Samples were then prepared by the usual technique, in 60% (v/v) ethylene glycol/D$_2$O. While the signal enhancements obtained were modest (300 to 2000-fold), solution spectra (including both carbonyl and aliphatic groups) were obtained in a single scan, in a L23 sample at only 15 μM. These findings suggest the potential to reduce the long experiment times of protein NMR in solution. In addition, DNP-NMR may be particularly well suited to studying transient processes in protein samples, such as ligand binding or folding. One potential limitation on DNP-enhanced protein studies is the relatively harsh conditions of current dissolution methods, and ensuring the structural integrity of these macromolecules would be important. Hilty *et al.* have also described a rapid sample injection device, which minimizes loss of signal during transfer of the HP sample to the magnet.[57] In the context of the observed apparent relaxation times of 1.3–5.1 s, this innovation is particularly relevant.

**3.1.3. Toxicity in living systems**—The concentrations of agents polarized using the DNP method are often quite high for *in vitro* and *in vivo* applications, in contrast to the tracer doses typically used for other metabolic imaging methods, for example PET. Clinical PET doses are quantified by radiation, with the typical dose of FDG at 10 mCi. Assuming a

specific activity of 5000 Ci per mmol for FDG,[58] this corresponds to 2 nmol. In contrast, if a typical HP [1-$^{13}$C] pyruvate dose administered to a 20 g mouse (200 μL of an 80 mM solution) were extrapolated to a 70 kg man, 0.056 mol of the agent would be given. The result is a $10^7$–$10^8$ difference in pharmacologic dose between the technologies. Therefore, toxicity is a consideration for use of HP molecules in biologic systems. For these applications, the DNP agent used is usually: (1) chemically identical, or similar to an endogenous metabolite, or (2) chemically inert. Inert substances, for example iodinated contrast media or Gd-chelates, are currently the mainstay for improving tissue contrast in clinical CT and MR scans, and are administered at fairly high doses (~500 mM in the case of Gd-chelates).[59]

Metabolically inert $^{13}$C compounds were described in some of the earliest DNP-NMR work, which used the nascent technology in angiography and catheter tracking.[60–62] More recently, these probes have been used in perfusion imaging, for example $^{13}$C urea. Urea is a natural end product of nitrogen metabolism in the human body, and one of the main components of urine. In the kidneys, urea is reabsorbed in the renal medulla and acts as an osmolyte as part of the natural water reclamation process. For HP imaging, the carbonyl of urea provides a long $T_1$ species for imaging (Fig. 2A). HP $^{13}$C urea experiments have been used to determine tissue perfusion, in both static and dynamic studies.[63] Urea has been used in conjunction with other probes as a co-polarized agent and potentially could be used to normalize for delivery in DNP studies since it is not metabolized on the time scale of the HP experiment.[64] Recent work has shown that it can also be used to measure absorption in diuresis and assess kidney function.[65] While many clinical studies employ CT and MR contrast agents, these tend to use high concentrations of iodinated contrast or Gd-chelates, which are not safe for patients with renal disease.[66,67] Thus perfusion imaging using HP $^{13}$C urea has high potential for clinical translation. Other inert DNP probes include [U-$^2$H$_9$, 2-$^{13}$C] methylpropan-2-ol[68] and (bis-1,1-(hydroxymethyl)-[1-$^{13}$C]cyclopropane-$^2$H$_8$) or HP001, the first HP agent used to study cerebral perfusion.[62]

## 3.2. Components of the DNP sample

A DNP sample preparation includes the $^{13}$C substrate to be polarized and an organic free radical in solution. This solution must form an amorphous solid on freezing, which may require the addition of a co-solvent. To increase polarization, a paramagnetic agent (often a Gd-chelate) may be used. Multiple $^{13}$C agents may be polarized simultaneously with minimal loss of polarization and $T_1$.

**3.2.1. Enriched $^{13}$C substrate**—For *in vivo* and most *in vitro* applications, the molecule is enriched in $^{13}$C at the atom of interest. Since the natural abundance of $^{13}$C is only 1.1%, this increases the observable NMR signal by at least two orders of magnitude (not accounting for $^{13}$C–$^{13}$C spin diffusion). One compelling feature of DNP-NMR is limited background signal, with a natural abundance $^{13}$C signatures (non-enriched nuclei) not generally observed in biologic applications. Several $^{13}$C-enriched metabolites and precursors are commercially available, although the cost of these DNP candidates can be prohibitively high. For this reason, natural abundance species can be used to answer critical questions regarding $T_1$ and receptor binding, prior to investing in costly enriched substrates. For

example, the binding of salicylic acid and ascorbic acid to albumin was studied *via* polarization of the natural abundance small-molecules, while the effect of hydrophobic binding on $T_1$ was analyzed by polarization of natural abundance benzoic acid and mixing with varying concentrations of β-cyclodextrin.[38,54]

**3.2.2. Organic free radical—**As discussed, the DNP mechanism requires the presence of unpaired electrons, which are often provided as an organic radical. In a typical experiment, irradiation of the electron paramagnetic resonance (EPR) spectrum of the radical with microwaves induces spin polarization transfer to the nucleus of interest. A narrow EPR line-width allows higher nuclear polarization when the line-width is larger than, or comparable to the nuclear Larmor frequency. Fig. 2B summarizes the organic radicals applied to DNP. The first, and most common radicals used for fast dissolution DNP-NMR are the trityls,[69] with several versions employed depending on the solvent used to prepare the sample. The most water-soluble, and versatile of these is OX063. Nitroxides (*e.g.*, TEMPO),[70] 1,3-bisdiphenylene-2-phenylallyl (BDPA),[71] 2,2-diphenyl-1-picryl-hydrazyl (DPPH),[72] and 2,6-di-*tert*-butyl-α-(3,5-di-*tert*-butyl-4-oxo-2,5-cyclohexadien-1-ylidene)-*p*-tolyloxy (galvinoxyl)[73] and their derivatives have also been studied. Recently, rigid biradical systems using nitroxides have been constructed (bTbk and relatives), for which large $^{13}$C enhancements were recorded; these were quite sensitive to the orientation of, and distance between, the NO moieties.[74] One of the bTbk radicals studied (bTbk-py) used tetrahydropyran groups to increase aqueous solubility, and performed well in a glycerol–water solvent matrix. Incorporation of sulfoxides and sulfones into this biradical scaffold has also been used to increase solubility.[75] Finally, mixtures of two radicals (a relative of BDPA and trityl) have been studied. Their EPR frequencies are separated by approximately the $^{13}$C nuclear Larmor frequency.[76]

**3.2.3. Solvents and glassing—**One of the requirements of DNP is formation of an amorphous solid on freezing of the $^{13}$C sample, to ensure homogeneous distribution of the radical. To accomplish this, a co-solvent such as glycerol, dimethyl sulfoxide (DMSO), or dimethylacetamide is usually added to aqueous preparations. The solvent and glassing agent are chosen to maximize the concentration of the $^{13}$C agent. A high sample molarity both enhances $^{13}$C–$^{13}$C spin diffusion during polarization, and allows a more concentrated solution following dissolution.[77] One strategy that has been used for zwitterionic compounds (*e.g.*, amino acids) at high concentrations has been to generate their corresponding sodium or chloride salts, by addition of NaOH or HCl.[78] In its present embodiment, the DNP technique is inherently dilutional, and high metabolite concentrations are needed for *in vivo* studies. Approaches to minimize the dilution of HP analytes include use of immiscible liquids for the melting and flushing of the DNP sample; this significantly reduces the amount of aqueous solvent required.[79]

Another approach to maximize $^{13}$C–$^{13}$C spin diffusion is use of enriched $^{13}$C solvents in the DNP sample.[80] [1-$^{13}$C] sodium pyruvate was dissolved in $^{13}$C-enriched DMSO, and the solution doped with the OX063 trityl radical. For this system, the authors determined that the build-up time ($\tau$) for polarization of the sample in $^{13}$C-enriched DMSO was approximately twice as fast as that observed for an identical sample using natural abundance

DMSO. However, the absolute enhancements recorded in solution were nearly identical for the two samples. These findings suggest that spin diffusion is the mechanism responsible for propagation of nuclear spin surrounding paramagnetic centers, altering the kinetics of DNP in this system, but not affecting the overall polarization magnitude. The extension of these results to other spin systems/solvents may increase the efficiency of the DNP process.

**3.2.4. Use of Gd-chelates**—A recent development is the addition of Gd-chelates to the DNP sample, which has been shown to increase polarization. $Gd^{3+}$ doping was accomplished *via* addition of gadolinium complex of 10-(2-hydroxy-propyl)-1,4,7,10-tetraazacyclododecane-1,4,7-triacetic acid (gadoteridol) to [1-$^{13}$C] pyruvic acid samples containing the OX063 trityl, 4-oxo-TEMPO, and BDPA.[81] In these experiments, the concentration of Gd-chelate was varied from 0–8 mM, with the solid-state polarization initially increasing, peaking at 1–2 mM, and decreasing with higher Gd-chelate concentrations. A 300% increase in solid-state polarization for the pyruvic acid-OX063 sample was observed following Gd-doping, *versus* only 5–20% for the other radicals. Improvement in the DNP-enhanced NMR intensity with $Gd^{3+}$ doping has been attributed to the shortening of the electronic spin–lattice relaxation time $T_{1e}$. Use of Gd-chelates to increase signal enhancements can be problematic in solution, since these paramagnetic agents may also shorten the $T_1$ of the $^{13}$C nucleus of interest, thereby limiting its observable lifetime in MR applications.[82] This is particularly important at low field strengths where the relaxivity of many lanthanide chelates is higher. Interestingly, Johannesson *et al.* observed only a modest effect on polarization when [1-$^{13}$C] pyruvate was polarized at 4.6 T with 1.5 mM Gd-chelate.[45] This finding suggests that the effect of Gd-chelates on DNP may be field-dependent, and warrants future study. Careful evaluation of these effects *in vitro* is suggested prior to considering use of Gd-chelates in biologic systems.

**3.2.5. Multi-metabolite polarization**—The chemical shift dispersion of metabolites in the $^{13}$C spectrum allows several probes and their products to be observed simultaneously, both *in vitro* and *in vivo*.[83] Multi-metabolite polarization can be accomplished with minimal effect on polarization and $T_1$. Fig. 4 depicts HP [1-$^{13}$C] pyruvate, [1,4-$C_2$] fumarate, $^{13}$C urea, and $^{13}$C bicarbonate in solution at 11.7 T. These agents could potentially be used to study lactate dehydrogenase (LDH) activity, necrosis, perfusion, and pH in the same MR imaging experiment. For several *in vivo* studies, $^{13}$C urea (or other biochemically inert agent) has been co-polarized with the metabolite of interest to determine the role of perfusion, which is often altered in angiogenic tumors.[64]

## 4. Chemical structures: carbonyls and beyond

Most $^{13}$C DNP substrates studied have been carbonyls, including carboxylic acids, ketones, esters, and amides. The classes of chemical structures polarized by DNP are summarized in Table 3. Carboxylic acids in particular are (1) abundant in endogenous molecules, (2) typically water-soluble, (3) often amenable to $^{13}$C enrichment, (4) have longer $T_1$'s, and (5) are involved directly in, or positioned near sites of biochemical modification. This last feature is critical, as most HP MR strategies rely on chemical shift to observe reactions *in vitro* and *in vivo*. The dicarbonyl structure of pyruvic acid (seen in other DNP substrates, *e.g.*, dehydroascorbic acid or benzoylformic acid) has a carboxylic acid at the 1-position and

a ketone at the 2-position, and both sites have been $^{13}C$-enriched for metabolic studies. [1-$^{13}C$] pyruvate has a long $T_1$ at clinically relevant field strengths (60 s at 3 T) due to weak dipole–dipole interactions. Its conversion to other acids, lactate, alanine, and bicarbonate is easily observed spectroscopically in a variety of biologic systems. [2-$^{13}C$] pyruvate is labeled at the adjacent ketone position and as expected has a lower $T_1$ (50 s at 3 T) due to stronger coupling with nearby spins. In biologic systems with a high rate of oxidative phosphorylation, conversion of HP [2-$^{13}C$] pyruvate to [1-$^{13}C$] citrate and [5-$^{13}C$] glutamate is observed[84] (Fig. 5).

Several $^{13}C$ esters have been polarized using the DNP technique. These may correspond to an endogenous metabolite, for example the lactone [1-$^{13}C$] dehydroascorbate employed in redox applications.[85,86] Alternatively, a non-endogenous ester that is the precursor of a metabolite of interest may be used. This is a "pro-drug" strategy that has been exploited in other imaging applications. For example, [1-$^{13}C$] ethyl pyruvate has been used to image the anesthetized rat brain, taking advantage of increased lipophilicity to cross the blood–brain barrier (BBB).[87] This agent is reasonably well-tolerated in animals, and has been shown to be neuroprotective in a cerebral ischemia model.[88] Rapid and preferential uptake into brain was shown in rats, as well as the metabolites [1-$^{13}C$] pyruvate and [1-$^{13}C$] lactate, which are formed by hydrolysis of the ethyl ester (to pyruvate and ethanol) and subsequent conversion to [1-$^{13}C$] lactate. These steps are depicted in Fig. 6. For esters, controlling the dissolution conditions is critical to avoid saponification. Hurd *et al.* used NaOH in the dissolution media to intentionally generate a combination of both [1-$^{13}C$] ethyl pyruvate and [1-$^{13}C$] pyruvate,[87] but a stable solution of the HP ester is also feasible.

Although carbonyls have dominated the DNP literature, the viability of other chemical structures has been established.[41,89] Non-carbonyl structures with sufficient $T_1$'s for DNP are common in biomolecules, and often commercially available (for example, the hemi-ketal [2-$^{13}C$] fructose).[90] One limitation is the synthetic feasibility of $^{13}C$ enrichment. For example, the tocopherol structure (vitamin E) has several carbons without directly attached protons, with potential applications to study reduction/oxidation (redox) chemistry (Fig. 7). In fact, $^{13}C$ enrichment of numerous atoms in α-tocopherol has been achieved.[91] However, synthesis of an appropriate $^{13}C$-enriched molecule at a long-$T_1$ site might prove difficult, especially at reasonable cost. Fortunately, for some applications natural abundance substrates are appropriate for DNP-NMR. Another strategy used is to increase the $T_1$ of a $^{13}C$ nucleus of interest by additional substrate enrichment. This has been accomplished by partial, or complete deuteration of molecules allowing DNP polarization of aliphatic $^{13}C$. These approaches will be further described in the following section.

## 5. Increasing $T_1$ by deuterium enrichment

Substitution of deuterium ($^2H$) into molecules for analytical study, above its natural abundance (0.0156%), has historically been used to follow chemical and biochemical reactions,[92] and to characterize molecular structure from small molecules[93] to proteins.[94] As a spin 1 nucleus, deuterium is a quadrupole and exhibits scalar coupling (*J*-coupling) with other spin 1/2 nuclei using the standard $2n + 1$ rule. The splitting pattern is then determined by the *J*-coupling constant, and in the case of $^{13}C$–$^2H$ bonds is on the order of 30 Hz. $^2H$

substitution of exchangeable protons permits exchange experiments in different solvent systems, providing a means to study the rates of these phenomena. More frequently, $^2H$ enrichment is performed at non-exchangeable sites, so $^2H$ can be followed through chemical and or biochemical conversions.

While HP MR affords a huge signal-to-noise ratio (SNR) increase, the lifetime of this signal is determined by the apparent $T_1$ relaxation rate of the nucleus of interest. One strategy for increasing the $T_1$ is to design chemical systems that are devoid of neighboring spin 1/2 nuclei, such as carboxylate carbons. Another viable approach is the replacement of directly attached, or 2-bond spin 1/2 nuclei with deuterium. This has been used in multiple HP probes and has resulted in a dramatically increased $T_1$ in some cases. It is important to note that the effect of deuterium substitution on $T_1$ is a function of the coupling of the $^1H$ it replaces, and in the context of stronger coupling can have a greater effect. Although the replacement of directly-bonded (strongly $J$-coupled) protons with $^2H$ would be expected to have the highest impact on $T_1$, in this case $^2H$ substitution also leads to splitting. This, in turn, can decrease overall SNR when moving to field strengths where $J$ is large relative to $\omega$. For long-range protons (>1 bond, weakly $J$-coupled), substitution with $^2H$ has a modest effect on $T_1$, and no observable splitting.

In addition to splitting of the $^{13}C$ resonance of interest, $^2H$ substitution also has a significant impact on metabolism in biologic symptoms due to the kinetic isotope effect, which has been considered in the context of HP $^{13}C$ studies.[95] The isotope effect may be primary or secondary. The primary isotope effect describes rate differences when the isotopic enrichment is in a chemical bond that is formed or broken in the rate-limiting step of a reaction.[96] In contrast, the secondary isotope effect describes rate differences observed when the isotopic substitution is remote from this bond. For the primary isotope effect, the heavier atom results in a higher activation energy for bond cleavage, lowering the measured reaction rate. In the latter case, electronic effects such as induction and hyperconjugation change the vibrational frequency of a remote chemical bond.[97–99] Rarely, a deuterated molecule will react faster than its $^1H$ analog.[100] The $^2H$-enriched metabolites evaluated by DNP-NMR are expected to (1) be dominated by the primary isotope effect, and (2) react more slowly than their $^1H$ counterparts. Of note, isotopic rate changes are most pronounced when the mass change is greatest. Substitution of $^1H$ by $^2H$ represents a doubling of mass, *versus* the 8% increase when $^{12}C$ is replaced by $^{13}C$. Therefore $^{13}C$ enrichment should not significantly impact the rate of biochemical reactions.

The kinetic isotope effect may impact the ability to observe certain deuterated $^{13}C$ metabolites by DNP-NMR. In some cases, $^2H$ substitution may retard the rate of metabolite formation. Alternatively, the isotope effect may actually aid in metabolite accumulation, if the rate of its subsequent conversion is decreased. The isotope effect may be partially responsible for the observation of dihydroxyacetone phosphate (DHAP) following metabolism of HP [U-$^{13}C$, U-$^2H$] glucose in yeast.[101] In glycolysis, fructose-bisphosphate aldolase splits the diphospho-hexose (fructose 1,6-bisphosphate, F1,6P) into two triose sugars, DHAP and glyceraldehyde 3-phosphate (GA3P). GA3P is predominantly taken downstream in glycolysis and the enzyme triosephosphate isomerase (TPI) catalyzes the rapid interconversion of DHAP and GA3P. Deuterium substitution in [1(R)-$^2H$] DHAP

leads to a 2.9 times smaller $k_{cat}$ for TPI,[102] *versus* natural abundance DHAP. If the isotope effect is partially responsible for the HP DHAP signal observed in yeast, $^2H$ substitution might be viewed as a kinetic "trapping" mechanism not unlike strategies commonly employed in PET.[103]

## 5.1. HP [2-$^{13}$C, 2-$^2$H$_4$] choline

One of the first HP molecules to be investigated as a deuterated species was $^{15}N$ enriched choline. Choline has been a staple of *in vivo* $^1H$ MRSI investigation as its MR signature is seen in a wide range of cancers,[104] and is readily visualized *in vivo* due to the sensitivity afforded it by 9 magnetically equivalent protons. For HP applications, both $^{15}N$ and $^{13}C$ enriched versions of the molecule have been studied. Enrichment with $^{15}N$ is particularly attractive, since the $^{15}N$ of the trimethylamine choline head group has a $T_1$ on the order of 200 s. The $J(^{15}N,^1H)$ is approximately 0.8 Hz and when substituted with $^2H$, the [1-$^{15}$N, $^2$H$_9$] choline has a $T_1$ of approximately 390 s split into a triplet, since all 9 deuteriums are equivalent.[105] *In vivo* applications of this molecule have been hindered by a small chemical shift difference to its products, including phosphocholine ($\delta_{15N}$ = 43.6 ppm, $\delta \approx 0.2$ ppm) and its relative toxicity, with the LD$_{50}$ of intravenous choline chloride reported as 53 mg kg$^{-1}$ body weight.[106] Given this extremely long $T_1$, the deuterated tri-methylamine of choline could play a role as a reporter molecule when integrated into other HP probe systems. Recent work has attempted to use the $^{13}C$ labeled and deuterated side chain moieties of choline, [2-$^{13}$C, 2-$^2$H$_4$] choline.[107] While it exhibits a relatively long carbon $T_1$ relaxation time (Table 3), a complex deuterium coupling pattern may limit its utility.

## 5.2. HP [2-$^{13}$C, U-$^2$H] fructose

For the hemi-ketal carbon of fructose, polarized resonances are observed for each of the predominant 5 and 6 membered ring forms (Fig. 8).[90] These have similar $T_1$ relaxation rates and polarizations since they are in fast isomeric exchange in solution. Additionally, these resonances are all approximately singlets since the long range $J$-coupling through the ring is small as compared with typical one bond C–H coupling constants. When all exchangeable protons of the fructose molecule are substituted for $^2H$, the $T_1$ relaxation time increases more than 2-fold at 11.7 T, from 16 to 34 s. Although the $T_1$ increases, importantly, the carbon resonances remain approximately singlets, even at high field, since the $J$-coupling constant to the ring deuterons is small.

Given the presumed role of fructose in diabetes,[108] fatty liver disease,[109] and certain forms of cancer,[110] HP [2-$^{13}$C] fructose holds strong potential for clinical translation, especially with the enhanced $T_1$ observed for the deuterated species. A study in the transgenic adenocarcinoma of the mouse prostate (TRAMP) model suggested increased phosphorylation of HP [2-$^{13}$C] fructose to [2-$^{13}$C] fructose-6P, although *in vivo* results were limited by inadequate chemical shift separation between the two metabolites.[90] In yeast, several metabolites were seen following application of [2-$^{13}$C] fructose, including [2-$^{13}$C] dihydroxyacetone phosphate (DHAP) as well as signals arising from anabolic reactions, corresponding to [2-$^{13}$C] glucose-6P and [5-$^{13}$C] fructose-1,6BP.[101] Glucose-6P is formed from fructose-6P by the activity of phosphofructose isomerase, while [5-$^{13}$C] fructose-1,6BP

results from the aldol condensation of DHAP with [2-$^{13}$C] glyceraldehyde-3P. The detection of these metabolites in relevant cell-lines and animal models has not been reported, but should be facilitated by partial or complete deuteration of the $^{13}$C species.

## 5.3. HP [U-$^{13}$C, U-$^2$H] glucose

As highlighted by the widespread clinical use of $^{18}$F-FDG, glucose is of great interest in metabolic imaging, particularly for cancer. However, its lack of long $T_1$ carbons limits HP MR applications.[48,49] Substitution of the non-exchangeable protons with $^2$H significantly increases $T_1$ of glucose carbons for [U-$^{13}$C, U-$^2$H] glucose, reported as approximately 12 s for $^{13}$C$_{1-5}$ and 10 s for $^{13}$C$_6$.[101] Allouche-Arnon *et al.* have also studied the effect of concentration, magnetic field, and variable enrichment on $T_1$.[111] A large polarization (approximately 25%) was obtained for this probe using the DNP technique. Several recent studies have examined the *in vitro* metabolism of [U-$^{13}$C, U-$^2$H] glucose, in living yeast (*Saccharomyces cerevisiae*), as well as bacteria (*Escherichia coli*).[95,101] In addition, the role of sulfur(IV) compounds (generally referred to as "sulfites") in glycolytic inhibition has been explored.[112] These experiments were remarkable for several reasons. First, a very large number of metabolites were observed, due to the high glycolytic activity of these organisms, and careful experimental design. Following administration of the HP [U-$^{13}$C, U-$^2$H] glucose dietary substrate, metabolism could be followed along entire metabolic pathways with accumulation of the corresponding end-products. The relevant metabolic pathways are summarized in Fig. 9. For *Saccharomyces cerevisiae*, these end-products were primarily ethanol and CO$_2$. Interestingly, the delay between CO$_2$ and HCO$_3^-$ formation was resolved in this system, which was not seen *in vivo* by Gallagher *et al.*, due to the high activity of carbonic anhydrase in animals.[37] For *Escherichia coli*, significant flux through pyruvate dehydrogenase (PDH) was observed with decarboxylation of pyruvate to acetyl-CoA, followed by formation of acetate. In addition, a significant resonance representing formate was seen, representing the activity of pyruvate formate lyase, which converts pyruvate to formate by a radical mechanism.[113]

Several other resonances were more characteristic of metabolism in mammals. These included fructose 1,6-bisphosphate, the aldolase products of DHAP and glyceraldehyde 3-phosphate (GA3P), phosphoenolpyruvic acid (PEP). The metabolites most familiar to DNP researchers were also seen, *i.e.*, lactate, pyruvate and alanine. Finally, the resonances of the pentose phosphate shunt 6-phosphogluconate (6-PG) and ribulose 5-phopshate were observed.

These studies were also remarkable for the resonances that were not seen. It is surprising that fructose 6-phosphate was not observed, given that its subsequent conversion by phosphofructokinase is one of the most tightly regulated steps of glycolysis.[114] Phosphofructokinase may have not been significantly inhibited under the experimental conditions, or the resonance of fructose 6-phosphate may overlap with that of fructose 1,6-bisphosphate. In other cases, it appears likely that glycolytic intermediates were not observed due to fast turnover. For example, 1,3-bisphosphoglycerate (1,3BPG), 3-phosphoglycerate (3PG) and 2-phosphoglycerate (2PG) were not detected, which may be secondary to the high activities of glyceraldehyde-3-phopsphate dehydrogenase (GAPDH),

phosphoglycerate kinase (PGK), and phosphoglycerate mutase (PGM) respectively.[115] Furthermore, in *Saccharomyces cerevisiae* although ethanol was readily seen, its direct precursor acetaldehyde was not. This finding is consistent with rapid flux through alcohol dehydrogenase (ADH).

Careful isotopic enrichment of glucose may allow further delineation of these pathways, and promote clinical translation of $^{13}C$-enriched glucose. Despite the dramatic results achieved with [U-$^{13}C$, U-$^{2}H$] glucose *in vitro*, a universally $^{13}C$-labeled, perdeuterated analog is not ideal for several reasons. First, the isotope effect will affect the rate of biochemical reactions, most dramatically when a bond to $^{2}H$ is broken or formed. Second, the complex *J*-coupling observed confounds the spectrum and limits SNR. Finally, the $T_1$ of $^{13}C$ nuclei may be reduced by dipolar interactions with adjacent $^{13}C$ nuclei. This was explicitly studied by comparing the $T_1$'s of [U-$^{13}C$, U-$^{2}H$] glucose carbons to those of [U-$^{2}H$] glucose.[49] In the natural abundance case, for which the probability of a given position being occupied by $^{13}C$ is 1.1%, the probability of adjacent $^{13}C$–$^{13}C$ nuclei is negligible. The $T_1$'s recorded for [U-$^{2}H$] glucose were 12.2 ± 1.3 s, *versus* 8.9 ± 1.4 s for [U-$^{13}C$, U-$^{2}H$] glucose. As applications for $^{13}C$ glucose continue to emerge, $^{2}H$ and $^{13}C$ substitution can be tailored to the specific pathway under investigation.

### 5.4. HP [5-$^{13}C$, 4-$^{2}H_2$] glutamine

Growing interest in glutaminolysis, as well as the role of 2-hydroxygluterate (2HG) in cancer metabolism, has sparked the need to develop noninvasive imaging markers for the rate of glutamine uptake and metabolism.[116,117] In the first demonstrations of HP glutamine, although the relaxation time of the C1 carbon was substantially longer than that of the C5 (Table 3), the chemical shift change of the C5 when converted to glutamate was large enough ( $\delta \approx 3.4$ ppm) to permit observation of the conversion.[118] The relaxation rates of both glutamine and glutamate may hinder their translation and recent work has investigated the synthesis of partially deuterated glutamine.[119] [5-$^{13}C$, 4-$^{2}H_2$] glutamine has been produced in a 7-step synthetic scheme with the resulting $T_1$ nearly 2-fold longer for the C5. Hyperpolarization of the partially deuterated probe permitted the visualization of real-time generation of deuterated HP glutamate in brain tumor cells. As with fructose, while the C5 carbon of glutamine has no directly attached protons, elimination of the long range *J*-coupling permits a dramatic lengthening of the carbonyl $T_1$.

### 5.5. HP [3-$^{13}C$, $^{2}H_3$] pyruvate

The vast majority of DNP studies employ [1-$^{13}C$] pyruvate, although there is increased interest in [2-$^{13}C$] pyruvate allowing detection of downstream metabolites in the mitochondria. Since the C3 carbon is protonated, its $T_1$ is much shorter making [3-$^{13}C$] pyruvate suitable for metabolic studies at thermodynamic equilibrium, but not DNP applications. Recently, [3-$^{13}C$, $^{2}H_3$] pyruvate was synthesized by chemical exchange in $D_2O$/ammonium carbonate and polarized by the usual method.[120] Following incubation with alanine transaminase [ALT] and glutamate, direct detection of $^{13}C$-β-L-alanine was observed, with SNR comparing favorably with that obtained for $^{13}C$-α-L-alanine seen in the [2-$^{13}C$] pyruvate case. ALT-catalyzed D/H exchange at the alanine methyl group was also noted.

### 5.6. Other deuterated species for DNP

As discussed, the DNP technique has been used to rapidly obtain $^{13}C$ spectra for large polypeptides and proteins that were partially deuterated.[56] Secondary polarization of amino acids and short polypeptides (*e.g.*, Arg-Gly-Asp or "RGD") has also been performed by acylation of their N-termini using $[1,1'-^{13}C_2, {}^2H_6]$ acetic anhydride, which resulted in significantly longer $T_1$'s than those obtained for the $^1H$ electrophile.[121] Recently, $^{29}Si$ has emerged as an attractive nucleus for DNP applications, and controlled incorporation of deuterons was shown to dramatically increase sensitivity in a series of organosilica materials that contain surface propylazide fragments.[122] Both $[^2H_9]$-TMS and $[^2H_3]$-methoxy groups were used to coat the silica surface, resulting in significantly larger $T_1$'s determined by both direct acquisition and cross-polarization. For perfusion imaging, both HP001 and perdeuterated $^{13}C$ 2-methylpropan-2-ol have incorporated deuterium to lengthen $T_1$.[68,123,124] As discussed in the next section, $[^{13}C, {}^2H_3]$-*p*-anisidine was developed to target hypochlorous acid (HOCl), employing a long-lived deuterated methoxy group.[125]

## 6. Beyond $T_1$-the singlet state

Another approach to extend HP spin lifetimes in solution includes conversion of HP magnetization into nuclear singlet order, where many relaxation mechanisms do not apply. Conceptually, this approach steps between symmetry and asymmetry. In the case of a symmetric molecule with 2 adjacent spin 1/2 nuclei, the singlet and triplet states are disconnected. This allows the singlet state to experience dramatically reduced relaxation, but it is difficult to populate and also observe. In the asymmetric case, the triplet and singlet states are connected, but a long-lived singlet state is difficult to maintain. Accessing the singlet state has been achieved *via* field cycling, continuous irradiation, and chemical modification,[39] although these are not readily feasible for *in vivo* imaging. Recently, a pulse sequence has been designed to populate the singlet state in a symmetric molecule, which also contains couplings that break magnetic equivalence.[126] In all cases a preparation is necessary to put the spins in the singlet state, typically labeled as M2S, followed by a time-reversed S2M sequence to bring the magnetization back into the triplet state to observe.

Pileio *et al.* reported a method for converting magnetization into singlet order and back again, that is compatible with the DNP technique.[127] The authors used a $^{15}N$-labelled nitrous oxide ($N_2O$) spin system; audio-frequency pulse trains were used to temporarily store magnetization as low-field singlet order. The decay measured outside the NMR magnet beyond 500 s had a constant of $25 \pm 3$ minutes, which is an order of magnitude larger than the conventional $T_1$'s for the $^{15}N$ nuclei. This method may be applied to molecules containing two spin-1/2 nuclei, which can exist as singlet and triplet nuclear spin isomers, and has been extended to $^{13}C$ molecules on a hardware setup typical of *in vivo* dissolution-DNP.[128] A sample of cyclohexyl-isopropyl-1,2-$^{13}C_2$-oxalate-$^2H_{18}$ (Fig. 2A) was HP by the usual method and MRI experiments were conducted on a 4.7 T preclinical horizontal bore scanner. When HP magnetization was converted into the singlet order, the resulting decay of MR signals (at later times) were fit to an exponential time constant of $77 \pm 12$ s, *versus* a measured time constant $T_1$ of $54 \pm 2$ s by conventional $T_1$ measurement at this field strength. Although only a modest improvement, this work demonstrated the ability to extend HP

signal lifetimes beyond those dictated by $T_1$. This was achieved using a molecule in which the two $^{13}C$ spins are highly coupled, having a spin-spin scalar coupling constant greater than the shielding-dependent frequency difference between the nuclei. However, as the authors describe, to access the singlet order a chemical shift difference between the two nuclei is required.

Storage of singlet magnetization has been extended further by incorporating singlet-friendly species into potential substrates of interest. Feng *et al.* demonstrate that for a molecule such as diethyl oxalate-$^{13}C_2$, $^{13}C$ labeled at the C2 and C3 positions, a duality of symmetries can be created for singlet storage.[126] In this scenario, the $^{13}C$ and $^1H$ pairs are symmetric around the same inversion center, with a singlet–singlet state (SS, with no dipole-allowed transitions to other states) and an additional triple–triplet state (TT). In this 4 spin system (AA′XX′), with the appropriate scalar couplings, the SS and TT states can communicate, allowing for storage from the TT to the SS. Taking advantage of this may provide a means of incorporating singlet state storage moieties into molecules of interest for hyperpolarization. In its current form, the technique is applicable to a limited class of chemical structures, and its relevance in biologic systems remains to be seen.

## 7. Observing fast chemistry by DNP-NMR

The marked MR signal enhancement afforded by DNP (up to $10^5$) has allowed observation of fundamental chemistry and biochemistry both *in vitro* and *in vivo*. Due to $T_1$-dependent signal decay of the HP $^{13}C$ signals, DNP-NMR is well-suited to the study of fast chemical reactions, and transient/dynamic molecular interactions. Chemical reactions that have been studied *in vitro* include polymerization, acetylation, oxidation, reduction, hydration/ dehydration, and acid–base. Binding in aqueous solution has also been studied by DNP-NMR, using the $T_1$-mediated loss of HP ligand signal seen with receptor binding. These methods are amenable to studying relatively weak interactions at high SNR and short experiment times, and may be useful for both drug discovery and *in vivo* imaging.

### 7.1. Hydration/dehydration

The most well-known reaction to a chemist studying HP [1-$^{13}C$] pyruvate is its reversible hydration at the 2-position, which is both temperature and pH-dependent.[124] Higher percentages of the hydrate exist when pH < p$K_a$ (2.2 for pyruvic acid), with lower percentages seen on the basic side. The rates of hydration and dehydration of pyruvate have been calculated with a broad range of catalysts. At near-physiologic pH, pH > p$K_a$ and the hydrate is <8%. The nonmetabolically-active HP $^{13}C$ pyruvate hydrate is readily observed in HP [1-$^{13}C$] pyruvate MR studies, as a resonance approximately 8 ppm downfield from the dominant keto resonance. For pyruvate esters, *e.g.*, ethyl pyruvate used in HP $^{13}C$ brain studies, the predominant form in water is the hydrated species.[87]

The hydration of $CO_2$ to carbonic acid, and subsequent deprotonation to bicarbonate may also be interrogated using HP DNP-NMR, as well as the reverse reactions.[37,129] As discussed further in Section 8 (Essential Biochemistry of DNP), HP $^{13}C$ bicarbonate may be used to determine the pH of a solution, by integrating the $^{13}C$ bicarbonate and $^{13}C$ $CO_2$ resonances and employing the Henderson–Hasselbalch equation. This exchange is rapid

even without catalysis by carbonic anhydrase, with the rate constant describing the flux between bicarbonate and $CO_2$ in solution estimated as 0.1 $s^{-1}$ using magnetization transfer methods.[37]

## 7.2. Oxidation

Reactive oxygen species (ROS) are implicated in a variety of diseases, including cancer, reperfusion injury, and neurodegeneration. Recent studies have also suggested a positive role for ROS in normal cell-signaling, mediated by the NADPH oxidase (NOX) enzymes.[130] A reaction-based approach was developed to detect $H_2O_2$ based on its oxidation of an α-ketoacid ($^{13}C$-benzoyl-formic acid or BFA) to a carboxylic acid ($^{13}C$-benzoic acid), readily observable by chemical shift[35] (Fig. 10). The oxidative decarboxylation of BFA was also shown to be relatively selective for $H_2O_2$ over other relevant ROS, for example $O_2^-$, NO, and hydroxyl radical using analytical HPLC. The reactivity of BFA towards $H_2O_2$ is easily manipulated by ring-substituents, potentially facilitating next-generation probes for *in vivo* use.

More recently, a deuterated DNP probe was developed to target hypochlorous acid (HOCl),[125] an oxidizer that reacts with a large range of biomolecules *in vivo*. The chemical structure of $[^{13}C, ^2H_3]$-*p*-anisidine (Fig. 11) incorporates a fully deuterated $^{13}C$ methoxy group. The basic mechanism of this probe is an alkoxy/aryloxy to alcohol conversion that has been used in a variety of environment-responsive chemical pro-drugs.[131] Therefore, the deuterated methoxy group may find a number of interesting applications, in the development of probes that interrogate ROS, pH, or a specific enzyme activity. In each case the liberated $^{13}C$ product would be $CD_3OH$, which has been reported to have a $T_1$ of 32.9 s at 9.4 T. The reaction of $[^{13}C,D_3]$-*p*-anisidine with HOCl demonstrates the formation of $CD_3OH$ in the HP spectrum. This exciting result suggests that other long-$T_1$ moieties might be employed in a similar fashion in HP chemical sensors. Practical considerations for *in vivo* applications, such as bio-orthogonality, sensitivity, and toxicity warrant further study.

## 7.3. Reduction

HP $[1-^{13}C]$ dehydroascorbate (DHA), the oxidized form of vitamin C (VitC), has recently been developed as an endogenous redox sensor. The direct chemical reduction of HP $[1-^{13}C]$ DHA has been studied *in vitro*, using the water-soluble reducing agents $NaBH_3CN$ and reduced glutathione.[85,86] In both cases, conversion to HP $[1-^{13}C]$ VitC depended on the concentration of the reducing agent. Interestingly, when $NaBH_3CN$ was added to a solution of HP $[1-^{13}C]$ DHA (1 major peak), several resonances were observed in the dynamic HP spectra. Following the DNP-NMR experiment, a spectrum at thermodynamic equilibrium was obtained revealing only the reduced VitC species (1 peak). Therefore, it is unclear what the multiple additional resonances observed in the HP spectra represent. Possibilities include semidehydroascorbate, the radical anion formed by a one-electron reduction, or tautomers of vitamin C, corresponding to transient species seen following reduction at the 2 or 3-positions.

### 7.4. Acetylation

Near quantitative acetylation of primary amines by HP [1,1-$^{13}$C] acetic anhydride has been employed to transfer polarization to a biomolecule of interest by chemical means.[40] This technique may be useful to (1) interrogate nucleophile-rich biofluids of interest (*e.g.*, cerebrospinal fluid [CSF], urine) with high SNR, and (2) polarize substrates that are not amenable to direct polarization, either due to crystalline properties in solution or high molecular weight (*e.g.*, peptides). Fig. 12 demonstrates the acetylation of an amino acid mixture using HP [1,1-$^{13}$C] acetic anhydride and the $T_1$-dependent signal loss for the various resolved *N*-acetyl adducts at 11.7 T. Recently, the fully deuterated analog [$^2$H$_6$, 1,1-$^{13}$C] acetic anhydride was used to label the Arg-Gly-Asp or "RGD" peptide, a common motif in cellular recognition.[121] The measured $T_1$ of the $^{13}$C-RGD adduct was 5.4 s at 14 T, but >30 s at 3 T highlighting the effect of CSA on $T_1$. The relevance of secondary polarization for *in vivo* applications is unclear, given the relatively modest signal enhancements obtained (on the order of $10^3$ for *N*-acetylglycine).

### 7.5. Polymerization

Hilty *et al.* have investigated the time-resolved spectroscopy of anionic polymerization reactions using DNP-NMR. The authors initially described formation of poly(ethyl-2-cyanoacrylate).[132] A 50:50 (v/v) mixture of natural abundance ethyl-2-cyanoacrylate and methyl methacrylate containing BDPA radical were polarized using the usual technique, dissolved in THF, mixed with tetra-methylethylenediamine (TMEDA) and studied by NMR. Rapid formation of long polymer chains was indicated by the line-broadening of product peaks. In a more recent paper, the anionic polarization of styrene was observed by DNP-NMR.[41] Although polystyrene can be synthesized by several methods, the anionic method was chosen to avoid formation of radical intermediates that might diminish the NMR signal by paramagnetic relaxation. For the DNP experiment, styrene monomer (natural abundance) was HP by the usual method, dissolved in dioxane, and mixed with the initiator sodium naphthalenide (NaC$_{10}$H$_8$) in THF. As described in Fig. 13, the reaction begins with dimerization of two styryl radical ions, and is followed by bidirectional propagation. Although the resulting HP $^{13}$C spectrum had a large contribution from the styrene monomer, additional resonances not seen in the styrene/polystyrene references at thermal equilibrium correspond to reaction intermediates. For these intermediates, the authors performed correlation experiments with selective inversion of a spin of interest, to unambiguously assign resonances to the anionic species. This is possible in DNP-NMR when two chemical species are transformed into each other.[133,134] These findings are ground-breaking not only for their elucidation of living polymerization reactions, but also for the potential utility of DNP-NMR to study a variety of transient phenomena.

### 7.6. Study of molecular interactions

The study of molecular interactions in solution using NMR at thermodynamic equilibrium is well-established. Screening studies for ligand–receptor interactions in solution are usually ligand-directed and have employed both $^1$H and $^{19}$F NMR.[135–137] Use of a $^{13}$C nucleus is attractive given the large $^{13}$C chemical shift range, but sensitivity has been limited by low natural abundance and $\gamma$. Hyperpolarization using the DNP technique has been suggested as

a means to circumvent this problem, allowing $^{13}C$ screening experiments that would be impractical at thermal equilibrium. In a proof-of-principle study, a HP ligand solution containing salicylate and ascorbate was mixed with human serum albumin.[38] In the presence of the receptor, resonances corresponding to salicylate were not seen, while the ascorbate resonances are clearly visible (Fig. 14A). These effects are due primarily to $T_1$-mediated HP signal decay, and the effect of exchange line-broadening. Attenuation of MR signal amplitude, line-broadening, and chemical shift changes in the presence of serum albumin were observed for HP salicylate in a separate experiment at an earlier time-point.

The relationship between binding and $T_1$ was studied explicitly using a model ligand–receptor system, namely the hydrophobic binding of benzoic acid to β-cyclodextrin, a cyclic sugar used in a variety of enzyme mimics.[54,138] Natural abundance benzoic acid was polarized using the DNP method and combined with β-cyclodextrin, with $T_1$'s calculated for varying concentrations of the ligand. The results were used to estimate log$K$, which was similar to that described previously for this ligand–receptor pair. In a second set of experiments, enriched [1-$^{13}C$] benzoic acid was HP and mixed with solutions with varied concentrations of the cyclodextrin host. A 3D frequency selective echo-planar imaging method was then used to image the HP benzoate, with attenuation of signals observed with the host present. Signal changes correlated with the cyclodextrin concentration (Fig. 14C). These findings suggest that HP MR may be used to determine the presence, and concentration of a relevant ligand–receptor pair *in vivo*, for example a polarized steroid and androgen receptors expressed by prostate cancer.

## 8. Essential biochemistry of DNP

The enzymatic conversion of HP probes plays a crucial role in the ability to visualize metabolism non-invasively. Key processes include the uptake/transport kinetics of substrates, their rapid enzymatically-catalyzed conversion and availability of cofactors. This section describes rapid enzyme mediated processes, which can be used as a primer for the understanding of biochemical mechanisms characterized by DNP.

### 8.1. Dehydrogenases and redox

The most well-studied reaction by DNP-NMR, namely the conversion of [1-$^{13}C$] pyruvate to [1-$^{13}C$] lactate, is a reduction. In many studies, this conversion has been linked to the aberrant metabolism seen in cancer. As Warburg and colleagues postulated,[139,140] many cancers undergo increased aerobic glycolysis even in the presence of oxygen. This adaptation is counterintuitive, given the energetic advantage of metabolizing glucose *via* the tricarboxylic acid cycle (TCA) and oxidative phosphorylation to produce energy (ATP). Warburg's hypothesis has driven extensive research into the reasons for this shift, and what competitive advantage is afforded cells in this state. *In vivo*, one important driving force is modulation in the ratio of reducing to oxidizing (redox) agents leading to increased metabolism to lactate.[141,142]

Generation of lactate from the glycolytic intermediate pyruvate is mediated by the enzyme lactate dehydrogenase (LDH, EC 1.1.1.27). At steady state, the kinetics of LDH can be characterized as an ordered bi-reactant scheme, specifically a Theorell–Chance

mechanism.[143,144] First the enzyme binds the reduced dinucleotide cofactor nicotinamide adenine dinucleotide (NADH). It then binds the substrate pyruvate and catalyzes its reduction to the product lactate *via* a hydride transfer (Fig. 15). At high concentrations of pyruvate, LDH has been shown to be substrate inhibited and the concentration of pyruvate in the cell is tightly regulated in glycolysis. In the case of HP [1-$^{13}$C] pyruvate, the labeled carbonyl is adjacent to the C2 carbon, which is the site of reduction. Pyruvate is rapidly transported into the cell by the monocarboxylate transporter family (MCT), predominantly MCT1 ($K_m = 0.7$–2 mM).[145–147] While there are sodium dependent MCTs, the greater density of MCT1 is a H$^+$ symporter, thus requiring a molar equivalent of H$^+$s to enter the cell upon uptake of pyruvate. In most experiments, HP pyruvate is introduced into the system at very high concentrations and thus the magnitude of conversion to labeled lactate can be limited by the specific activity of MCT.[148] Once in the cell, the high availability of NADH and LDH allows for near instantaneous conversion to lactate. It is important to note that if the lifetime of the pyruvate–LDH complex were long during the conversion to lactate, the HP signal would decrease more rapidly due to through space relaxation and increased molecular correlation time. Once reduced, the HP lactate is incorporated into the intracellular lactate pool. The label can also be transported out of the cell, predominantly through MCT4,[149,150] which has also been shown to be upregulated in cancer cells.[151,152] Given the ubiquitous nature of this dehydrogenase reaction, HP pyruvate has been studied extensively, demonstrating rapid conversion in cells[152–155] and animal models.[155–159]

While pyruvate provides a window into the predominantly cytosolic NAD(H)-dependent redox pool, the network of redo-related enzymes and cofactors is both complicated and expansive. Many other redox networks have been targeted for metabolic study.[130,160–162] The generation of reactive oxygen species and its subsequent quenching has been a topic of great interest and the antioxidants glutathione [GSH] and ascorbate (vitamin C) have been found to be critical in maintaining redox.[161,163] Interestingly, the oxidized form of vitamin C, dehydroascorbate, is rapidly transported into the cell by glucose transporters (GLUTs), predominantly GLUT1. It then takes part in a 2-electron reduction to ascorbate catalyzed by a range of redox enzymes including GSH-dependent glutaredoxin (EC 1.20.4.1), protein disulfide isomerase (PDI, EC 5.3.4.1), and glutathione transferase (GSTO, EC 2.5.1.18). Reduced glutathione levels can then be maintained by through NADPH-dependent reactions, including glutathione reductase (EC 1.8.1.7). Given the robustness of this redox network, [1-$^{13}$C] DHA was developed as a redox probe for monitoring intracellular reducing capacity. Following application to cells or intravenous administration, HP DHA is rapidly transported into the cell and reduced to HP [1-$^{13}$C] vitamin C. It is important to note that the export of vitamin C from the cell is relatively slow and, on the time scale of the HP experiment, would be expected to accumulate intracellularly.

HP DHA conversion to vitamin C has been demonstrated in cancer cells as well as in animal models.[85,86] High rates of conversion are observed in organs whose exposure to ROS is high, including the brain, liver, and kidneys. High rates of reduction are also observed in tumors,[85] consistent with both high concentrations of glutathione as well as over-expression of redox enzymes.[164]

### 8.2. Transaminases

Conversion of HP [1-$^{13}$C] pyruvate to [1-$^{13}$C] alanine has been observed by DNP-NMR. The rapid enzymatic conversion of α-keto-acids to amino acids is typically catalyzed by transaminases. These enzymes are responsible for many processes including the maintenance of nitrogen homeostasis, catabolism and shuttling of substrates. The reversible conversion of pyruvate to alanine is mediated by the enzyme alanine aminotransferase (ALT, EC 2.6.1.2), which uses glutamate as the amine donor. ALT, like all transaminases, requires pyridoxal-phosphate, which is converted into pyridoxamine post-reaction with an amino acid. When HP [1-$^{13}$C] pyruvate is enzymatically converted *via* ALT *in vivo*, [1-$^{13}$C] alanine is observed in many tissues, most predominantly the liver[165–167] (Fig. 16). Liver pathologies can impact the observed alanine signal and increased metabolism of HP pyruvate to alanine has been seen in early development of myc-driven hepatocellular carcinoma.[168] Since transport of HP pyruvate into the cell is regulated by the MCTs, the reaction rate of ALT becomes dependent on its balance with other processes, including reduction of pyruvate to lactate. This can be envisioned as real-time enzymatic competition.

This HP probe design has been extended to other keto-acids, including [1-$^{13}$C] ketoisocaproic acid (KIC).[169] Like pyruvate, KIC's conversion to leucine through the branch chain aminotransferases (BCAT, EC 2.6.1.42) requires glutamate as the amine donor. KIC is transported into the cell using similar transporters to pyruvate and its compartmentalization is dependent on the activity of both a cytosolic and mitochondrial isoform BCAT. In recent work, the conversion of HP KIC to leucine was observed in tumors with high BCAT activity.[169] In the brain, HP KIC metabolism is expected to inform on glutamate transport between neurons and astroglia.[170]

### 8.3. Decarboxylases

In tissues with a high rate of oxidative phosphorylation, such as the heart, HP $^{13}$C bicarbonate (a surrogate for $^{13}$C $CO_2$) is seen following administration of [1-$^{13}$C] pyruvate, both *in vivo* and in perfused systems. Removal of a carboxyl group from amino and keto-acids is catalyzed by the family of decarboxylases. These reactions tend to be fast and since they can easily be traced using a labeled carboxyl group, they are readily addressed by long $T_1$ HP probes. The decarboxylation of pyruvate is typically catalyzed by the pyruvate dehydrogenase complex (PDC), which is comprised of 3 enzyme units.[171] Pyruvate dehydrogenase (EC 1.2.4.1), with the cofactor thiamine pyrophosphate (TPP – vitamin B$_1$) catalyzes the conversion of pyruvate to $CO_2$ in the first step of metabolism of pyruvate to acetyl-CoA. In this mechanism, pyruvate and TPP are bound by the enzyme and the C2 carbon of TPP performs a nucleophilic attack on the C2 of pyruvate, leading to the decarboxylation of pyruvate and production of $CO_2$. This is considered the rate-limiting step of the PDC. Using HP [1-$^{13}$C] pyruvate in highly oxidative cells and organs, the flux through PDC was monitored by $CO_2$ formation and found to be sensitive to physiologic perturbations.[157,172] The $CO_2$ observed is readily converted to bicarbonate through both carbonic anhydrase and acid–base chemistry (Fig. 17). Production of $^{13}CO_2$, and in turn $^{13}$C bicarbonate, has been linked to changes in cardiac status[173,174] as well as response to chemotherapeutics such as dichloroacetate.[175,176]

While [1-$^{13}$C] pyruvate can interrogate decarboxylation in the first step of the PDC, labeling using HP [2-$^{13}$C] pyruvate has demonstrated flux into the TCA cycle.[84] TCA intermediates can be observed in real time showing flux from [2-$^{13}$C] pyruvate directly to [1-$^{13}$C] citrate and [5-$^{13}$C] glutamate. Using HP [1,2-$^{13}$C] pyruvate, flux though both pathways has been compared.[177] While the $T_1$ relaxation rates of these intermediates must be determined to quantify differences in observed flux, relative changes can be used to assess changes with disease state such as ischemia. It is important to note that the relative signal intensities of these TCA metabolites to the injected C2 pyruvate is quite low, due to both the faster relaxation times of these intermediates as well as potential extended relaxation due to interaction with multiple enzymes.

A resonance corresponding to [1-$^{13}$C] oxaloacetate has been seen following HP [1-$^{13}$C] pyruvate infusion. Addition of a carboxyl group to keto-acids is mediated by the ligase class of carboxylases.[178] Pyruvate carboxylase (PC, EC 6.4.1.1) catalyzes the irreversible carboxylation of pyruvate to oxaloacetate (OAA), using both ATP and acetyl-CoA. OAA can then take part in many reactions including shuttling from the mitochondria to the cytosol as malate, converted back to OAA and decarboxylated and phosphorylated to phosphoenolpyruvate (PEP) for gluconeogenesis. Regulation of the fate of OAA derived from PC is dependent on glucose concentration and upstream enzymatic processes as well as the anaplerotic role of replenishing carbons in TCA. In conditions of high glucose, high PC activity can lead to pyruvate cycling in pancreatic β-cells in order to facilitate glycolysis.[179] HP [1-$^{13}$C] pyruvate injected into perfused livers has demonstrated conversion through OAA to malate and aspartate, indicative of PC activity[167] as well as *in vivo*.[166] Interestingly, the researchers show label scrambling of both malate and aspartate as a result of malate's hydration reaction through fumarase (EC 4.2.1.2) to the symmetric TCA intermediate fumarate, leading to both [1-$^{13}$C] and [4-$^{13}$C] malate and aspartate. The contribution of flux through fumarase is visualized in the relative resonance amplitudes for the C1 and C4 carbons.

## 8.4. Peptidases, acetyltransferases, and acylases

As discussed, translocation of carboxyl groups provides a convenient means of following enzymatic conversion by HP MR due to the long $T_1$ relaxation of the carboxyl moiety. This has been extended to the cleaving of carboxyl groups from substrate mimics in an effort to report on the activity of the enzyme. Importantly, although a peptide bond can spontaneously hydrolyze in water (taking on the order of 1000 years), it is enzymatically facilitated *in vivo*, releasing nearly 4 kcal mol$^{-1}$ (ref. 180) of energy; the ability to visualize this process by HP MR is striking.

Carboxypeptidases are protease enzymes (EC 3.4.16-18) that hydrolyze a C-terminal peptide bond.[181] Typically these are involved in protein regulation and have also been the target of developing chemotherapeutics,[182] treatment of neurodegenerative/inflammatory diseases,[183] and even detection of prostate cancer (PSMA).[184] Typically this is a Zn$^{2+}$-dependent mechanism where the carboxyl carbon of the peptide bond to be cleaved is coordinated by the zinc ion. This mechanism has not yet been applied to *in vivo* HP study, however *ex vivo* work has shown the ability to visualize peptide carboxyl cleavage. 3,5-Diflurobenzoyl-L-

glutamate was HP at natural abundance and reacted with carboxypetidase G2 (CPG2) as a reporter probe, with cleavage to glutamate indicating CPG2 activity.[185] Interestingly, the amide carbonyl is not observed; its lifetime shortening is attributed to depolarization *via* an exchange effect with zinc and is reversed by addition of a chelator (*i.e.*, EDTA). The $T_1$'s of the carbons of interest in solution were relatively short, thus limiting clinical translation, but its important to note the C1 carbonyl resonance of glutamate survives the reaction and is readily observed.

Like removal of carboxyl groups, acetyltransferases are capable of removing acetyl moieties from peptides and small molecules and transferring them. In the brain, choline acetyltransferase (EC 2.3.1.6) catalyzes the cleavage of the acetyl group from acetyl-CoA and its ligation with choline to form the neurotransmitter acetylcholine.[186] Histone acetyltransferase (EC 2.3.1.48) catalyzes the acetylation of *N*-acetyl-lysine, removing the acetyl from acetyl-CoA and playing a major role in gene regulation.[187] For this reason, acetyl transferases have been studied using HP precursors, but they have yet been shown to be robustly translatable to living systems. This is most likely due to the slow uptake of the precursor, for example choline. Recently, researchers have used a similar mechanism, aminoacylase (EC 3.5.1.14), as a reporter.[188] This probe catalyzes the cleavage of a carboxylate from an *N*-acyl-amino acid. By genetically modifying HEK cells to include the Acyl-1 gene, Chen *et al.* were able to demonstrate that cells expressing elevated aminoacylase cleaved *N*-acetyl-methionine to methionine on the timescale of the HP experiment. In these cases, the acylase probes have been shown to be potentially transport-limited and using the transport architecture of the cell, may provide a means to yield higher signals. While intracellular incorporation may prove difficult when investigating endogenous reactions, enzymatic enrichment may be a beneficial tool for non-invasive cell tracking.

## 8.5. Kinases

The prevalence of phosphorylation reactions in metabolism and cell-signaling cascades make these a novel and high-yield application of $^{13}$C DNP-NMR. The phosphorylation of both $^{13}$C hexoses and $^{13}$C choline derivatives has been demonstrated *in vitro*. This transfer of phosphate groups from high-energy molecules, such as adenine triphosphate (ATP), to metabolites of interest is catalyzed by the kinase family of enzymes. Due to phosphate bond strengths, phosphorylation stores approximately 7 kcal mol$^{-1}$ of energy.[189] Over the last two decades a great deal of effort has been directed toward the elucidation of protein kinase pathways and their regulation of disease state, leading to many therapeutic targets. The metabolic elucidation of kinases began with older studies describing glycolysis. Hexokinase (EC 2.7.1.1) catalyzes the phosphorylation of hexoses and is the first step in the glycolytic metabolism of glucose, resulting in glucose-6-phosphate.[190] Hexokinase has been shown to be regulated and recruited by a number of mechanisms, including insulin response, and hexokinase 2 (encoded by the HK2 gene), which localizes to the outer mitochondrial membrane and is upregulated in many rapidly dividing cancer cells.[191] In order to investigate this metabolic process, multiple HP probes have been developed. The first was [2-$^{13}$C] fructose,[90] which exists as multiple hexose isomers, predominantly the β-fructopyranose and fructofuranose rings. This was chosen since the hemi-ketal carbon of

fructose has a long $T_1$ relative to the short glucose $T_1$'s. *In vitro*, with the addition of hexokinase, phosphorylation could be observed and resolved, since fructose-6-phosphate only exists as a furanose isomer. *In vivo*, fructose is transported by the GLUTs, predominantly GLUT5, which is upregulated in some cancers. Changes in the ratio of phosphorylated to total fructose can be anticipated in regions of both high GLUT mediated uptake and resulting hexokinase activity. In more recent studies, fully deuterated glucose and fructose have been HP (see Sections 5.2 and 5.3) and have tremendous *in vivo* promise since metabolism assessed by GLUTs and glycolysis may be more representative of the upstream oncogenic phenotype.

Another kinase that has been extensively studied for clinical translation is choline kinase (EC 2.7.1.32). Choline and its phosphorylated intermediates of the Kennedy cycle, phosphocholine (PC) and glycerophosphocholine (GPC), have been observed by ^{1}H NMR and are related to stage and progression in a number of cancer types.[192–194] Recently it was shown that CHK plays a role in a complex with the EGF receptor (EGFR) in a c-Src-dependent manner, and functions cooperatively with EGFR and c-Src in regulating cell proliferation pathways.[195] Choline uptake and trapping *via* CHK have also been exploited as the radioactive PET analogue ^{11}C-choline. Given this level of interest in choline metabolism, both ^{15}N and ^{13}C labeled choline molecules have been HP for study.[26,105,107] While *ex vivo* experiments have demonstrated the phosphorylation of HP choline by CHK, detecting this conversion *in vivo* may be limited by the kinetics of the choline transporter.

## 8.6. Hydratases

Enzyme-catalyzed hydration and dehydration reactions have been interrogated by ^{13}C DNP-NMR, using probes with high potential for clinical translation. Specifically, the hydration of HP [1,4-[13]C$_2$] fumarate to malate has been seen in necrotic cells, while the carbonic anhydrase-mediated hydration of [13]C $CO_2$ to [13]C $HCO_3^-$ (and the reverse reaction) have been studied in the context of extracellular pH.[37] Due to the high concentration of water in cells, these reactions contrast with previously discussed cases, for which enzymatic conversion of HP probes is reactant-limited. For example, with depletion of NAD(H) in chemotherapy, LDH flux observed by HP [1-^{13}C] pyruvate is decreased. For reactions using $H_2O$, the presence of this virtually unlimited reactant allows a more precise understanding of metabolic flux.

Recently, Gallagher *et al.* have used [1,4-[13]C$_2$] fumarate to study necrosis both *in vitro* and *in vivo*.[196] In normal tissue, fumarate is transported into the cell by sodium dependent dicarboxylic acid transporters (DCATs) and rapidly hydrated by fumarate hydratase (FH, EC 4.2.1.2) to malate. Tumor, as well as normal tissues have demonstrated very low, if any, detectable HP malate. When treated with chemotherapies that induce high levels of necrosis, [1,4-[13]C$_2$] malate is detected and was correlated to levels of necrosis (Fig. 18). Observing the static FH activity and ubiquitous availability of the cofactor ($H_2O$), the researchers postulate that this increased malate production is due to the increased membrane permeability, which accompanies necrosis. Importantly, HP fumarate addresses one of the most exciting applications of DNP, namely monitoring response to therapy.

The determination of extracellular pH ($pH_e$) non-invasively has been a goal of many researchers in the last 3 decades. Acidification of the extracellular matrix (ECM) has been related to many diseases, particularly cancer. While nuclear medicine and MRI techniques have been developed to image an acidic $pH_e$, these efforts have been plagued by quantification inaccuracies and sensitivity. Using the unlimited reactant water, Gallagher *et al.* have developed HP $^{13}$C-bicarbonate as a means for measuring $pH_e$.[37,83] Bicarbonate remains extracellular and its conversion to $CO_2$ can happen fairly rapidly by acid–base chemistry (10's of seconds). *In vivo*, the interconversion of bicarbonate and $CO_2$ is facilitated by the family of carbonic anhydrases (CA, EC 4.2.1.1) because the non-catalyzed rate of interconversion is slow relative to the metabolic fluxes, which generate (and consume) $H^+$.[197,198] CA can increase this inter-conversion $10^4$–$10^6$ fold and exists both on the cell surface as well as on the mitochondrial membrane. The rapid chemical exchange of $^{13}$C $HCO_3^-$ and $^{13}$C $CO_2$, catalyzed by carbonic anhydrase, was investigated in a series of saturation experiments *in vivo* (Fig. 19). In these experiments, selective saturation of the $^{13}$C $CO_2$ resonance was performed, with and without treatment with acetazolamide, a CA inhibitor. These studies showed more rapid decay of the $^{13}$C $HCO_3^-$ resonance with $^{13}$C $CO_2$ saturation, as expected in a fast-exchanging pair. By contrast, when acetazolamide was administered, $^{13}$C $CO_2$ saturation had little effect on the decay of the $^{13}$C $HCO_3^-$ resonance (dominated by its $T_1$). Therefore, the role of CA in facilitating this equilibrium was unambiguously established. $^{13}$C cesium bicarbonate was used to demonstrate CA-catalyzed interconversion both *in vitro* and in tumor-bearing mice, demonstrating lower pH within tumor (Fig. 19). The ratio of $^{13}$C $HCO_3$ to $^{13}CO_2$ is governed by the Henderson–Hasselbach equation and pH can be readily determined from a ratiometric image. Recent work has extended this to hyperpolarizing $^{13}$C sodium bicarbonate, a non-toxic salt, showing this method has great potential for non-invasive imaging of $pH_e$.[83] It is important to note that intracellular CA activity is also observed in most tissues *via* conversion of the $CO_2$ derived from HP pyruvate to bicarbonate. The pH derived in this way is of the intracellular compartment and is typically observed in cardiac experiments.

## 9. Engineered cell and tissue culture systems (bioreactors)

The study of HP probes and their biochemistry requires tissue culture systems that interface with DNP-NMR. Due to limited HP MR lifetimes, it is difficult to use traditional cell and tissue culture to investigate HP probe metabolism. Moreover, reproducibility and robustness of the measurement is confounded by variations in cell density, the concentrations of metabolic precursors, and media components. To study changes in metabolism with HP probes as well as characterize biochemical mechanisms, MR-compatible systems have been developed, deemed bioreactors.[199–201] These systems may be studied using both NMR at thermal equilibrium and DNP-NMR, with several key modifications needed for the latter. These modifications include (1) a fast injection system, so that the $^{13}$C substrate of interest reaches the cells/tissues within its useful HP lifetime, (2) the ability to adjust key parameters (for example flow rate) to investigate rapid kinetic mechanisms, and (3) maintenance of magnetic field homogeneity, to resolve $^{13}$C probes and their metabolites by chemical shift.

First incarnations of these perfusion systems were adapted from predecessors designed for large cultures and used to monitor dynamic and steady state metabolism of small molecules,

including $^{13}C$ and $^{19}F$ labeled probes.[202,203] In recent work, systems that perfuse immortal cells with injection of HP pyruvate[148,153] have measured changes in cell uptake,[148] response to therapy,[154] and reproducibility of measurements.[153] Similar to perfused organ and murine studies, metabolic pathways are readily visualized in real time. Of greater importance is the ability to control parameters such as oxygenation, flow, pH, and substrate availability to introduce perturbations in microenvironment. Additionally, these systems can be used to accurately measure kinetics and derive parameters of interest for translation. With a well-controlled system, typical confounders such as variability in cell bioenergetics state can be controlled for using $^{31}P$ MR and HP $^{13}C$ kinetics can be assessed. A recent study demonstrated that not only does transporter uptake govern the HP lactate observed, derived from pyruvate and MCT1, but also the transport of lactate out of the cell (MCT4). Because this was observed in cell lines of differing aggressiveness, MCT4 may be a potential cancer target.[152]

The extension of this approach to more biologically relevant model systems is of great importance. Over the years, many targeted therapies and biomarkers that have been discovered in immortal cell lines and mouse models, have yielded poor clinical translation.[204,205] In recent work, living primary human tissue slice cultures (TSCs) have been integrated into a bioreactor platform for metabolic study.[206] These TSCs are derived from patients at surgery and kept alive under perfusion inside of an NMR spectrometer for metabolic study using injected HP probes (Fig. 20). Metabolism of HP pyruvate to lactate in these cultures was shown to increase in prostate cancer relative to benign prostate tissues and will be important in validating studies in prostate cancer patients.

## 10. HP kinetic measurements

While the focus of this review is on the chemistry and biochemistry of HP MR, it is important to consider the relevant parameters needed to assess observed kinetics. Each HP probe has a characteristic $T_1$ relaxation rate at a given field strength, which affects the observed signals in time. In order to analyze *ex vivo* kinetic data for a given probe, the $T_1$ of the substrate and product must first be measured at the proposed field strength, using a low flip angle ($a$) pulse and acquire sequence. After correcting for pulse saturation due to excitation (*i.e.* $\cos^n(a)$), the $T_1$ can be fit to a mono-exponential decay using standard methods. Using these $T_1$'s, one can apply standard kinetic analysis methods to the acquired HP MR data. In the case of first order chemical kinetics, $T_1$ relaxation can be incorporated into a first order rate equation and used to derive measured rates.

$$A \xrightarrow{k} B \quad (1)$$
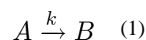
$$\frac{\mathrm{d}A}{\mathrm{d}t} = -kA - \frac{1}{T_{1A}} \quad (2)$$

$$\frac{\mathrm{d}B}{\mathrm{d}t} = kA - \frac{1}{T_{1B}}B \quad (3)$$

The reaction rate is represented by $k$ with the relaxation rates of $A$ and $B$ as $T_{1A}$ and $T_{1B}$, respectively. These coupled ordinary differential equations can then be integrated:

$$A(t) = A_0 e^{-\left(k + \frac{1}{T_{1A}}\right)t} \quad (4)$$

$$B(t) = \frac{A_0 k \left(e^{-\frac{t}{T_{1B}}} - e^{-\left(k + \frac{1}{T_{1A}}\right)t}\right) + B_0 \left(k + \frac{1}{T_{1A}} - \frac{1}{T_{1B}}\right) e^{-\frac{t}{T_{1B}}}}{k + \frac{1}{T_{1A}} - \frac{1}{T_{1B}}} \quad (5)$$

$A_0$ and $B_0$ are the starting measurements of substrate and product. This approach can be used as a primer for extending to higher order kinetics using standard methods and has been applied to chemical reactions.[134]

This method can also be applied to enzyme kinetics, with the inclusion of the appropriate rate equation. Recent work has modeled monocarboxylate transport kinetics using an exchange model[155] and then standard Michaelis–Menten kinetics[148] while others have modeled lactate dehydrogenase kinetics using a Theorell–Chance mechanism.[144] Others have attempted to include additional information such as mass spectroscopy derived concentrations to aid in the quantification.[207] Additionally, this modeling has been extended to include delivery dynamics both in cell and *in vivo* systems.[153,208] Each approach makes assumptions to reduce the number of variables and allow for numerical solution. These approximations typically assume that the substrate and product have similar relaxation rates or that the reaction is unidirectional. For the purposes of quantifying *in vivo* kinetics, it is important to note that relaxation parameters are difficult to assess for different tissues and this must be accounted for to develop quantitative rates. Diffusion and perfusion of substrates as well as products[64,121,209] will also influence the observed signals and these limitations must be addressed to calculate absolute rates *in vivo*. While rates, in the classical sense, are important for understanding the underlying biochemical mechanism of conversion, a high range of contrast between normal and malignant tissues can be determined using simple approaches such as resonance ratios.[85,156,168,210] These are typically used for *in vivo* experiments and provide a robust measurement for tissue comparison. As in other imaging methods, *e.g.*, dynamic contrast enhanced MRI, modeling of HP parameters will play a major role in the future quantification of observed metabolic conversions and a better appreciation of these kinetic changes may yield other more sensitive parameters for tissue characterization.

## 11. *In vivo* success stories: pyruvate, dehydroascorbate, and fumarate

Many ^{13}C substrates have been polarized using the DNP technique, but only a handful have been useful for detailed *in vivo* study, during which metabolites are not only detected but also localized to an organ/tissue of interest. Simply stated, this requires large ^{13}C metabolite signals and chemical shift imaging [CSI] methods to parse those signals into voxels. For the prototype agent [1-^{13}C] pyruvate, this was described as early as 2006, but several newer ^{13}C agents have also demonstrated rapid *in vivo* metabolism amenable to CSI. Two recent

examples are dehydroascorbate and fumarate. This section presents the chemical and biochemical features of pyruvate, dehydroascorbate, and fumarate that render these metabolic agents potentially useful in the clinic.

The identification of chemical structures amenable to hyperpolarization by DNP has already been discussed. These three small molecules (1) have a long $T_1$ carbon nucleus, (2) are endogenous, (3) are highly soluble, and (4) experience a chemical reaction that is observable by chemical shift. For *in vivo* applications, several additional features are critical. Since HP $^{13}$C agents are administered intravenously as a concentrated bolus (mM range), toxicity may limit the dose delivered. Transport of the $^{13}$C agent into the cellular compartment (or organ) of interest is also an important consideration. For example, for studying cerebral metabolism the introduced $^{13}$C probe must cross the blood–brain barrier at a sufficient rate, which is not the case for many small-molecule metabolites. The conversion of the introduced $^{13}$C agent to its metabolic products must also occur at a high rate, to be observed on the time-scale of the HP MR experiment. The $^{13}$C metabolic products formed must also have longer $T_1$'s, and be maintained at a high steady-state concentration. This requirement is highlighted by studies in yeast using [U-$^2$H, U-$^{13}$C] glucose, remarkable not only for the number of resonances observed, but also for the resonances *not* observed, corresponding to intermediates in the glycolytic pathway. Although these intermediates (*e.g.*, 3-phospoglycerate) are certainly formed, they are themselves consumed too rapidly to permit detection, reflected by their low steady-state concentrations in the cell. This is also the case for intermediates of the TCA cycle that are not seen following administration of [2-$^{13}$C] pyruvate.

## 11.1. HP [1-$^{13}$C] pyruvate

Pyruvate is the most prolific HP $^{13}$C agent, and numerous studies have been performed in preclinical models, including transgenic and implanted murine tumors, perfused organs, and bioreactors. Many outstanding studies have been published that not only validate [1-$^{13}$C] lactate as a cancer biomarker, but also demonstrate the utility of [1-$^{13}$C] pyruvate in cardiac and cerebral imaging, and investigate fundamental cellular processes. Further discussion of these reports are beyond the scope of this review, but have been addressed elsewhere.[211–213] HP [1-$^{13}$C] lactate signals have been correlated with tumor grade in a TRAMP model.[156] Tumor response to therapy has been investigated *in vivo* in a murine lymphoma model comparing HP [1-$^{13}$C] pyruvate to $^{18}$F-FDG.[214] In cardiac imaging, decarboxylation of [1-$^{13}$C] pyruvate by the pyruvate dehydrogenase (PDH) complex results in large bicarbonate signals in the normal heart, that are significantly decreased in ischemia.[215] Metabolism of HP [1-$^{13}$C] pyruvate has been observed both in the normal brain, and implanted glial tumors where increased lactate signals were observed.[216] Several basic cellular processes have been investigated using HP [1-$^{13}$C] pyruvate, including a recent study describing the role of carbonic anhydrase-rich domains in facilitating mitochondrial respiration in myocytes.[217]

These studies are possible due to the previously described chemical and biochemical features of pyruvate, as well as its central role in metabolism. Increasingly, HP [2-$^{13}$C] pyruvate has been studied, which also has a long $T_1$ and is amenable to DNP. Metabolites of the citric acid (TCA) cycle cannot be observed in biologic systems using [1-$^{13}$C] pyruvate,

since it is the C2 carbon that enters TCA as acetyl-CoA, with C1 "lost" as $CO_2$. HP [2-$^{13}$C] pyruvate has been used in the heart, which has a high rate of oxidative phosphorylation.

## 11.2. HP [1-$^{13}$C] dehydroascorbic acid

As noted earlier, the oxidized form of vitamin C (VitC), dehydroascorbic acid (DHA) has been developed as a redox probe and studied *in vivo*.[85,86] It shares a dicarbonyl structure with pyruvate, although in aqueous solution various hydrates and intramolecular hemi-ketal forms are seen, that complicate its MR spectrum. Like pyruvate, it has a long $T_1$, high solubility (in DMA and DMSO), and may be injected at concentrations for which physiologic effects in animals are not observed (up to 15 mM). *In vivo*, dehydroascorbate shares an uptake mechanism with glucose *via* the GLUT 1,3,4 transporters and is rapidly converted to vitamin C. This reduction is considered glutathione (GSH) dependent, although a host of redox enzymes, NADPH, and vitamin C itself are also implicated. As discussed previously, direct reduction of DHA by GSH *in vitro* is possible, but this rate is too slow to account for the large *in vivo* signals VitC signals observed following administration of HP [1-$^{13}$C] DHA. In the TRAMP model, the largest VitC signals were observed in the kidneys, liver, brain, and prostate tumor (Fig. 21).[85,164] This reduction is probably best considered a measure of redox capacity,[218] rather than redox state.[219] While the former term refers to the cell's ability to reduce oxidizing species (reflected in both reducing agent concentration and its maintenance), the latter may be defined as the [GSH]/[GSSG] ratio. It is not clear that [GSSG] may be interrogated using the DHA–VitC pair. Following administration of HP [1-$^{13}$C] VitC, only trace DHA is observed, which may not depend on the concentration of oxidized glutathione.

## 11.3. HP [1,4-$^{13}$C$_2$] fumarate

Tumors may respond to therapy by both apoptotic and non-apoptotic mechanisms including necrosis, with unregulated digestion of cellular components. While necrosis may be imaged macroscopically using traditional $^1$H methods, early necrosis is of great interest in observing a tumor's response to therapy. HP [1,4-$^{13}$C$_2$] fumarate has been used to image necrosis in a murine lymphoma model, with formation of [1,4-$^{13}$C$_2$] malate correlated with the percentage of cells that had lost plasma membrane integrity.[196] Following treatment with etoposide, there was Hyperpos a significant (2.4-fold) increase in [1,4-$^{13}$C$_2$] malate production that correlated with tumor cell necrosis (Fig. 22). As previously discussed, fumarate is a TCA intermediate that is maintained at low concentrations in the mitochondria, and converted to malate by the activity of fumarase. Gallagher *et al.* found that the increased [1,4-$^{13}$C$_2$] malate signal observed was unlikely to be due to fumarase expression, or increased transport *via* the sodium-dependent dicarboxylate transporter. Rather, the primary mechanism appears to be spilling of fumarase from damaged necrotic cells. Use of HP [1,4-$^{13}$C$_2$] fumarate in the clinic might therefore allow observation of both pathological states and response to treatment.

# 12. Summary

The development of rapid dissolution DNP methods has facilitated previously impossible *in vitro* and *in vivo* study of small molecules. The DNP technique is generalizable to a large

number of analytes, in contrast to other hyperpolarization methods. Several considerations for identifying compatible chemistries are presented in this review, for example the $T_1$ of the $^{13}C$ nucleus of interest, and the biochemistry of endogenous substrates. New approaches are overcoming the limitations imposed by $T_1$, for example controlled incorporation of enriched nuclei, and storage of spin polarization in the singlet state. The former approach will require development of new (and cheaper) synthetic methodologies, while the latter demands focused investigation of fundamental physical chemistry. HP NMR using DNP holds special promise in the interrogation of rapid and dynamic chemistries in solution, for which equilibrium spin magnetizations do not suffice. In addition, the technique has the potential to revolutionize the way patients are diagnosed and treated in the clinic, *via* non-invasive insights into basic metabolism.

## Acknowledgments

## References

1. Thakur ML, Lentle BC. J Nucl Med. 2005; 46:11N–13N. 42N.

2. Ardenkjaer-Larsen JH, Fridlund B, Gram A, Hansson G, Hansson L, Lerche MH, Servin R, Thaning M, Golman K. Proc Natl Acad Sci U S A. 2003; 100:10158–10163. [PubMed: 12930897]

3. Nelson SJ, Kurhanewicz J, Vigneron DB, Larson PE, Harzstark AL, Ferrone M, van Criekinge M, Chang JW, Bok R, Park I, Reed G, Carvajal L, Small EJ, Munster P, Weinberg VK, Ardenkjaer-Larsen JH, Chen AP, Hurd RE, Odegardstuen LI, Robb FJ, Tropp J, Murray JA. Sci Transl Med. 2013; 5:198ra108.

4. Macovski A. J Magn Reson Imaging. 2009; 30:919–923. [PubMed: 19856404]

5. DeFeo EM, Wu CL, McDougal WS, Cheng LL. Nat Rev Urol. 2011; 8:301–311. [PubMed: 21587223]

6. Duarte JM, Lei H, Mlynarik V, Gruetter R. Neuroimage. 2012; 61:342–362. [PubMed: 22227137]

7. Kemp GJ, Brindle KM. Diabetes. 2012; 61:1927–1934. [PubMed: 22826313]

8. Boesch C. J Magn Reson Imaging. 2007; 25:321–338. [PubMed: 17260389]

9. Ten Hove M, Neubauer S. Heart Failure Rev. 2007; 12:48–57.

10. Ouwerkerk R. J Am Coll Radiol. 2007; 4:739–741. [PubMed: 17903762]

11. Thulborn KR, Davis D, Snyder J, Yonas H, Kassam A. Neuroimag Clin N Am. 2005; 15:639–653. xi–xii.

12. Li S, Zhang Y, Wang S, Yang J, Ferraris Araneta M, Farris A, Johnson C, Fox S, Innis R, Shen J. Magn Reson Med. 2009; 62:565–573. [PubMed: 19526500]

13. Bluck LJ, Clapperton AT, Coward WA. Clin Sci. 2005; 109:513–521. [PubMed: 16091018]

14. Stevens AN, Morris PG, Iles RA, Sheldon PW, Griffiths JR. Br J Cancer. 1984; 50:113–117. [PubMed: 6743508]

15. van Zijl PC, Chesnick AS, DesPres D, Moonen CT, Ruiz-Cabello J, van Gelderen P. Magn Reson Med. 1993; 30:544–551. [PubMed: 8259054]

16. Jensen JE, Drost DJ, Menon RS, Williamson PC. NMR Biomed. 2002; 15:338–347. [PubMed: 12203225]

17. Zhu H, Barker PB. Methods Mol Biol. 2011; 711:203–226. [PubMed: 21279603]

18. Haase A, Frahm J, Hanicke W, Matthaei D. Phys Med Biol. 1985; 30:341–344. [PubMed: 4001160]

19. Prost E, Sizun P, Piotto M, Nuzillard JM. J Magn Reson. 2002; 159:76–81. [PubMed: 12468306]

20. Smith MA, Gillen J, McMahon MT, Barker PB, Golay X. Magn Reson Med. 2005; 54:691–696. [PubMed: 16086301]

21. Prescot AP, Renshaw PF. J Magn Reson Imaging. 2013; 37:642–651. [PubMed: 23055387]

22. Cocuzzo D, Lin A, Ramadan S, Mountford C, Keshava N. Conf Proc IEEE Eng Med Biol Soc. 2011; 2011:4929–4934. [PubMed: 22255444]

23. Roussel T, Giraudeau P, Ratiney H, Akoka S, Cavassila S. J Magn Reson. 2012; 215:50–55. [PubMed: 22227288]

24. Cudalbu C, Comment A, Kurdzesau F, van Hees-wijk RB, Uffmann K, Jannin S, Denisov V, Kirik D, Gruetter R. Phys Chem Chem Phys. 2010; 12:5818–5823. [PubMed: 20461252]

25. Reineri F, Viale A, Ellena S, Alberti D, Boi T, Giovenzana GB, Gobetto R, Premkumar SS, Aime S. J Am Chem Soc. 2012; 134:11146–11152. [PubMed: 22663300]

26. Gabellieri C, Reynolds S, Lavie A, Payne GS, Leach MO, Eykyn TR. J Am Chem Soc. 2008; 130:4598–4599. [PubMed: 18345678]

27. Atkins TM, Cassidy MC, Lee M, Ganguly S, Marcus CM, Kauzlarich SM. ACS Nano. 2013; 7:1609–1617. [PubMed: 23350651]

28. Aptekar JW, Cassidy MC, Johnson AC, Barton RA, Lee M, Ogier AC, Vo C, Anahtar MN, Ren Y, Bhatia SN, Ramanathan C, Cory DG, Hill AL, Mair RW, Rosen MS, Walsworth RL, Marcus CM. ACS Nano. 2009; 3:4003–4008. [PubMed: 19950973]

29. Jindal AK, Merritt ME, Suh EH, Malloy CR, Sherry AD, Kovacs Z. J Am Chem Soc. 2010; 132:1784–1785. [PubMed: 20102196]

30. Lumata L, Jindal AK, Merritt ME, Malloy CR, Sherry AD, Kovacs Z. J Am Chem Soc. 2011; 133:8673–8680. [PubMed: 21539398]

31. Kuzma NN, Pourfathi M, Kara H, Manasseh P, Ghosh RK, Ardenkjaer-Larsen JH, Kadlecek SJ, Rizi RR. J Chem Phys. 2012; 137:104508. [PubMed: 22979875]

32. Shchepin RV, Coffey AM, Waddell KW, Chekmenev EY. J Am Chem Soc. 2012; 134:3957–3960. [PubMed: 22352377]

33. Zacharias NM, Chan HR, Sailasuta N, Ross BD, Bhattacharya P. J Am Chem Soc. 2012; 134:934–943. [PubMed: 22146049]

34. Bhattacharya P, Chekmenev EY, Perman WH, Harris KC, Lin AP, Norton VA, Tan CT, Ross BD, Weitekamp DP. J Magn Reson. 2007; 186:150–155. [PubMed: 17303454]

35. Lippert AR, Keshari KR, Kurhanewicz J, Chang CJ. J Am Chem Soc. 2011; 133:3776–3779. [PubMed: 21366297]

36. Nonaka H, Hata R, Doura T, Nishihara T, Kumagai K, Akakabe M, Tsuda M, Ichikawa K, Sando S. Nat Commun. 2013; 4:2411. [PubMed: 24022444]

37. Gallagher FA, Kettunen MI, Day SE, Hu DE, Ardenkjaer-Larsen JH, Zandt RI, Jensen PR, Karlsson M, Golman K, Lerche MH, Brindle KM. Nature. 2008; 453:940–943. [PubMed: 18509335]

38. Lerche MH, Meier S, Jensen PR, Baumann H, Petersen BO, Karlsson M, Duus JO, Ardenkjaer-Larsen JH. J Magn Reson. 2010; 203:52–56. [PubMed: 20022775]

39. Warren WS, Jenista E, Branca RT, Chen X. Science. 2009; 323:1711–1714. [PubMed: 19325112]

40. Wilson DM, Hurd RE, Keshari K, Van Criekinge M, Chen AP, Nelson SJ, Vigneron DB, Kurhanewicz J. Proc Natl Acad Sci U S A. 2009; 106:5503–5507. [PubMed: 19276112]

41. Lee Y, Heo GS, Zeng H, Wooley KL, Hilty C. J Am Chem Soc. 2013; 135:4636–4639. [PubMed: 23461287]

42. Abragam A, Goldman M. Rep Prog Phys. 1978; 41:395–467.

43. Overhauser AW. Phys Rev. 1953; 92:411–415.

44. de Boer W, Borghini M, Morimoto K, Niinikoski TO, Udo F. J Low Temp Phys. 1974; 15:249–267.

45. Johannesson H, Macholl S, Ardenkjaer-Larsen JH. J Magn Reson. 2009; 197:167–175. [PubMed: 19162518]

46. Lau AZ, Chen AP, Ghugre NR, Ramanan V, Lam WW, Connelly KA, Wright GA, Cunningham CH. Magn Reson Med. 2010; 64:1323–1331. [PubMed: 20574989]

47. Blicharski JS. Z Naturforsch. 1972; A:1456–1458.

48. Harada M, Kubo H, Abe T, Maezawa H, Otsuka H. Jpn J Radiol. 2010; 28:173–179. [PubMed: 20182855]

49. Allouche-Arnon H, Wade T, Waldner LF, Miller VN, Gomori JM, Katz-Brull R, McKenzie CA. Contrast Media Mol Imaging. 2013; 8:72–82. [PubMed: 23109395]

50. Levitt, MH. Spin Dynamics: Basics of Nuclear Magnetic Resonance. 2. John Wiley & Sons Ltd; West Sussex, England: 2008.

51. Allouche-Arnon H, Lerche MH, Karlsson M, Lenkinski RE, Katz-Brull R. Contrast Media Mol Imaging. 2011; 6:499–506. [PubMed: 22144028]

52. Chen AP, Tropp J, Hurd RE, Van Criekinge M, Carvajal LG, Xu D, Kurhanewicz J, Vigneron DB. J Magn Reson. 2009; 197:100–106. [PubMed: 19112035]

53. Mieville P, Jannin S, Bodenhausen G. J Magn Reson. 2011; 210:137–140. [PubMed: 21393034]

54. Keshari KR, Kurhanewicz J, Macdonald JM, Wilson DM. Analyst. 2012; 137:3427–3429. [PubMed: 22655289]

55. Chattergoon N, Martinez-Santiesteban F, Handler WB, Ardenkjaer-Larsen JH, Scholl TJ. Contrast Media Mol Imaging. 2013; 8:57–62. [PubMed: 23109393]

56. Ragavan M, Chen HY, Sekar G, Hilty C. Anal Chem. 2011; 83:6054–6059. [PubMed: 21651293]

57. Bowen S, Hilty C. Phys Chem Chem Phys. 2010; 12:5766–5770. [PubMed: 20442947]

58. Hariharan R, Bray M, Ganim R, Doenst T, Goodwin GW, Taegtmeyer H. Circulation. 1995; 91:2435–2444. [PubMed: 7729031]

59. Runge VM, Ai T, Hao D, Hu X. Invest Radiol. 2011; 46:807–816. [PubMed: 22094366]

60. Magnusson P, Johansson E, Mansson S, Petersson JS, Chai CM, Hansson G, Axelsson O, Golman K. Magn Reson Med. 2007; 57:1140–1147. [PubMed: 17534914]

61. Olsson LE, Chai CM, Axelsson O, Karlsson M, Golman K, Petersson JS. Magn Reson Med. 2006; 55:731–737. [PubMed: 16538605]

62. Svensson J, Mansson S, Johansson E, Petersson JS, Olsson LE. Magn Reson Med. 2003; 50:256–262. [PubMed: 12876701]

63. Golman K, Ardenkjaer-Larsen JH, Petersson JS, Mansson S, Leunbach I. Proc Natl Acad Sci U S A. 2003; 100:10435–10439. [PubMed: 12930896]

64. von Morze C, Larson PE, Hu S, Yoshihara HA, Bok RA, Goga A, Ardenkjaer-Larsen JH, Vigneron DB. Magn Reson Imaging. 2012; 30:305–311. [PubMed: 22169407]

65. von Morze C, Bok RA, Sands JM, Kurhanewicz J, Vigneron DB. Am J Physiol Renal Physiol. 2012; 302:F1658–F1662. [PubMed: 22492940]

66. Kaewlai R, Abujudeh H. AJR Am J Roentgenol. 2012; 199:W17–W23. [PubMed: 22733927]

67. Laville M, Juillard L. J Nephrol. 2010; 23:387–398. [PubMed: 20349411]

68. Grant AK, Vinogradov E, Wang X, Lenkinski RE, Alsop DC. Magn Reson Med. 2011; 66:746–755. [PubMed: 21432901]

69. Reddy TJ, Iwama T, Halpern HJ, Rawal VH. J Org Chem. 2002; 67:4635–4639. [PubMed: 12098269]

70. Jannin S, Comment A, Kurdzesau F, Konter JA, Hautle P, van den Brandt B, van der Klink JJ. J Chem Phys. 2008; 128:241102. [PubMed: 18601309]

71. Lumata L, Ratnakar SJ, Jindal A, Merritt M, Comment A, Malloy C, Sherry AD, Kovacs Z. Chemistry. 2011; 17:10825–10827. [PubMed: 21919088]

72. Lumata L, Merritt M, Khemtong C, Ratnakar SJ, van Tol J, Yu L, Song L, Kovacs Z. RSC Adv. 2012; 2:12812–12817. [PubMed: 23205273]

73. Lumata LL, Merritt ME, Malloy CR, Sherry AD, van Tol J, Song L, Kovacs Z. J Magn Reson. 2013; 227:14–19. [PubMed: 23246650]

74. Kiesewetter MK, Corzilius B, Smith AA, Griffin RG, Swager TM. J Am Chem Soc. 2012; 134:4537–4540. [PubMed: 22372769]

75. Dane EL, Corzilius B, Rizzato E, Stocker P, Maly T, Smith AA, Griffin RG, Ouari O, Tordo P, Swager TM. J Org Chem. 2012; 77:1789–1797. [PubMed: 22304384]

76. Michaelis VK, Smith AA, Corzilius B, Haze O, Swager TM, Griffin RG. J Am Chem Soc. 2013; 135:2935–2938. [PubMed: 23373472]

77. Comment A, Van Den Brandt B, Uffmann K, Kurdzesau F, Jannin S, Konter J, Hautle P, Wenckebach W, Gruetter R, Van Der Klink J. Concepts Magn Reson Part B. 2007; 31:255–269.

78. Jensen PR, Karlsson M, Meier S, Duus JO, Lerche MH. Chemistry. 2009; 15:10010–10012. [PubMed: 19714690]

79. Harris T, Bretschneider C, Frydman L. J Magn Reson. 2011; 211:96–100. [PubMed: 21531156]

80. Lumata L, Kovacs Z, Malloy C, Sherry AD, Merritt M. Phys Med Biol. 2011; 56:N85–92. [PubMed: 21285486]

81. Lumata L, Merritt ME, Malloy CR, Sherry AD, Kovacs Z. J Phys Chem A. 2012; 116:5129–5138. [PubMed: 22571288]

82. Gabellieri C, Leach MO, Eykyn TR. Contrast Media Mol Imaging. 2009; 4:143–147. [PubMed: 19330792]

83. Wilson DM, Keshari KR, Larson PE, Chen AP, Hu S, Van Criekinge M, Bok R, Nelson SJ, Macdonald JM, Vigneron DB, Kurhanewicz J. J Magn Reson. 2010; 205:141–147. [PubMed: 20478721]

84. Schroeder MA, Atherton HJ, Ball DR, Cole MA, Heather LC, Griffin JL, Clarke K, Radda GK, Tyler DJ. FASEB J. 2009; 23:2529–2538. [PubMed: 19329759]

85. Keshari KR, Kurhanewicz J, Bok R, Larson PE, Vigneron DB, Wilson DM. Proc Natl Acad Sci U S A. 2011; 108:18606–18611. [PubMed: 22042839]

86. Bohndiek SE, Kettunen MI, Hu DE, Kennedy BW, Boren J, Gallagher FA, Brindle KM. J Am Chem Soc. 2011; 133:11795–11801. [PubMed: 21692446]

87. Hurd RE, Yen YF, Mayer D, Chen A, Wilson D, Kohler S, Bok R, Vigneron D, Kurhanewicz J, Tropp J, Spielman D, Pfefferbaum A. Magn Reson Med. 2010; 63:1137–1143. [PubMed: 20432284]

88. Yu YM, Kim JB, Lee KW, Kim SY, Han PL, Lee JK. Stroke. 2005; 36:2238–2243. [PubMed: 16141417]

89. Svensson J. Acta Radiol, Suppl. 2003; 429:1–30. [PubMed: 12757468]

90. Keshari KR, Wilson DM, Chen AP, Bok R, Larson PE, Hu S, Van Criekinge M, Macdonald JM, Vigneron DB, Kurhanewicz J. J Am Chem Soc. 2009; 131:17591–17596. [PubMed: 19860409]

91. Urano S, Iida M, Otani I, Matsuo M. Biochem Biophys Res Commun. 1987; 146:1413–1418. [PubMed: 3619937]

92. Cleland WW. Arch Biochem Biophys. 2005; 433:2–12. [PubMed: 15581561]

93. Khripach V, Zhabinskii V. Chem Rec. 2007; 7:265–274. [PubMed: 17924439]

94. Pan Y, Konermann L. Analyst. 2010; 135:1191–1200. [PubMed: 20498872]

95. Meier S, Jensen PR, Duus JO. FEBS Lett. 2011; 585:3133–3138. [PubMed: 21907715]

96. Westheimer FH. Chem Rev. 1961; 61:265–273.

97. Glad SS, Jensen F. J Am Chem Soc. 1997; 119:227–232.

98. Lee I. Chem Soc Rev. 1995; 24:223–229.

99. Storer JW, Raimondi L, Houk KN. J Am Chem Soc. 1994; 116:9675–9683.

100. Stutz J, Ezell MJ, FinlaysonPitts BJ. J Phys Chem A. 1997; 101:9187–9190.

101. Meier S, Karlsson M, Jensen PR, Lerche MH, Duus JO. Mol BioSyst. 2011; 7:2834–2836. [PubMed: 21720636]

102. Leadlay PF, Albery WJ, Knowles JR. Biochemistry. 1976; 15:5617–5620. [PubMed: 999836]

103. Pauwels EK, Ribeiro MJ, Stoot JH, McCready VR, Bourguignon M, Maziere B. Nucl Med Biol. 1998; 25:317–322. [PubMed: 9639291]

104. Glunde K, Bhujwalla ZM, Ronen SM. Nat Rev Cancer. 2011; 11:835–848. [PubMed: 22089420]

105. Sarkar R, Comment A, Vasos PR, Jannin S, Gruetter R, Bodenhausen G, Hall H, Kirik D, Denisov VP. J Am Chem Soc. 2009; 131:16014–16015. [PubMed: 19848401]

106. Agut J, Font E, Sacristan A, Ortiz JA. Arzneimittel-forschung. 1983; 33:1016–1018. [PubMed: 6684453]

107. Allouche-Arnon H, Gamliel A, Barzilay CM, Nalbandian R, Gomori JM, Karlsson M, Lerche MH, Katz-Brull R. Contrast Media Mol Imaging. 2011; 6:139–147. [PubMed: 21698772]

108. Johnson RJ, Perez-Pozo SE, Sautin YY, Manitius J, Sanchez-Lozada LG, Feig DI, Shafiu M, Segal M, Glassock RJ, Shimada M, Roncal C, Nakagawa T. Endocr Rev. 2009; 30:96–116. [PubMed: 19151107]

109. Lim JS, Mietus-Snyder M, Valente A, Schwarz JM, Lustig RH. Nat Rev Gastroenterol Hepatol. 2010; 7:251–264. [PubMed: 20368739]

110. Zamora-Leon SP, Golde DW, Concha II, Rivas CI, Delgado-Lopez F, Baselga J, Nualart F, Vera JC. Proc Natl Acad Sci U S A. 1996; 93:1847–1852. [PubMed: 8700847]

111. Allouche-Arnon H, Wade T, Waldner LF, Miller VN, Gomori JM, Katz-Brull R, McKenzie CA. Contrast Media Mol Imaging. 2013; 8:72–82. [PubMed: 23109395]

112. Meier S, Solodovnikova N, Jensen PR, Wendland J. ChemBioChem. 2012; 13:2265–2269. [PubMed: 22961998]

113. Becker A, Kabsch W. J Biol Chem. 2002; 277:40036–40042. [PubMed: 12163496]

114. Wegener G, Krause U. Biochem Soc Trans. 2002; 30:264–270. [PubMed: 12023862]

115. Teusink B, Passarge J, Reijenga CA, Esgalhado E, van der Weijden CC, Schepper M, Walsh MC, Bakker BM, van Dam K, Westerhoff HV, Snoep JL. Eur J Biochem. 2000; 267:5313–5329. [PubMed: 10951190]

116. Yen KE, Bittinger MA, Su SM, Fantin VR. Oncogene. 2010; 29:6409–6417. [PubMed: 20972461]

117. Daye D, Wellen KE. Semin Cell Dev Biol. 2012; 23:362–369. [PubMed: 22349059]

118. Gallagher FA, Kettunen MI, Day SE, Lerche M, Brindle KM. Magn Reson Med. 2008; 60:253–257. [PubMed: 18666104]

119. Qu W, Zha Z, Lieberman BP, Mancuso A, Stetz M, Rizzi R, Ploessl K, Wise D, Thompson C, Kung HF. Acad Radiol. 2011; 18:932–939. [PubMed: 21658976]

120. Barb AW, Hekmatyar SK, Glushka JN, Prestegard JH. J Magn Reson. 2013; 228:59–65. [PubMed: 23357427]

121. Koelsch BL, Keshari KR, Peeters TH, Larson PE, Wilson DM, Kurhanewicz J. Analyst. 2013; 138:1011–1014. [PubMed: 23304699]

122. Zagdoun A, Rossini AJ, Conley MP, Gruning WR, Schwarzwalder M, Lelli M, Franks WT, Oschkinat H, Coperet C, Emsley L, Lesage A. Angew Chem Int Ed. 2013; 52:1222–1225.

123. Johansson E, Mansson S, Wirestam R, Svensson J, Petersson JS, Golman K, Stahlberg F. Magn Reson Med. 2004; 51:464–472. [PubMed: 15004786]

124. Pocker Y, Meany JE, Nist BJ, Zadorojn C. J Phys Chem. 1969; 73:2879–2882.

125. Doura T, Hata R, Nonaka H, Ichikawa K, Sando S. Angew Chem Int Ed. 2012; 51:10114–10117.

126. Feng Y, Davis RM, Warren WS. Nat Phys. 2012; 8:831–837. [PubMed: 23505397]

127. Pileio G, Carravetta M, Levitt MH. Proc Natl Acad Sci U S A. 2010; 107:17135–17139. [PubMed: 20855584]

128. Laustsen C, Pileio G, Tayler MC, Brown LJ, Brown RC, Levitt MH, Ardenkjaer-Larsen JH. Magn Reson Med. 2012; 68:1262–1265. [PubMed: 22851334]

129. Gallagher FA, Kettunen MI, Brindle KM. NMR Biomed. 2011; 24:1006–1015. [PubMed: 21812047]

130. Dickinson BC, Peltier J, Stone D, Schaffer DV, Chang CJ. Nat Chem Biol. 2011; 7:106–112. [PubMed: 21186346]

131. Rautio J, Kumpulainen H, Heimbach T, Oliyai R, Oh D, Jarvinen T, Savolainen J. Nat Rev Drug Discovery. 2008; 7:255–270.

132. Hilty C, Bowen S. Org Biomol Chem. 2010; 8:3361–3365. [PubMed: 20556296]

133. Bowen S, Hilty C. Anal Chem. 2009; 81:4543–4547. [PubMed: 19388628]

134. Zeng H, Lee Y, Hilty C. Anal Chem. 2010; 82:8897–8902. [PubMed: 20942386]

135. Akke M. Biochem Soc Trans. 2012; 40:419–423. [PubMed: 22435823]

136. Calle LP, Canada FJ, Jimenez-Barbero J. Nat Prod Rep. 2011; 28:1118–1125. [PubMed: 21487589]

137. Jenkins BG. Life Sci. 1991; 48:1227–1240. [PubMed: 2002752]

138. Bellia F, La Mendola D, Pedone C, Rizzarelli E, Saviano M, Vecchio G. Chem Soc Rev. 2009; 38:2756–2781. [PubMed: 19690752]

139. Warburg O. Science. 1956; 123:309–314. [PubMed: 13298683]

140. Warburg O, Wind F, Negelein E. J Gen Physiol. 1927; 8:519–530. [PubMed: 19872213]

141. Cairns RA, Harris IS, Mak TW. Nat Rev Cancer. 2011; 11:85–95. [PubMed: 21258394]

142. Ward PS, Thompson CB. Cancer Cell. 2012; 21:297–308. [PubMed: 22439925]

143. Theorell H, Chance B. Acta Chem Scand. 1951; 5:1127–1144.

144. Witney TH, Kettunen MI, Brindle KM. J Biol Chem. 2011; 286:24572–24580. [PubMed: 21596745]

145. Bonen A. Eur J Appl Physiol. 2001; 86:6–11. [PubMed: 11820324]

146. Halestrap AP, Price NT. Biochem J. 1999; 343(Pt 2):281–299. [PubMed: 10510291]

147. Garcia CK, Goldstein JL, Pathak RK, Anderson RG, Brown MS. Cell. 1994; 76:865–873. [PubMed: 8124722]

148. Harris T, Eliyahu G, Frydman L, Degani H. Proc Natl Acad Sci U S A. 2009; 106:18131–18136. [PubMed: 19826085]

149. Hertz L, Dienel GA. J Neurosci Res. 2005; 79:11–18. [PubMed: 15586354]

150. Manning Fox JE, Meredith D, Halestrap AP. J Physiol. 2000; 529(Pt 2):285–293. [PubMed: 11101640]

151. Ganapathy V, Thangaraju M, Prasad PD. Pharmacol Ther. 2009; 121:29–40. [PubMed: 18992769]

152. Keshari KR, Sriram R, Koelsch BL, Van Criekinge M, Wilson DM, Kurhanewicz J, Wang ZJ. Cancer Res. 2013; 73:529–538. [PubMed: 23204238]

153. Keshari KR, Kurhanewicz J, Jeffries RE, Wilson DM, Dewar BJ, Van Criekinge M, Zierhut M, Vigneron DB, Macdonald JM. Magn Reson Med. 2010; 63:322–329. [PubMed: 20099325]

154. Ward CS, Venkatesh HS, Chaumeil MM, Brandes AH, Vancriekinge M, Dafni H, Sukumar S, Nelson SJ, Vigneron DB, Kurhanewicz J, James CD, Haas-Kogan DA, Ronen SM. Cancer Res. 2010; 70:1296–1305. [PubMed: 20145128]

155. Day SE, Kettunen MI, Gallagher FA, Hu DE, Lerche MH, Wolber J, Golman K, Ardenkjaer-Larsen JH, Brindle KM. Nat Med. 2007; 13:1382–1387. [PubMed: 17965722]

156. Albers MJ, Bok R, Chen AP, Cunningham CH, Zierhut ML, Zhang VY, Kohler SJ, Tropp J, Hurd RE, Yen YF, Nelson SJ, Vigneron DB, Kurhanewicz J. Cancer Res. 2008; 68:8607–8615. [PubMed: 18922937]

157. Schroeder MA, Cochlin LE, Heather LC, Clarke K, Radda GK, Tyler DJ. Proc Natl Acad Sci U S A. 2008; 105:12051–12056. [PubMed: 18689683]

158. Lau AZ, Chen AP, Hurd RE, Cunningham CH. NMR Biomed. 2011; 24:988–996. [PubMed: 21751271]

159. Dodd MS, Ball DR, Schroeder MA, Le Page LM, Atherton HJ, Heather LC, Seymour AM, Ashrafian H, Watkins H, Clarke K, Tyler DJ. Cardiovasc Res. 2012; 95:69–76. [PubMed: 22593200]

160. Ushio-Fukai M, Nakamura Y. Cancer Lett. 2008; 266:37–52. [PubMed: 18406051]

161. Balendiran GK, Dabur R, Fraser D. Cell Biochem Funct. 2004; 22:343–352. [PubMed: 15386533]

162. Morgan B, Ezerina D, Amoako TN, Riemer J, Seedorf M, Dick TP. Nat Chem Biol. 2013; 9:119–125. [PubMed: 23242256]

163. Linster CL, Van Schaftingen E. FEBS J. 2007; 274:1–22. [PubMed: 17222174]

164. Keshari KR, Sai V, Wang ZJ, Vanbrocklin HF, Kurhanewicz J, Wilson DM. J Nucl Med. 2013; 54:922–928. [PubMed: 23575993]

165. Kohler SJ, Yen Y, Wolber J, Chen AP, Albers MJ, Bok R, Zhang V, Tropp J, Nelson S, Vigneron DB, Kurhanewicz J, Hurd RE. Magn Reson Med. 2007; 58:65–69. [PubMed: 17659629]

166. Lee P, Leong W, Tan T, Lim M, Han W, Radda GK. Hepatology. 2013; 57:515–524. [PubMed: 22911492]

167. Merritt ME, Harrison C, Sherry AD, Malloy CR, Burgess SC. Proc Natl Acad Sci U S A. 2011; 108:19084–19089. [PubMed: 22065779]

168. Hu S, Balakrishnan A, Bok RA, Anderton B, Larson PE, Nelson SJ, Kurhanewicz J, Vigneron DB, Goga A. Cell Metab. 2011; 14:131–142. [PubMed: 21723511]

169. Karlsson M, Jensen PR, in't Zandt R, Gisselsson A, Hansson G, Duus JO, Meier S, Lerche MH. Int J Cancer. 2010; 127:729–736. [PubMed: 19960440]

170. Butt SA, Sogaard LV, Magnusson PO, Lauritzen MH, Laustsen C, Akeson P, Ardenkjaer-Larsen JH. J Cereb Blood Flow Metab. 2012; 32:1508–1514. [PubMed: 22453630]

171. Zhou ZH, McCarthy DB, O'Connor CM, Reed LJ, Stoops JK. Proc Natl Acad Sci U S A. 2001; 98:14802–14807. [PubMed: 11752427]

172. Merritt M, Harrison C, Storey C, Jeffrey FM, Sherry AD, Malloy CR. Proc Natl Acad Sci U S A. 2007; 104:19773–19777. [PubMed: 18056642]

173. Merritt ME, Harrison C, Storey C, Sherry AD, Malloy CR. Magn Reson Med. 2008; 60:1029–1036. [PubMed: 18956454]

174. Atherton HJ, Dodd MS, Heather LC, Schroeder MA, Griffin JL, Radda GK, Clarke K, Tyler DJ. Circulation. 2011; 123:2552–2561. [PubMed: 21606392]

175. Hu S, Yoshihara HA, Bok R, Zhou J, Zhu M, Kurhanewicz J, Vigneron DB. Magn Reson Imaging. 2012; 30:1367–1372. [PubMed: 22819176]

176. Dodd MS, Ball V, Bray R, Ashrafian H, Watkins H, Clarke K, Tyler DJ. J Cardiovasc Magn Reson. 2013; 15:19. [PubMed: 23414451]

177. Chen AP, Hurd RE, Schroeder MA, Lau AZ, Gu YP, Lam WW, Barry J, Tropp J, Cunningham CH. NMR Biomed. 2012; 25:305–311. [PubMed: 21774012]

178. Jitrapakdee S, St Maurice M, Rayment I, Cleland WW, Wallace JC, Attwood PV. Biochem J. 2008; 413:369–387. [PubMed: 18613815]

179. Liu YQ, Han J, Epstein PN, Long YS. Am J Physiol Endocrinol Metab. 2005; 288:E471–478. [PubMed: 15507531]

180. Martin RB. Biopolymers. 1998; 45:351–353.

181. Kilshtain AV, Warshel A. Proteins. 2009; 77:536–550. [PubMed: 19480013]

182. Bouchelouche K, Choyke PL, Capala J. Discov Med. 2010; 9:55–61. [PubMed: 20102687]

183. Rahn KA, Watkins CC, Alt J, Rais R, Stathis M, Grishkan I, Crainiceau CM, Pomper MG, Rojas C, Pletnikov MV, Calabresi PA, Brandt J, Barker PB, Slusher BS, Kaplin AI. Proc Natl Acad Sci U S A. 2012; 109:20101–20106. [PubMed: 23169655]

184. Ghosh A, Heston WD. J Cell Biochem. 2004; 91:528–539. [PubMed: 14755683]

185. Jamin Y, Gabellieri C, Smyth L, Reynolds S, Robinson SP, Springer CJ, Leach MO, Payne GS, Eykyn TR. Magn Reson Med. 2009; 62:1300–1304. [PubMed: 19780183]

186. Oda Y. Pathol Int. 1999; 49:921–937. [PubMed: 10594838]

187. Lee KK, Workman JL. Nat Rev Mol Cell Biol. 2007; 8:284–295. [PubMed: 17380162]

188. Chen AP, Hurd RE, Gu YP, Wilson DM, Cunningham CH. NMR Biomed. 2011; 24:514–520. [PubMed: 21674653]

189. Ferrannini E. Metabolism. 1988; 37:287–301. [PubMed: 3278194]

190. Stocchi V, Magnani M, Canestrari F, Dacha M, Fornaini G. J Biol Chem. 1982; 257:2357–2364. [PubMed: 7061426]

191. Cao X, Bloomston M, Zhang T, Frankel WL, Jia G, Wang B, Hall NC, Koch RM, Cheng H, Knopp MV, Sun D. Clin Cancer Res. 2008; 14:1831–1839. [PubMed: 18347186]

192. Podo F. NMR Biomed. 1999; 12:413–439. [PubMed: 10654290]

193. Ackerstaff E, Glunde K, Bhujwalla ZM. J Cell Biochem. 2003; 90:525–533. [PubMed: 14523987]

194. Keshari KR, Tsachres H, Iman R, Delos Santos L, Tabatabai ZL, Shinohara K, Vigneron DB, Kurhanewicz J. NMR Biomed. 2011; 24:691–699. [PubMed: 21793074]

195. Miyake T, Parsons SJ. Oncogene. 2012; 31:1431–1441. [PubMed: 21822308]

196. Gallagher FA, Kettunen MI, Hu D-E, Jensen PR, in't Zandt R, Karlsson M, Gisselsson A, Nelson SK, Witney TH, Bohndiek SE, Hansson G, Peitersen T, Lerche MH, Brindle KM. Proc Natl Acad Sci U S A. 2009; 106:19801–19806. [PubMed: 19903889]

197. Tripp BC, Smith K, Ferry JG. J Biol Chem. 2001; 276:48615–48618. [PubMed: 11696553]

198. Supuran CT. Nat Rev Drug Discovery. 2008; 7:168–181.

199. Gillies RJ, Galons JP, McGovern KA, Scherer PG, Lien YH, Job C, Ratcliff R, Chapa F, Cerdan S, Dale BE. NMR Biomed. 1993; 6:95–104. [PubMed: 8457432]

200. Mancuso A, Fernandez EJ, Blanch HW, Clark DS. Biotechnology. 1990; 8:1282–1285. [PubMed: 1366962]

201. Macdonald JM, Grillo M, Schmidlin O, Tajiri DT, James TL. NMR Biomed. 1998; 11:55–66. [PubMed: 9608589]

202. DeBerardinis RJ, Mancuso A, Daikhin E, Nissim I, Yudkoff M, Wehrli S, Thompson CB. Proc Natl Acad Sci U S A. 2007; 104:19345–19350. [PubMed: 18032601]

203. Jeffries RE, Gamcsik MP, Keshari KR, Pediaditakis P, Tikunov AP, Young GB, Lee H, Watkins PB, Macdonald JM. Tissue Eng Part C. 2013; 19:93–100.

204. Hutchinson L, Kirk R. Nat Rev Clin Oncol. 2011; 8:189–190. [PubMed: 21448176]

205. Begley CG, Ellis LM. Nature. 2012; 483:531–533. [PubMed: 22460880]

206. Keshari KR, Sriram R, Van Criekinge M, Wilson DM, Wang ZJ, Vigneron DB, Peehl DM, Kurhanewicz J. Prostate. 2013; 73:1171–1181. [PubMed: 23532911]

207. Harrison C, Yang C, Jindal A, DeBerardinis RJ, Hooshyar MA, Merritt M, Dean Sherry A, Malloy CR. NMR Biomed. 2012; 25:1286–1294. [PubMed: 22451442]

208. Zierhut ML, Yen YF, Chen AP, Bok R, Albers MJ, Zhang V, Tropp J, Park I, Vigneron DB, Kurhanewicz J, Hurd RE, Nelson SJ. J Magn Reson. 2010; 202:85–92. [PubMed: 19884027]

209. Larson PE, Kerr AB, Reed GD, Hurd RE, Kurhanewicz J, Pauly JM, Vigneron DB. IEEE Trans Med Imaging. 2012; 31:265–275. [PubMed: 22027366]

210. Gallagher FA, Kettunen MI, Hu DE, Jensen PR, Zandt RI, Karlsson M, Gisselsson A, Nelson SK, Witney TH, Bohndiek SE, Hansson G, Peitersen T, Lerche MH, Brindle KM. Proc Natl Acad Sci U S A. 2009; 106:19801–19806. [PubMed: 19903889]

211. Brindle KM, Bohndiek SE, Gallagher FA, Kettunen MI. Magn Reson Med. 2011; 66:505–519. [PubMed: 21661043]

212. Viale A, Aime S. Curr Opin Chem Biol. 2010; 14:90–96. [PubMed: 19913452]

213. Hurd RE, Yen YF, Chen A, Ardenkjaer-Larsen JH. J Magn Reson Imaging. 2012; 36:1314–1328. [PubMed: 23165733]

214. Witney TH, Kettunen MI, Day SE, Hu DE, Neves AA, Gallagher FA, Fulton SM, Brindle KM. Neoplasia. 2009; 11:574–582. 571. following 582. [PubMed: 19484146]

215. Tyler DJ. Curr Cardiovasc Imaging Rep. 2011; 4:108–115. [PubMed: 21475403]

216. Chaumeil MM, Ozawa T, Park I, Scott K, James CD, Nelson SJ, Ronen SM. Neuroimage. 2012; 59:193–201. [PubMed: 21807103]

217. Schroeder MA, Ali MA, Hulikova A, Supuran CT, Clarke K, Vaughan-Jones RD, Tyler DJ, Swietach P. Proc Natl Acad Sci U S A. 2013; 110:E958–E967. [PubMed: 23431149]

218. Martinovich GG, Martinovich IV, Cherenkevich SN, Sauer H. Cell Biochem Biophys. 2010; 58:75–83. [PubMed: 20676800]

219. Schafer FQ, Buettner GR. Free Radical Biol Med. 2001; 30:1191–1212. [PubMed: 11368918]

220. Ardenkjaer-Larsen JH, Laustsen C, Pullinger B, Kadlecek SJ, Emami K, Rizi RR. Proc Intl Soc Mag Reson Med 19 Montreal Canada. 2011

221. Chiavazza E, Kubala E, Gringeri CV, Duwel S, Durst M, Schulte RF, Menzel MI. J Magn Reson. 2013; 227:35–38. [PubMed: 23262330]

222. Merritt ME, Harrison C, Mander W, Malloy CR, Sherry AD. J Magn Reson. 2007; 189:280–285. [PubMed: 17945520]

223. Jensen PR, Meier S, Ardenkjaer-Larsen JH, Duus JO, Karlsson M, Lerche MH. Chem Commun. 2009:5168–5170.

224. Jensen PR, Peitersen T, Karlsson M, In't Zandt R, Gisselsson A, Hansson G, Meier S, Lerche MH. J Biol Chem. 2009; 284:36077–36082. [PubMed: 19861411]

225. Hu S, Zhu M, Yoshihara HA, Wilson DM, Keshari KR, Shin P, Reed G, von Morze C, Bok R, Larson PE, Kurhanewicz J, Vigneron DB. Magn Reson Imaging. 2011; 29:1035–1040. [PubMed: 21855243]

226. Colombo Serra S, Karlsson M, Giovenzana GB, Cavallotti C, Tedoldi F, Aime S. Contrast Media Mol Imaging. 2012; 7:469–477. [PubMed: 22821881]

227. Chen AP, Kurhanewicz J, Bok R, Xu D, Joun D, Zhang V, Nelson SJ, Hurd RE, Vigneron DB. Magn Reson Imaging. 2008; 26:721–726. [PubMed: 18479878]

228. Bowen S, Hilty C. Angew Chem Int Ed. 2008; 47:5235–5237.

229. Gore, JC.; Kennan, RP. Magn Reson Imaging. 3. Stark, DD.; Bradley, WG., editors. Vol. 1. Mosby; St. Louis: 1999.

## Biographies



**Kayvan R. Keshari**

Kayvan R. Keshari is an Assistant Attending in the Department of Radiology and Assistant Member in the Molecular Pharmacology and Chemistry Program at Memorial Sloan-Kettering Cancer Center (MSKCC). He received his bachelor's degrees in Biochemistry and Applied Mathematics from the University of California, Berkeley in 2003. He completed his PhD in 2009 under Professor J. M. Macdonald in Biomedical Engineering at the University of North Carolina, Chapel Hill. He then moved to the University of California, San Francisco and completed a post-doctoral training in Cancer Metabolic Imaging in the Departments of Radiology and Bioengineering and Therapeutic Sciences under the supervision of Professor J. Kurhanewicz. He has authored over 20 manuscripts and 3 patents in metabolism, with a focus on hyperpolarized MR. His research focuses on the development of imaging approaches and bioengineered systems to study cancer metabolism, particularly in the realm of hyperpolarized MR and oxidative stress.



**David M. Wilson**

David M. Wilson is an Assistant Professor in the Department of Radiology and Biomedical Engineering at University of California, San Francisco (UCSF) where he is an attending radiologist in the neuroradiology section. He received his BS in biochemistry from Harvard University in 1997, and finished his MD-PhD training in 2004 working under Professor Ronald Breslow in the Columbia University Department of Chemistry. His clinical training including both residency in general radiology and fellowship in neuroradiology were completed at UCSF in 2010 at which time he joined the faculty. David has published 15 peer-reviewed papers on hyperpolarized $^{13}$C spectroscopy since 2009 and has patents on two new hyperpolarized agents. His work focuses on developing new $^{13}$C probes, comparing them to their $^{11}$C and $^{18}$F correlates used in positron emission tomography, and understanding their biochemical mechanisms.
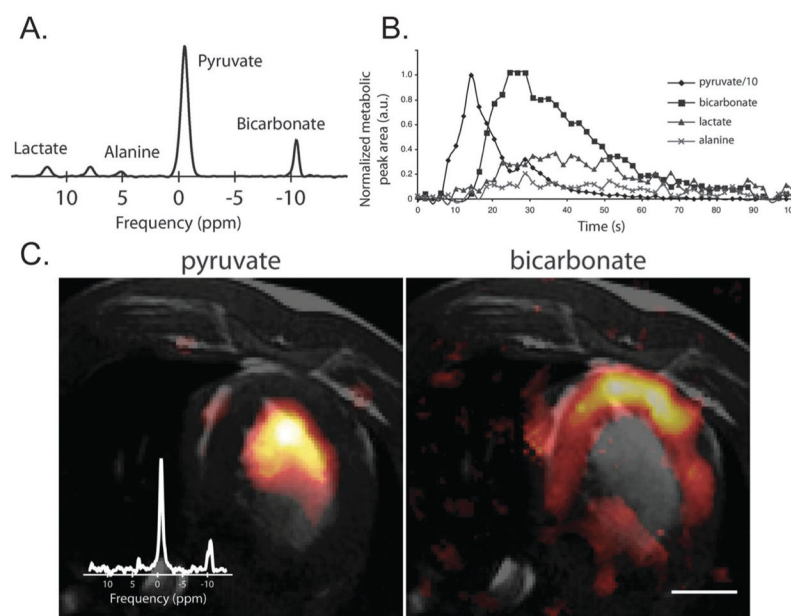
**Fig. 1.**
(A) Single $^{13}C$ spectrum acquired following injection of 15 ml of HP [1-$^{13}C$] pyruvate at 3 T in a porcine heart. The pyruvate was injected at a constant rate from 0 to 15 s. (B) To generate the time course, spectra were acquired every 2 s using a 10° flip angle and a 10 cm slice. The peak height plot demonstrates the time course of pyruvate delivery and lactate, alanine and bicarbonate labeling. (C) Axial $T_2$-weighted $^1H$ image depicting the porcine heart with color overlays reconstructed from MRSI data. Cardiac-gated data demonstrate the spatial distribution of pyruvate and bicarbonate in a single 10 mm axial slice. The inset spectrum is a sum over all magnitude spectra. The scale bar indicates 2 cm. The color scale for both images ranges from 15 to 100% of the image intensity maximum. Adapted from ref. 46.
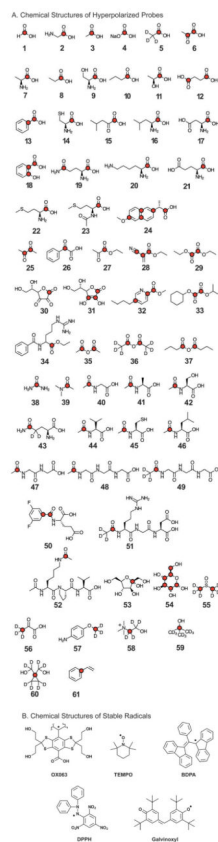
**Fig. 2.**
(A) Chemical structures of compounds that have been HP. Long-$T_1$ nuclei (those without directly attached $^1$H) that have been studied by DNP-NMR are labeled. These correspond to Table 3. (B) Chemical structures of stable organic free radicals used for hyperpolarization.
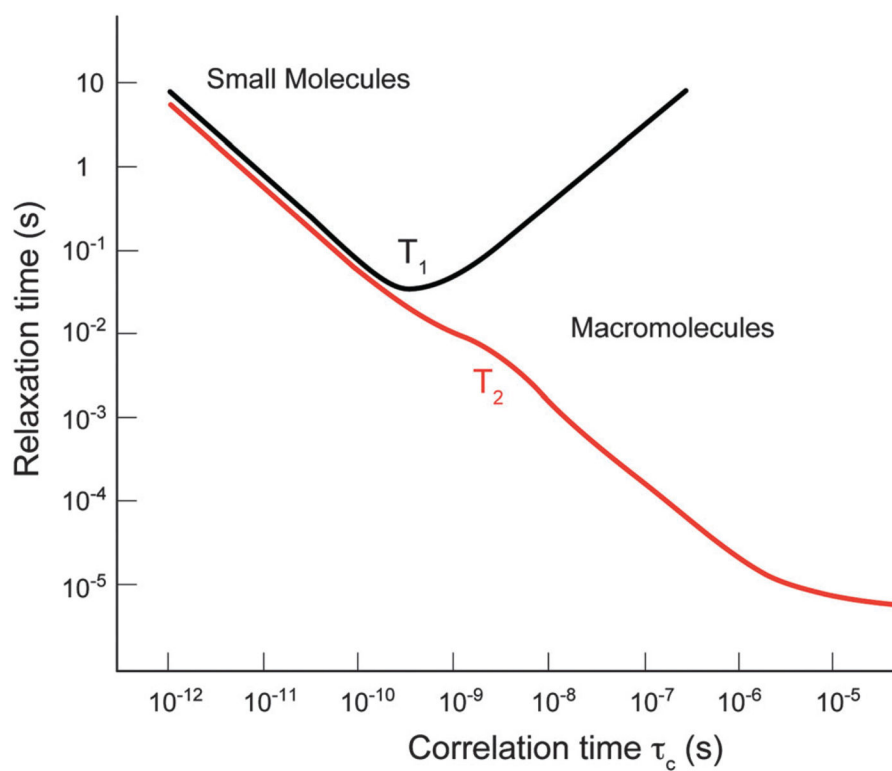
**Fig. 3.**
Plot of relaxation time *versus* correlation time ($\tau_c$) demonstrates the expected changes in $T_1$ and $T_2$ relaxation with molecule size. Adapted from ref. 229.
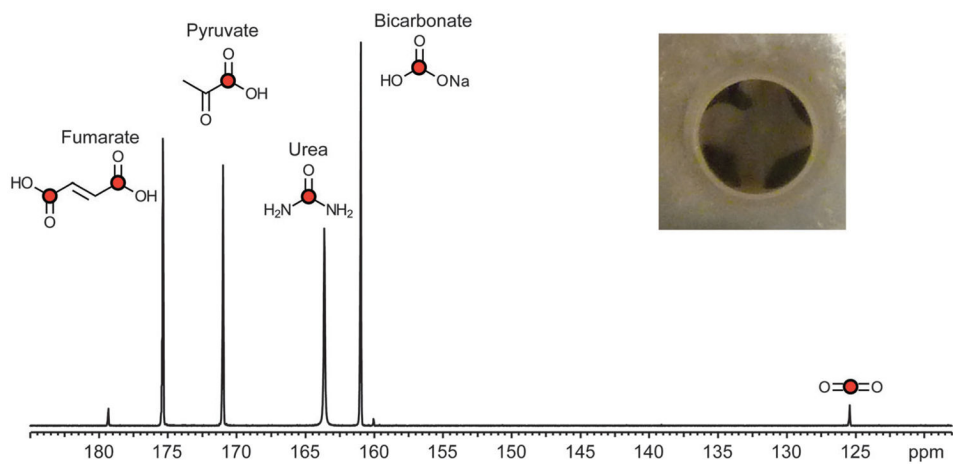
**Fig. 4.**
Multi-compound polarization demonstrates the simultaneous dissolution of [1-$^{13}$C] pyruvate, $^{13}$C-bicarbonate, $^{13}$C-urea, [1,4-$^{13}$C$_2$] fumarate at 11.7 T. The inlay image is a top down view of a standard sample cup with all 4 compound preparations frozen together prior to placement in the hyperpolarizer. Adapted from ref. 83.
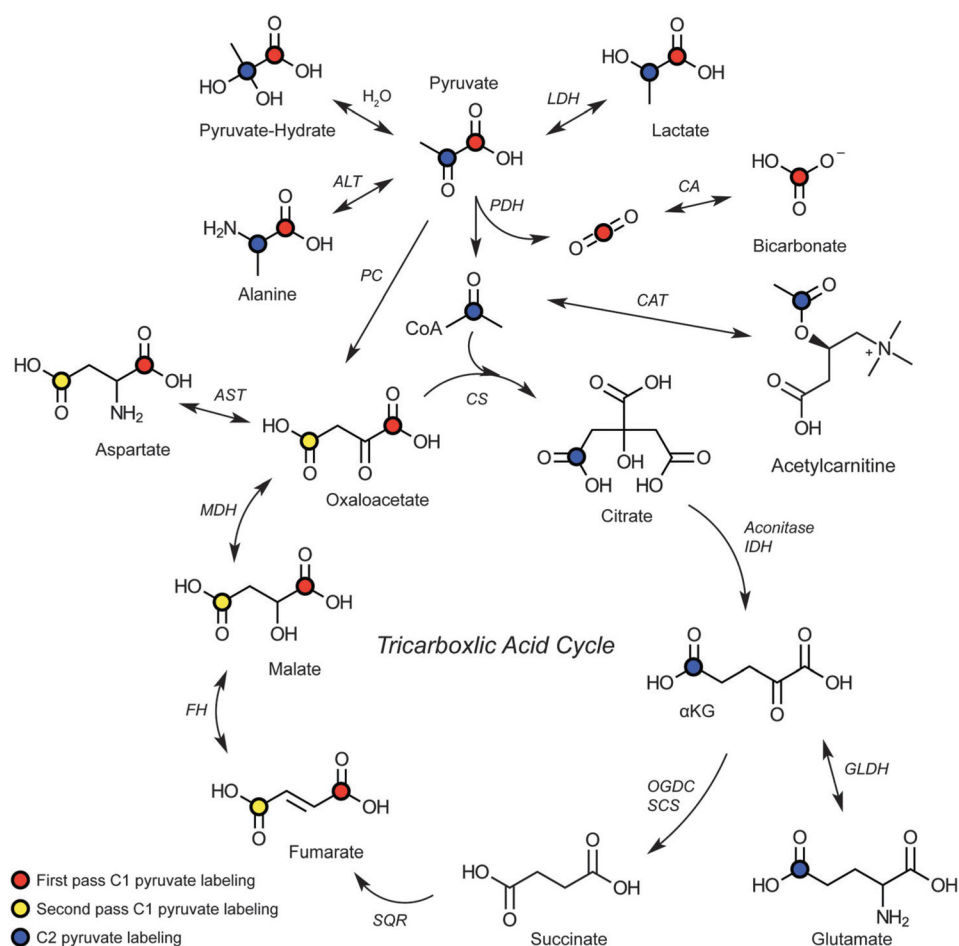
**Fig. 5.**
Biochemical scheme of labeling resulting from the injection of HP pyruvate. Carbons that have been observed *via* metabolism of HP substrates are labeled. Red dots indicate labeling from the C1 of pyruvate in the first pass of metabolism. Yellow dots indicate the fate of the C1 carbon if it were to enter through pyruvate carboxylase and progress backward to fumarate. At this point, the label can scramble due to symmetry. The blue dots indicate the labeled intermediates derived from metabolism of C2 pyruvate. TCA has been abbreviated for the purposes of clarity, though the necessary enzymes are listed and cofactors have been omitted. Abbreviations: LDH – lactate dehydrogenase (EC 1.1.2.4), ALT – alanine transaminase (EC 2.6.1.2), CA – carbonic anhydrase (EC 4.2.1.1), PDH – pyruvate dehydrogenase complex (EC 1.2.4.1, 2.3.1.12 and 1.8.1.4), CAT – carnitine *o*-acetyltransferase (EC 2.3.1.7), PC – pyruvate carboxylase (EC 6.4.1.1), CS – citrate synthase (EC 2.3.3.1), aconitase (EC 4.2.1.3), IDH – isocitrate dehydrogenase (EC 1.1.1.42), OGDC – oxoglutarate dehydrogenase complex (EC 1.2.4.2), SCS – succinyl coenzyme A synthetase (EC 6.2.1.4), SQR – succinate dehydrogenase (EC 1.3.5.1), FH – fumarate hydratase (EC 4.2.1.2), MDH – malate dehydrogenase (EC 1.1.1.37), AST – aspartate transaminase (EC 2.6.1.1), GLDH – glutamate dehydrogenase (EC 1.4.1.2). CoA – coenzyme A.
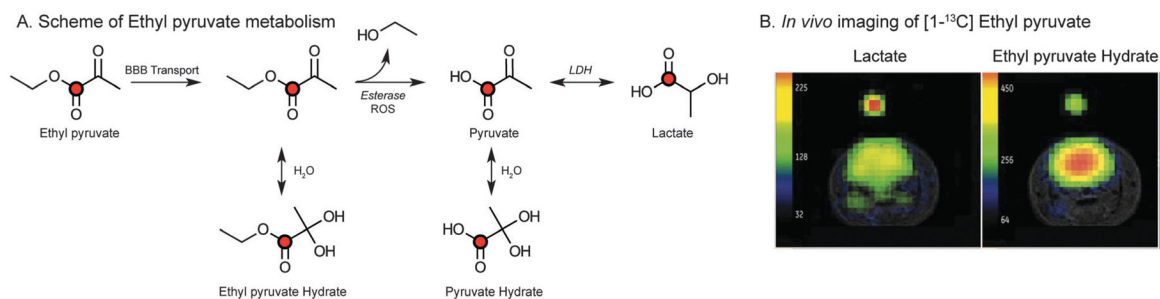
**Fig. 6.**

(A) Scheme of transport across the blood brain barrier (BBB) and subsequent metabolism of ethyl pyruvate. Ethyl pyruvate can be hydrolyzed by either esterases or reactive oxygen species (ROS). LDH – lactate dehydrogenase. (B) Representative axial imaging of a normal rat brain demonstrating the distribution of HP ethyl pyruvate hydrate and subsequent lactate generated at 3 T. HP images are overlaid on standard $T_2$-weighted anatomic images. Adapted from ref. 87.
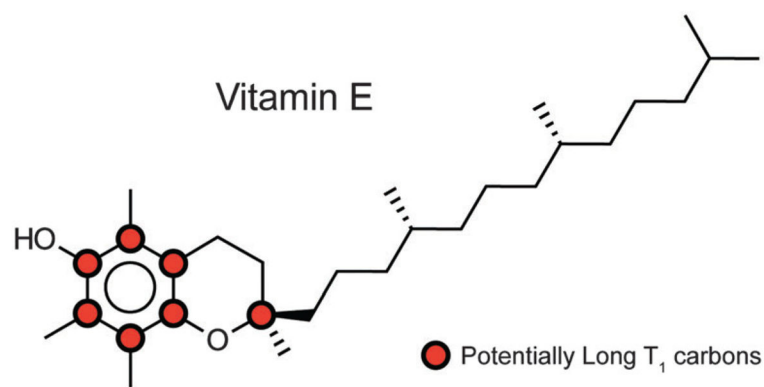
**Fig. 7.**
Chemical structure of tocopherol (vitamin E) demonstrating carbons with long $T_1$s for potential labeling and hyperpolarization. These carbons are indicated by the red dots.
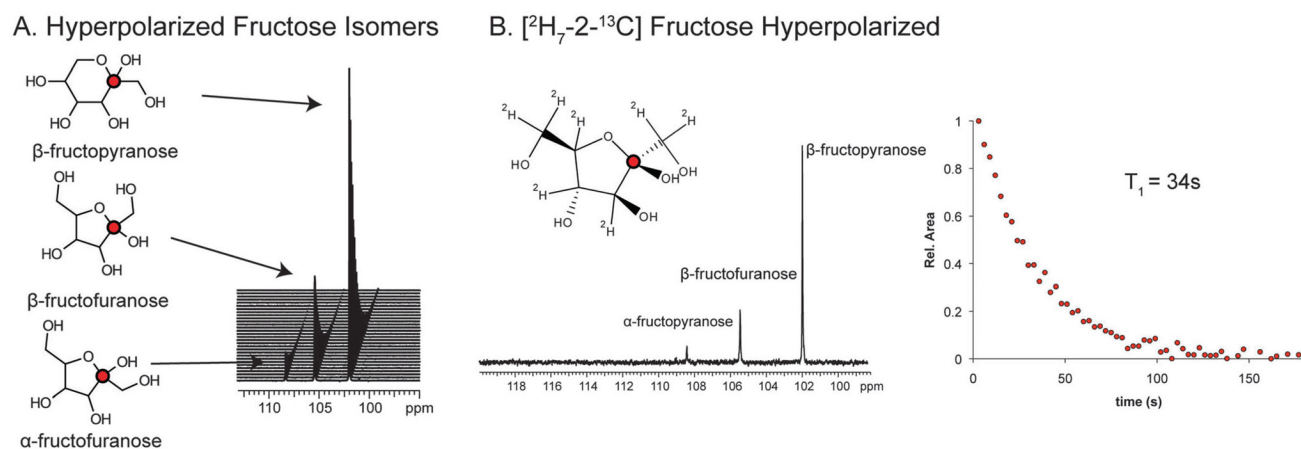
**Fig. 8.**
(A) Chemical structures of fructose isomers with accompanying HP resonances. HP [2-$^{13}$C] fructose was dissolved in 1× phosphate buffered saline (PBS, pH = 7.6) to a concentration of 5 mM. The dynamic spectra were acquired on an 11.7 T with a temporal resolution of 3 s and flip angle of 5°. Adapted from ref. 90. (B) Chemical structure of the furanose isomer of fructose uniformly deuterated with a HP spectrum acquired on 10 mM fructose in PBS (pH = 7.5) using a flip angle of 5°. Corresponding apparent $T_1$ decay of the HP signal is shown at the right, nearly 34 s in solution.
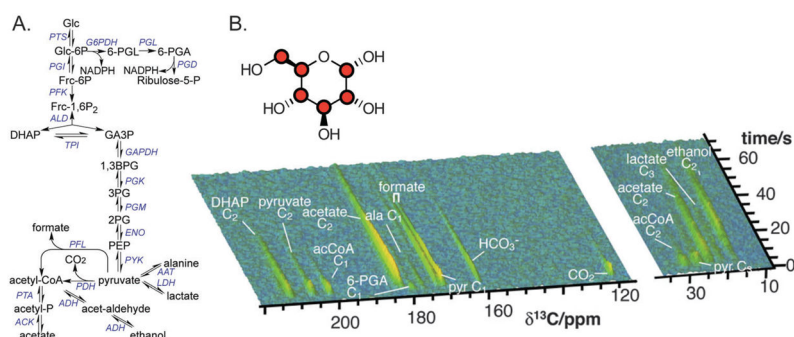
**Fig. 9.**
(A) Overview of metabolism observed in *Escherichia coli* interrogated using HP [U-$^{13}$C, U-$^{2}$H] glucose. The reactions of glycolysis, the pentose phosphate shunt, and fermentation are displayed. These pathways are nearly identical to those observed in yeast (*Saccharomyces cerevisiae*). (B) Time-resolved HP $^{13}$C NMR spectra recorded every 0.5 s demonstrating generation of $^{13}$C metabolites in real time. The overall signal decreases with loss of hyperpolarization. Adapted from ref. 95. Abbreviations: 1,3BPG – 1,3 bisphosphoglycerate, 2PG – 2-phosphoglycerate, 3PG – 3-phosphoglycerate, 6-PG – 6-phosphogluconate, 6-PGL – 6-phospho-  -gluconolactone, AAT – alanine aminotransferase (EC 2.6.1.2), Ac – acetate, Ac-CoA – acetyl-CoA, ACK –acetyl kinase (EC 2.7.2.1), ADH – alcohol dehydrogenase (EC 1.1.1.1), ALD – aldolase (EC 4.1.2.13), DHAP – dihydroxyacetone phosphate, ENO – enolase (EC 4.2.1.11), Frc-1,6P$_2$ – fructose-1,6-bisphosphate, Frc-6P – fructose-6phosphate, G6PDH – glucose-6-phosphate dehydrogenase (EC 1.1.1.49), GA3P – glyceraldehyde 3-phosphate, GAPDH – glyceraldehydes-3-phosphate dehydrogenase (EC 1.2.1.12), Glc – glucose, Glc-6P – glucose-6phosphate, LDH – lactate dehydrogenase (EC 1.1.1.27), PDC – pyruvate decarboxylase (EC 4.1.1.1), PEP – phosphoenolpyruvate, PFL – pyruvate formate lyase (EC 2.3.1.54), PFK – phosphofructokinase (EC 2.7.1.11), PGD – 6-phosphogluconate dehydrogenase (EC 1.1.1.43), PGL – 6-phosphogluconate lactonase (EC 3.1.1.31), PGK – phosphoglycerate kinase (EC 2.7.2.3), PGM – phosphoglycerate mutase (EC 5.4.2.1), PTA – phosphotransacetylase (EC 2.3.1.8), PTS –glucose-specific enzyme II of the phosphotransferase system (2.7.1.63), Pyr – pyruvate, PYK – pyruvate kinase (EC 2.7.1.40), TPI – triosephosphate isomerase (EC 5.3.1.1).
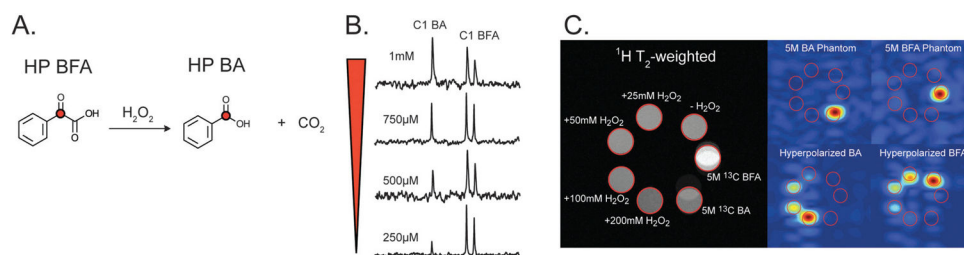
**Fig. 10.**
(A) Reaction scheme of HP [2-$^{13}$C] benzoylformic acid (BFA) reaction with $H_2O_2$ to form HP [1-$^{13}$C] benzoic acid (BA). (B) With increasing concentrations of $H_2O_2$, a proportional amount of HP BA is formed. These spectra were acquired with a single 90° pulse after incubation of HP BFA with $H_2O_2$ at 11.7 T. (C) Phantom images of 5 M thermally polarized $^{13}$C BFA in $H_2O$, 5 M thermally polarized $^{13}$C BA in DMA, and 20 mM HP $^{13}$C BFA in 100 mM phosphate, 0.3 mM EDTA buffered at pH 7.8 with 0, 25, 50, 100, and 200 mM $H_2O_2$. HP Images were acquired after ~37 s of reaction with $H_2O_2$ with a TR = 150 ms, FOV $40 \times 40 \times 40$ mm, $16 \times 12 \times 12$ matrix, and zero-filled to a final resolution of 1.25 mm isotropic, at 14 T. Adapted from ref. 35.
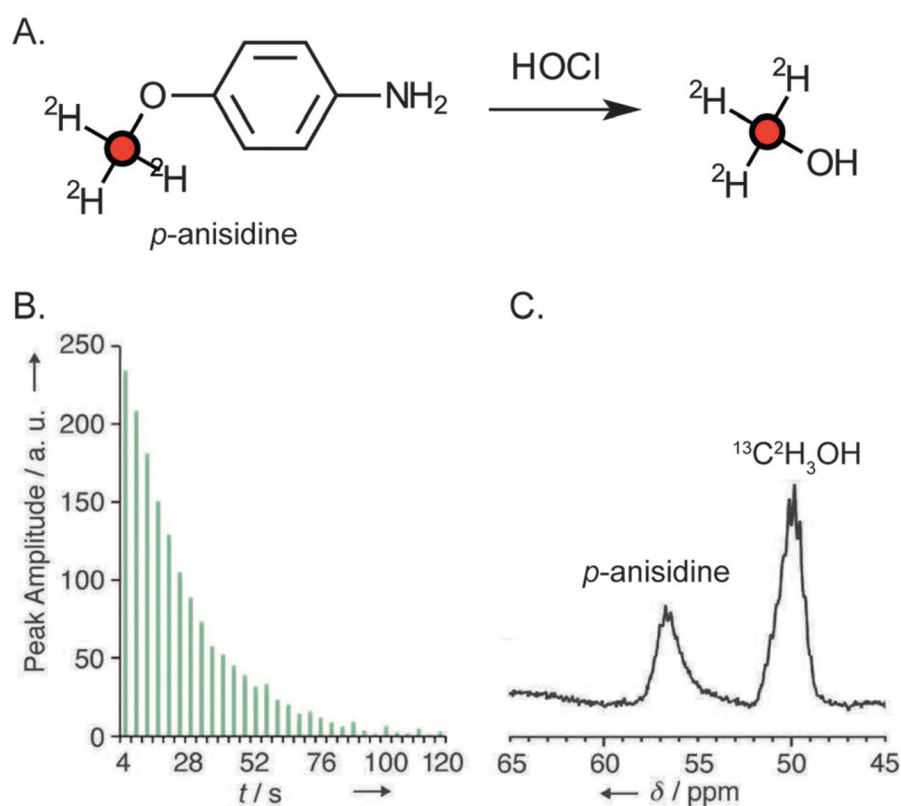
**Fig. 11.**
(A) Reaction of [$^{13}$C,D$_3$]-*p*-anisidine with hypochlorous acid (HOCl), resulting in liberation of deuterated methanol. (B) Time-resolved $^{13}$C NMR spectra of a 1.7 mM solution of HP [$^{13}$C,D$_3$]-*p*-anisidine acquired every 4 seconds, using a 18° tip angle. The calculated $T_1$ for this probe was 44.4 s (9.4 T, 37 °C). (C) $^{13}$C NMR spectrum of HP [$^{13}$C,D$_3$]-*p*-anisidine acquired 4 s after addition of HOCl (final concentration 20 mM), using a 90° tip angle. Adapted from ref. 125.
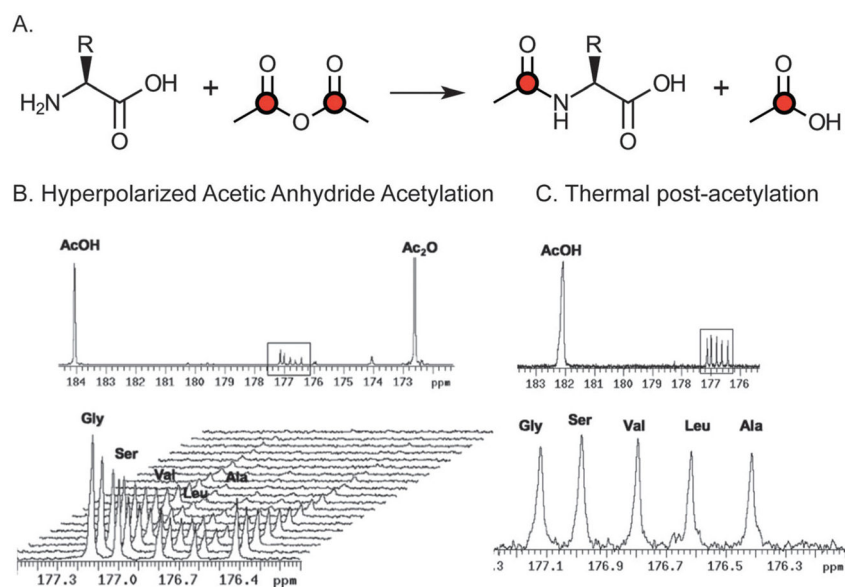
**Fig. 12.**
(A) General strategy for secondary hyperpolarization of amino acids using prepolarized [1,1-$^{13}$C] acetic anhydride. Red dots indicate HP carbons. (B) HP spectrum obtained when a buffered solution (100 mM phosphate, pH 7.8) containing the amino acids gly, ser, val, leu, ala (3.5 mM amino acid) is reacted with a 2-fold excess of HP acetic anhydride at 11.7 T. (B, top) Full spectrum ($t = 0$) including large peaks corresponding to unreacted acetic anhydride and hydrolysis product acetic acid, and acetylated amino acid products (outlined). (B, bottom) Dynamic HP spectrum with resolved acetylated amino acid products. (C) Thermal spectrum corresponding to the HP data in B. (C, top) After addition of Magnevist Gd-chelate to a final concentration of 5 mM, the only peaks observed correspond to [1-$^{13}$C] AcOH and the previously observed acetylated amino acid products (outlined). (C, bottom) Expanded region of interest in the $^{13}$C spectrum. Adapted from ref. 40.
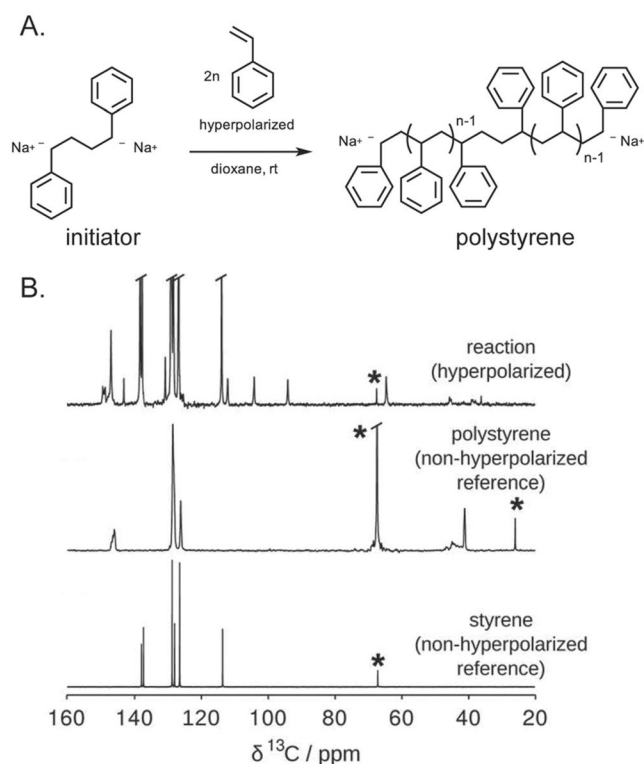
**Fig. 13.**
(A) Anionic polymerization using HP styrene. This scheme shows the propagation of polystyrene from bifunctional initiator in dioxane. (B) HP $^{13}$C NMR spectrum obtained when HP styrene is mixed with $NaC_{10}H_8$ initiator compared to the non-HP $^{13}$C spectra obtained for the synthesized polystyrene and for the styrene monomer. The * labels signify dioxane and THF resonances. A large number of peaks are observed in the HP $^{13}$C spectrum during polymer formation, which are not seen in the reference spectra obtained at thermal equilibrium. Correlation experiments with selective spin inversion were used to identify the chemical shifts of these reaction intermediates unambiguously. Adapted from ref. 41.
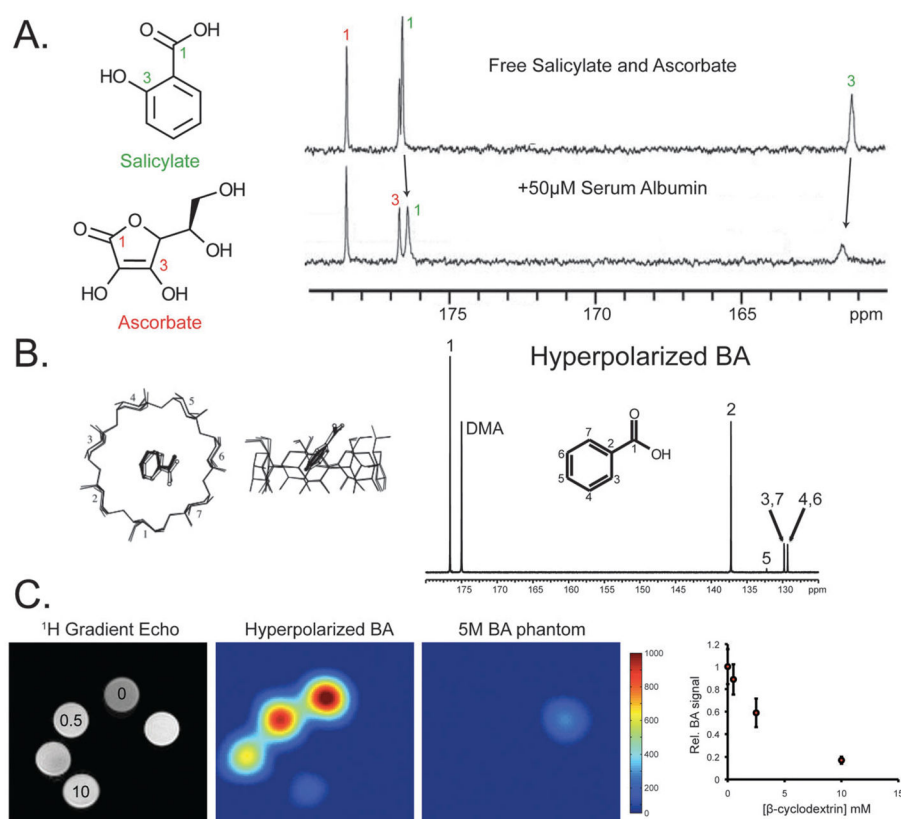
**Fig. 14.**

(A) Spectra of 200 mM HP salicylate and ascorbate at natural $^{13}$C isotopic abundance injected into buffer and into solutions of 50 mM human serum albumin at 9.4 T. Spectra are recorded 2 s after injections. $^{13}$C signals of the salicylate are detected in the binding reaction and show attenuated signal amplitude, line broadening and shift changes. Adapted from ref. 38. (B) Structure of the β-cyclodextrin–benzoic acid complex, as solved by X-ray crystallography and $^{13}$C NMR spectrum of natural abundance HP benzoic acid, obtained in a single 5° pulse at 36.4 mM (310 K, pH 7.8) at 11.7 T. All carbons are observed: C1-176.6 ppm, C2-137.3 ppm, C3,C7-129.8 ppm, C4,C6-129.3 ppm and C5-132.2 ppm. (C) HP $^{13}$C MR imaging experiment conducted at 14 T. (C, left) $^{1}$H imaging shows the orientation of tubes containing variable β-cyclodextrin concentration (0–10 mM final concentration). Also included is a [1-$^{13}$C] benzoic acid phantom (5 M). The HP $^{13}$C MR imaging study was performed using a 3D frequency-selective sequence after administration of HP [1-$^{13}$C] benzoic acid (final concentration 2.5 mM), and demonstrates loss of signal corresponding with increasing [β-cyclodextrin]. (C, right) Plot of HP [1-$^{13}$C] benzoic acid MR signals observed with variable [β-cyclodextrin], quantified for the imaging experiment. Adapted from ref. 54.
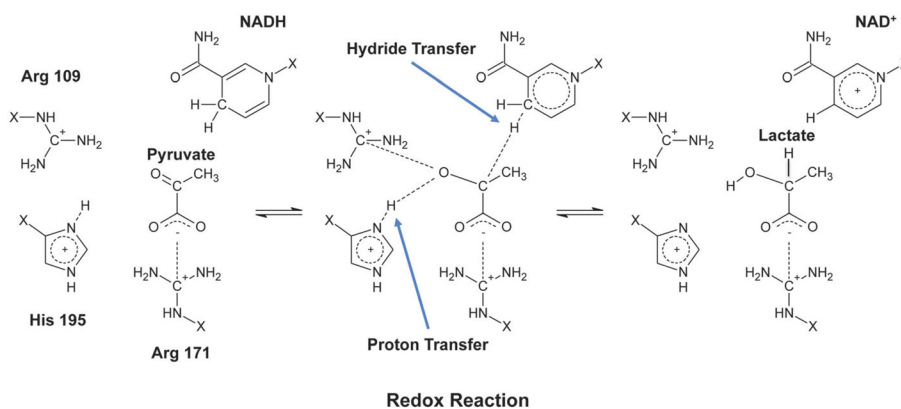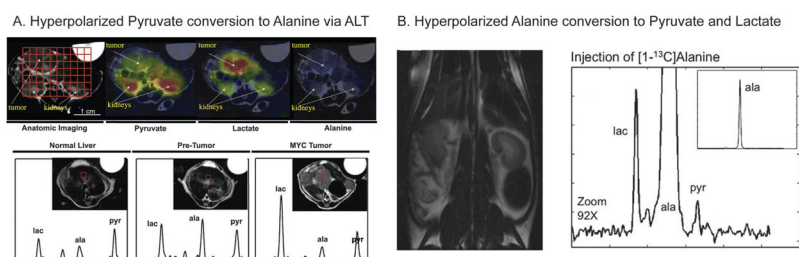
**Fig. 15.**
Lactate dehydrogenase (LDH) enzymatic conversion of pyruvate to lactate. The hydride transfer from nicotinamide adenine dinucleotide (NADH) is shown in the enzyme pocket. Amino acids are shown abbreviated with –X to simplify the scheme.

A. Hyperpolarized Pyruvate conversion to Alanine via ALT

B. Hyperpolarized Alanine conversion to Pyruvate and Lactate

**Fig. 16.**

(A, top) HP images acquired post-injection of 80 mM [1-$^{13}$C] pyruvate in a myc inducible transgenic model of liver cancer at 3 T. Color overlay maps from spectroscopic grids show clear differences in metabolic profiles between liver tumors and other tissues. (A, bottom) HP imaging of varying stages in tumor induction. Images demonstrate changes in metabolic profile during Myc-driven tumor formation. High pyruvate is detected in normal liver. Elevated alanine is associated with pretumor liver with modest MYC induction but no apparent phenotypic changes. A substantial increase in lactate is seen in developed tumor masses. Adapted from ref. 168. (B) $T_2$-Weighted coronal image derived from a normal rat with corresponding representative $^{13}$C spectrum post-injection of [1-$^{13}$C] alanine. Resonances corresponding to pyruvate and lactate are observed. Adapted from ref. 225.

## Generation of Hyperpolarized Bicarbonate in the heart
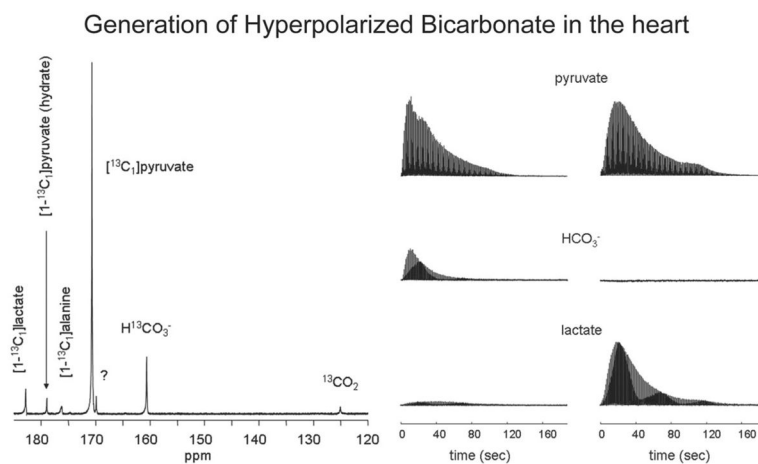


**Fig. 17.**

(left) $^{13}C$ NMR spectrum of an isolated rat heart at 14 T. The summed spectrum (100 consecutive scans) demonstrates resonances for $CO_2$, $HCO_3$, pyruvate, lactate, alanine, and pyruvate hydrate. (right) Stacked plot of $^{13}C$ NMR spectra from hearts supplied with [1-$^{13}C$] pyruvate. Each resonance is a single scan showing the dynamic production of each metabolite. The left column is from a heart supplied with [1-$^{13}C$] pyruvate, while the right was also incubated with octanoate. Adapted from ref. 172.
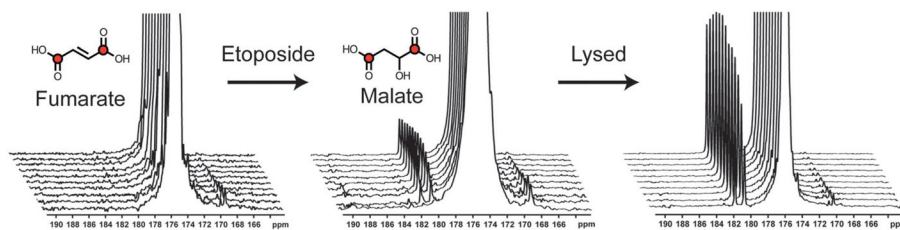
**Fig. 18.**
$^{13}$C spectra acquired over a period of 1 min after injection of HP [1,4-$^{13}$C$_2$] fumarate into suspensions of intact murine lymphoma cells (5 × 10$^7$ cells), cells treated with etoposide for 16 h and lysed cells. (B) Cells 16 h after etoposide treatment. Increased malate is observed with increased necrosis. Adapted from ref. 210.
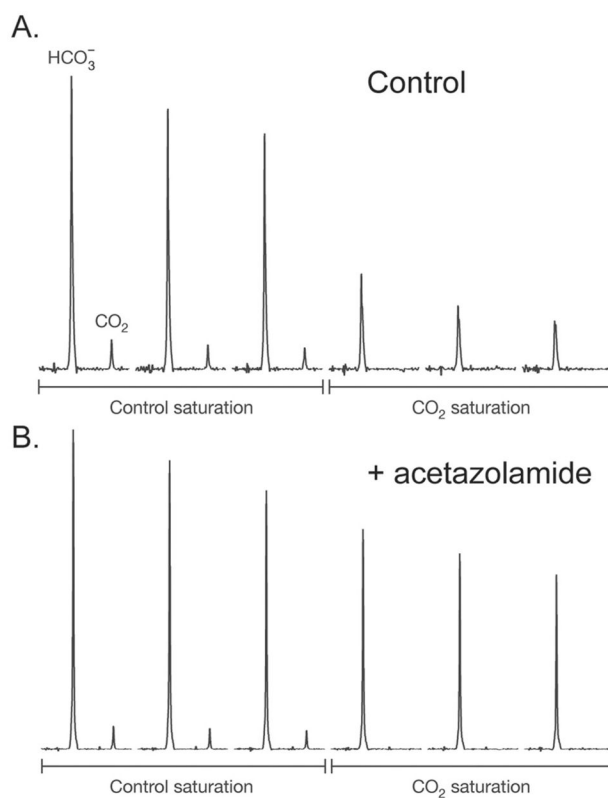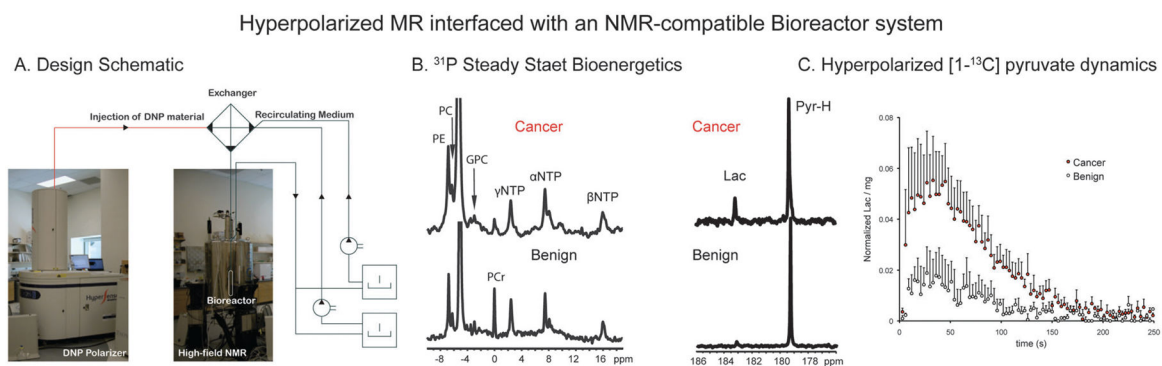
**Fig. 19.**
*In vivo* saturation experiment demonstrating that $^{13}C$ $HCO_3^-$ and $^{13}C$ $CO_2$ are in rapid chemical exchange, catalyzed by carbonic anhydrase. (A) Spectra acquired from a EL4 lymphoma tumor using a surface coil with a control saturation (first three spectra) and $^{13}C$ $CO_2$ saturation (second three spectra). (B) Identical experiment, but the mouse was treated with acetazolamide, a carbonic anhydrase inhibitor. Adapted from ref. 37.

Hyperpolarized MR interfaced with an NMR-compatible Bioreactor system

A. Design Schematic

B. $^{31}$P Steady Staet Bioenergetics

C. Hyperpolarized [1-$^{13}$C] pyruvate dynamics



**Fig. 20.**
(A) Design schematic for NMR-compatible bioreactor system, including interface between a DNP polarizer and high-field NMR magnet (11.7 T). (B) $^{31}$P spectra from living human malignant and benign tissue slice cultures (TSCs) perfused in a 10 mm NMR-compatible bioreactor. (C) Representative single $^{13}$C spectrum taken at 90 s post-injection of HP [1-$^{13}$C] pyruvate in the bioreactor with benign (*N* = 4) or malignant TSCs (*N* = 4) and accompanying average HP lactate dynamics for TSCs. Significantly increased lactate is observed in malignant prostate TSCs as compared to benign. PCr –phosphocreatine, PC – phosphocholine, PE – phosphoethanolamine, GPC – glycerophosphocholine, α,β,γ-NTPs – nucleotide triphosphates. Adapted from ref. 206.

HP $^{13}$C DHA *in vivo* conversion to Vitamin C
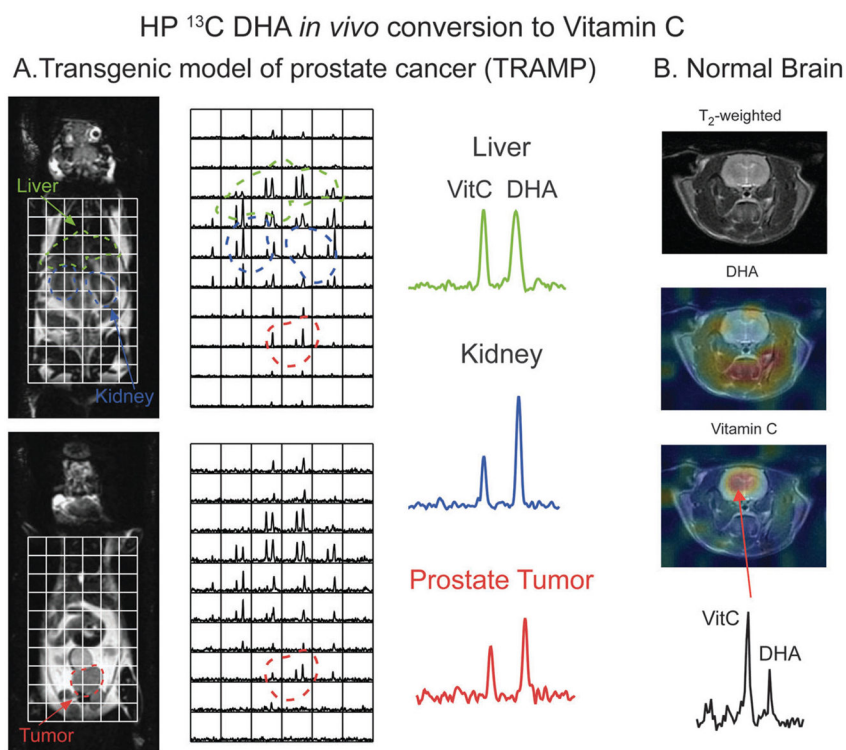
**Fig. 21.**
(A) Sequential coronal $T_2$-weighted images and corresponding $^{13}$C 3D MRSI demonstrating distribution of HP DHA and vitamin C (VitC) in a TRAMP mouse post intravenous injection of 350 μL of 15 mM HP [1-$^{13}$C] DHA at 3 T. The liver and kidneys are best seen in (A, top) and prostate tumor in (A, bottom), but both imaging slices contain significant amounts of liver, kidney, and tumor tissue. Regions of liver, kidney, and prostate tumor are segmented and superimposed on the spectral grid (color-coded dashed lines). Differences in metabolite ratios are seen between normal organs and between prostate tumor and normal surrounding tissues with representative spectra from liver, kidney, and prostate tumor. (B) Axial $T_2$-weighted images and corresponding color overlays of HP DHA and vitamin C (VitC) signal in a normal rat brain. Adapted from ref. 85.
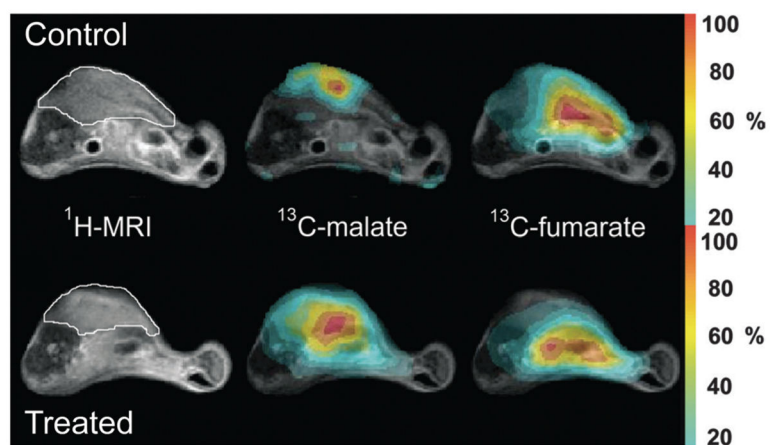
**Fig. 22.**
Representative axial images from untreated and etoposide-treated mice with implanted lymphoma tumors. Color overlays demonstrate increased total malate produced in etoposide treated mice in comparison to untreated tumors. Adapted from ref. 210.

**Table 1**

NMR active nuclei typically used for biomedical applications

| Nuclei | $m$ (spin) | Natural abundance (%) | $\gamma$ (rel to $^1$H) | $\delta$ (ppm) | $T_1$ range | Example biomedical application |
|---|---|---|---|---|---|---|
| $^1$H | 1/2 | 99.98 | 1 | 13 | 0.1–2 s | Total body MRI and MRSI |
| $^2$H | 1 | 0.02 | 0.1535 | 13 | <1 s | Metabolic tracer injection using MRSI |
| $^{13}$C | 1/2 | 1.11 | 0.2515 | 200 | 0.1–100 s | Metabolic tracer injection using MRSI |
| $^{15}$N | 1/2 | 0.37 | 0.1013 | 900 | 0.1–400 s | Metabolic tracer injection using MRSI |
| $^{17}$O | 5/2 | 0.04 | 0.1355 | 1160 | 5–50 ms | Oxidative metabolism using MRSI |
| $^{19}$F | 1/2 | 100.00 | 0.9409 | 700 | 0.1–1 s | Tracer injection of therapies using MRSI |
| $^{23}$Na | 3/2 | 100.00 | 0.2645 | 72 | 10–50 ms | Neurodegeneration and cardiac using MRI |
| $^{31}$P | 1/2 | 100.00 | 0.4048 | 430 | 0.05–2 s | Bioenergetics and pH using MRSI |

MRI – magnetic resonance imaging, MRSI – magnetic resonance spectroscopic imaging, $m$ – quantum spin number, $\gamma$ – gyromagnetic ratio, $\delta$ – chemical shift.
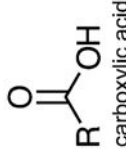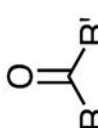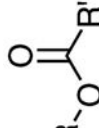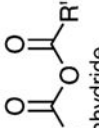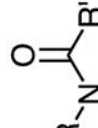
**Table 2**

Nuclei that have been HP using the dissolution dynamic nuclear polarization method (DNP)

| HP nuclei | Natural abundance (%) | $\gamma$ (rel to $^1$H) | Example molecules | Example $T_1$'s (field strength) |
|---|---|---|---|---|
| $^1$H | 99.98 | 1 | $H_2O$ | 3.7 s (4.7 T)[220] |
| $^{13}$C | 1.11 | 0.2515 | Fructose, urea | 13 s (11.7 T)[90]–85 s (3 T)[221] |
| $^{15}$N | 0.37 | 0.1013 | choline | 189 s–390 s (7 T)[105] |
| $^{29}$Si | 4.70 | 0.1987 | Nano-particles | 100–10 000 s (2.9 T)[28] |
| $^{89}$Yi | 100.00 | 0.17605 | DOTA chelates | 264–620 s (14.1 T)[29] |

**Table 3**

Chemical structures of HP probes

| Chemical structure | Index | HP agent | MW (Da) | Apparent $T_1$ (s) | Application | Ref. |
|---|---|---|---|---|---|---|
|  carboxylic acid | 1 | $^{13}C$ sodium formate | 69 | NR | C | 222 |
| | 2 | [1-$^{13}C$] glycine | 76 | 50 (9.4 T) | C | 78 |
| | 3 | [1-$^{13}C$] sodium acetate | 83 | 40 (9.4 T); 46 (14.1 T) | A, C | 121, 223 and 224 |
| | 4 | $^{13}C$-sodium bicarbonate | 85 | 49 (11.7 T); 50 (3 T); 34 (3 T) | A, C | 83 and 177 |
| carboxylic acid | 5 | [1-$^{13}C$, $^2H_3$] sodium acetate | 86 | 50 (14.1 T) | C | 121 |
| | 6 | [1-$^{13}C$] pyruvic acid | 89 | 67 (3 T); 48 (11.7 T); 44 (14.1 T) | A, B, C | 83 and 121 |
| | 6 | C$_1$ of [1,2-$^{13}C$] pyruvic acid | 90 | 56 (3 T) | A, C | 177 |
| | 7 | [1-$^{13}C$] alanine | 90 | 42 (3 T); 29 (9.4 T) | A, C | 78 and 225 |
| | 8 | [1-$^{13}C$] sodium proprionate | 97 | NR | A, C | 224 |
| | 9 | [1-$^{13}C$] serine | 106 | 23 (9.4 T) | C | 78 |
| | 6 | [1-$^{13}C$] sodium pyruvate | 111 | NR | C | 80 |
| | 10 | [1-$^{13}C$] sodium butyrate | 111 | 43 (14.1 T) | C | 226 |
| | 11 | [1-$^{13}C$] sodium lactate | 113 | 45, 50.6 (3 T); 32, 33.4 (14.1 T) | A, C | 52 and 227 |
| | 12 | [1,4-$^{13}C_2$] fumaric acid | 118 | 24 (9.4 T); 29 (11.7 T) | A, B, C | 83 and 196 |
| | 13 | C$_1$ of benzoic acid | 122 | 35 (11.7 T) | C | 54 |
| | 14 | [1-$^{13}C$] cysteine | 122 | 30 (9.4 T) | C | 78 |
| | 13 | [1-$^{13}C$] benzoic acid | 123 | 35 (11.7 T) | C | 54 |
| | 15 | [1-$^{13}C$] ketoisocaproic acid | 131 | 55 (9.4 T) | A, C | 169 |
| | 16 | [1-$^{13}C$] leucine | 132 | 24 (9.4 T) | C | 78 |
| | 17 | [1-$^{13}C$] aspartic acid | 134 | 29 (9.4 T) | C | 78 |
| | 18 | C$_1$ of salicylic acid | 138 | NR | C | 38 |
| | 19 | [1-$^{13}C$] glutamine | 147 | 25 (9.4 T) | C | 78 |
| | 20 | [1-$^{13}C$] lysine | 147 | 26 (9.4 T) | C | 78 |
| | 21 | [1-$^{13}C$] glutamate | 148 | 26 (9.4 T); 34 (9.4 T) FG | A, C | 78 |
| | 22 | [1-$^{13}C$] methionine | 150 | 17 (9.4 T) | C | 78 |
| | 23 | [1-$^{13}C$] $N$-acetyl-methionine | 192 | 28 (3 T) | A, B, C | 188 |

| Chemical structure | Index | HP agent | MW (Da) | Apparent $T_1$ (s) | Application | Ref. |
|---|---|---|---|---|---|---|
| | 4 | $^{13}$C-cesium bicarbonate | 195 | NR | A, C | 37 |
| | 24 | 2-Napthaleneacetic acid-6-methoxy-α-methyl (NA) | 230 | 15 (11.7 T) | C | 54 |
| | 25 | [2,3-$^{13}$C$_2$] diacetyl | 88 | 30 (7 T) | C | 39 |
| | 6 | [2-$^{13}$C] pyruvic acid | 89 | NR | B, C | 84 |
| | 6 | C2 of [1,2-$^{13}$C$_2$] pyruvic acid | 90 | 44 (3 T) | A, C | 177 |
| ketone | 26 | [2-$^{13}$C] benzoylformic acid | 151 | 24 (11.7 T); 19 (14.1 T) | C | 35 |
| | 27 | [1-$^{13}$C] ethyl pyruvate | 117 | 45 (3 T) | A, C | 87 |
| | 28 | Ethyl-2-cyanoacrylate (NA) | 125 | NR | C | 132 |
| | 29 | [1,1'-$^{13}$C$_2$] diethyl oxalate | 148 | 22 (8.4 T) | C | 126 |
| ester | 30 | [1-$^{13}$C] dehydroascorbic acid | 175 | 56 (3 T); 21 (9.4 T); 21 (11.7 T) | A, B, C | 85 and 86 |
| | 31 | C$_1$ of ascorbic acid (NA) | 176 | NR | C | 38 |
| | 31 | [1-$^{13}$C] ascorbic acid | 177 | 29 (3 T); 16 (9.4 T); 16 (11.7 T) | A, B, C | 85 and 86 |
| | 32 | Methyl fusarate (NA) | 193 | NR | C | 132 |
| | 33 | Cyclohexyl-isopropyl-1,2-$^{13}$C$_2$-oxalate-$^2$H$_{18}$ | 234 | 54 (4.7 T) | C | 128 |
| | 34 | Nα-benzoyl-L-arginine-ethyl ester | 306 | NR | C | 228 |
| anhydride | 35 | [1,1'-$^{13}$C$_2$] acetic anhydride | 104 | 34 (11.7 T); 45,50 (14.1 T) | C | 40 |
| | 36 | [1,1'-$^{13}$C$_2$, $^2$H$_6$] acetic anhydride | 110 | NR | C | 121 |
| | 37 | [1,1'-$^{13}$C$_2$] butyric anhydride | 160 | 39,40 (14.1 T) | C | 226 |
| | 38 | $^{13}$C-urea | 61 | 44 (11.7 T); 35 (14.1 T) | A, C | 83 |
| | 39 | Dimethyl acetamide (NA) | 87 | NR | C | 85 |
| | 40 | N-[Acetyl-1-$^{13}$C] glycine | 118 | 15 (11.7 T); 17 (14.1 T) | C | 40 |
| amide | 41 | N-[Acetyl-1-$^{13}$C] alanine | 132 | 15 (11.7 T) | C | 40 |
| | 19 | [5-$^{13}$C] glutamine | 145 | 16 (9.4 T) | B, C | 118 |
| | 42 | N-[Acetyl-1-$^{13}$C] serine | 148 | 11 (11.7 T) | C | 40 |
| | 43 | [5-$^{13}$C, 4-$^2$H$_2$] glutamine | 149 | 33 (9.4 T) | B, C | 40 |
| | 44 | N-[Acetyl-1-$^{13}$C] valine | 160 | 10 (11.7 T) | C | 40 |

| Chemical structure | Index | HP agent | MW (Da) | Apparent $T_1$ (s) | Application | Ref. |
|---|---|---|---|---|---|---|
| | 45 | N-[Acetyl-1-$^{13}$C] cysteine | 164 | NR | C | 40 |
| | 46 | N-[Acetyl-1-$^{13}$C] leucine | 174 | 9 (11.7 T) | C | 40 |
| | 47 | N-[Acetyl-1-$^{13}$C] gly-gly | 175 | 10 (11.7 T) | C | 40 |
| | 48 | N-[Acetyl-1-$^{13}$C] triglycine | 232 | 9 (11.7 T) | C | 40 |
| | 49 | N-[Acetyl-1-$^{13}$C,$^2$H$_3$] triglycine | 235 | 10 (14.1 T) | C | 40 |
| | 50 | C$_1$ of 3,5-difluorobenzoyl-L-glutamate (NA) | 287 | 7 (11.7 T) | C | 185 |
| | 51 | N-[Acetyl-1-$^{13}$C,$^2$H$_3$] RGD peptide | 393 | 5 (14.1 T) | C | 40 |
| | 52 | Lys-N-[acetyl-1-$^{13}$C] adduct of N-acetyl-α-MSH (11–13) peptide | 426 | 10 (11.7 T) | C | 40 |
| hemi-ketal | 53 | [2-$^{13}$C] fructose | 181 | 13–15 (3 T); 16 (11.7 T) | A, B, C | 90 |
| hemi-acetal | 54 | C$_1$ of [U-$^{13}$C, U-$^2$H] glucose | 193 | 12 (14.1 T)$^a$ | A, B, C | 101 and 111 |
| primary carbon | 55 | [$^{13}$C$_2$, $^2$H$_6$] DMSO | 86 | NR | C | 80 |
| | 56 | [3-$^{13}$C, $^2$H$_3$] pyruvic acid | 92 | 56 (14.1 T) | C | 120 |
| | 57 | [$^{13}$C, $^2$H$_3$]-p-anisidine | 127 | 44.4 (9.4 T) | C | 125 |
| primary alcohol | 54 | C$_6$ of [U-$^{13}$C, U-$^2$H] glucose | 193 | 10 (14.1)$^a$ | A, B, C | 101 and 111 |

| Chemical structure | Index | HP agent | MW (Da) | Apparent $T_1$ (s) | Application | Ref. |
|---|---|---|---|---|---|---|
|  secondary carbon | 58 | [2-$^{13}$C, 1,2-$^2$H$_4$] choline chloride | 142 | 47 (14.1 T) | C | 107 |
| primary alcohol | | | | | | |
|  secondary alcohol | 54 | C2-5 of [U-$^{13}$C, U-$^2$H] glucose | 193 | 12 (14.1 T)$^a$ | A, B, C | 101 and 111 |
| secondary alcohol | | | | | | |
|  tertiary alcohol | 59 | [U-$^2$H, $^{13}$C]methylpropan-2-ol | 84 | 46 (9.4 T) | A, C | 68 |
| tertiary alcohol | | | | | | |
|  | 60 | Bis-1,1-(hydroxymethyl)-[1-$^{13}$C]cyclopropane-$^2$H$_8$ | 111 | 82 (2.4 T) | A, C | 89 |
|  alkene | 28 | Ethyl-2-cyanocrylate (NA) | 125 | NR | C | 132 |
| alkene | | | | | | |
|  nitrile | 28 | Ethyl-2-cyanoacrylate | 125 | NR | C | 132 |
| nitrile | | | | | | |

| Chemical structure | Index | HP agent | MW (Da) | Apparent $T_1$ (s) | Application | Ref. |
|---|---|---|---|---|---|---|
| enediol (reductone) | 31 | $C_2$, $C_3$ of ascorbic acid (NA) | 176 | NR | C | 38 |
| enediol (reductone) | | | | | | |
| phenyl | 61 | $C_1$ of styrene (NA) | 104 | 37 (9.4 T) | C | 41 |
| | 13 | $C_2$ of benzoic acid (NA) | 122 | 19 (11.7 T) | C | 54 |
| | 18 | $C_2$ of salicylic acid (NA) | 138 | NR | C | 38 |
| | 32 | $C_2$ of methyl fusarate (NA) | 193 | NR | C | 132 |
| | 32 | $C_5$ of methyl fusarate (NA) | 193 | NR | C | 132 |
| phenyl | 50 | $C_2$ of 3,5-difluorobenzoyl-L-glutamate (NA) | 287 | 6 (11.7 T) | C | 185 |
| phenol | 18 | $C_3$ of salicylic acid (NA) | 138 | NR | C | 38 |
| phenol | | | | | | |
| naphthalene | 24 | $C_3$, $C_5$, $C_8$, $C_{10}$ of 2-napthaleneacetic acid-6-methoxy-α-methyl (NA) | 230 | NR | C | 54 |
| naphthalene | | | | | | |
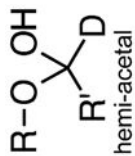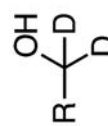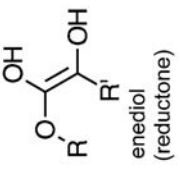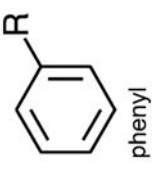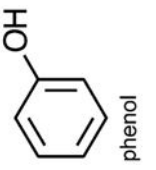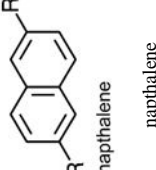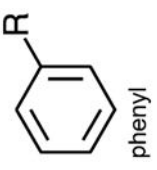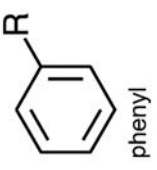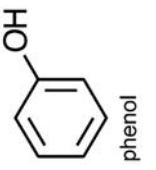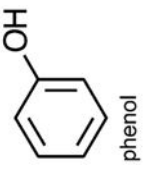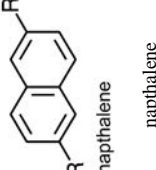
Apparent $T_1$ relaxation rates are reported in seconds with the corresponding field strength. Application abbreviation: A – *in vivo* studies, B – studies in cells, tissues, and perfused organs, C – solution studies (basic physiochemical properties, chemical reactions).

[a] For [U-$^{13}$C, U-$^2$H] glucose, $T_1$ studies were performed at a wide range of field strengths, concentrations, and enrichment sites. For further analysis please refer to Allouche-Arnon *et al.*[111]